Universidad Michoacana de San Nicolás de Hidalgo
Instituto de Física y Matemáticas

Diagrama de Fase de la QCD con Masas de Quarks Constantes

Tesis presentada al

Instituto de Física y Matemáticas

para obtener el grado de

Doctor en Ciencias en el Área de la Física

Por

Aftab Ahmad

Asesor

Dr. Alfredo Raya Montaño
(IFM-UMSNH)

Morelia, Micoacán, México.-Enero, 2016

University of Michoacan de San Nicolás de Hidalgo
Institute of Physics and Mathematics

QCD Phase Diagram from Constant Quark Masses

Thesis is presented to the

Institute of Physics and Mathematics

for the degree of

Doctor of Sciences in the Area of Physics

By

Aftab Ahmad

Supervisor

Dr. Alfredo Raya Montaño
(IFM-UMSNH)

Morelia, Micoacán, México.-January, 2016

Contents

Acknowledgements

First of all, I am thankful to almighty Allah, most Gracious, most Compassionate, who has given me courage, potential and good health to tackle the problem in my life.

I would like to express my sincere gratitude to my supervisor Prof. Dr. Alfredo Raya for the continuous support of my Ph.D study and research, for his patience, motivation, enthusiasm and immense knowledge. His guidance help me in all the time of research and writing of this thesis.

Besides my advisor, I would like to thank the rest of my thesis committee: Dr. Adnan Bashir, Dr. Alejandro Ayala, Dr. Christian Schubert and Dr. Axel Weber for their advices, insightful comments and encouragement.

I would like to acknowledge financial, academic and technical support from the IFM-UMSNH. I also would like to acknowledge the Conacyt-Mexico for providing me 4-year scholarship to complete this desertion. This scholarship not only provide me the support but also make the links between UMSNH University Mexico and Gomal University Pakistan. I also thank to academic and non academic staff of IFM-UMSNH.

I thank to Dr. Marcelo Loewe for inviting me to PUC, Chile, where a part of the work has been done.
My sincere thanks also goes to Prof. Dr. N.A.D Khattak, Chairman, Department of physics, Gomal University, Pakistan for his kind support and help in the process of study leave to complete my Ph. D thesis.

I am grateful to my best friend Paola for providing me the help in learning Spanish and support in academic and non academic matter, nice memories both in Mexico as well as in Chile. I also thanks to J. J. Cobos, Pietro Dall'ilo for valuable academic discussion. I would have nice memories with my friends Kappini Raya, Deric, Luis albino and rest of the friends from the IFM-UMSNH and outside the institute.

Last but not the least, I would like to thank my family: my parents and to my brothers, sister antes and uncle and rest of the family member for supporting me spiritually throughout writing this thesis and my life in general.

Dedication

“To My Family”

Resumen

En esta tesis estudiamos el diagrama de fase de la cromodinámica cuántica (QCD por sus siglas en inglés) en el plano de temperatura T y potencial químico μ en el marco de las ecuaciones de Schwinger-Dyson (SDE) implementando truncamientos que involucran masas de los quarks constantes. Truncamos la ecuación de brecha para el propagador del fermión de tres maneras diferentes. Primero, consideramos la aproximación de masa constante (CMA por sus siglas en inglés), donde consideramos un acoplamiento efectivo que depende del momentum y la temperatura y un propagador del gluón inspirado por recientes resultados de lattice dentro del llamado escenario refinado de confinamiento de Gribov-Zwanziger, pero truncamos la ecuación de brecha de modo que la renormalización de la función de onda se mantenga trivial y entonces obtenemos una masa dinámica independiente del momentum; Segundo, consideramos una variante del modelo de Nambu–Jona-Lasinio, regularizado dentro de un esquema de tiempo propio que en la literatura se ha llamado modelo de interacción de contacto (CI por sus siglas en inglés), donde el acoplamiento, el propagador del gluón y la masa dinámica de los quarks se toman como independientes del momentum. Finalmente, mejoramos el modelo de CI (refiriéndonos a éste como ICI por sus siglas en inglés), donde ajustamos nuestras predicciones a los resultados de lattice para el condensado de quark-antiquark. La temperatura críticua a μ cero para la transición de rompimiento a restauración de la simetría quiral se obtiene de la posición del máximo del gradiente térmico del condensado quiral en los tres casos. Para la transición de fase de confinamiento a desconfinamiento, considerando la CMA, usamos parámetros relacionados a la violación del axioma de reflexión de positividad del propagador del quark (derivados del "propagador del quark promediado espacialmente") y para la interacción de contacto usamos el condensado dual de quarks y la escala de longitud de confinamiento. Extendemos nuestros cálculos a T finita incluyendo el potencial químico μ y esbozamos el diagrama de fase en todos los casos. Las transiciones son un cross-over en presencia de una masa de corriente para los quarks y son de segundo orden en el límite quiral hasta que se alcanza el punto crítico final. Este punto se define como el punto en el plano $T-\mu$ donde las transiciones de fase continuas se vuelven de primer orden. El punto crítico final para el truncamiento de la CMA se encuentra en $(\mu_E/T_c = 0.42, T_E/T_c = 0.8)$, para la CI en $(\mu_E/T_c = 1.68, T_E/T_c = 0.4)$ con masa de corriente y en el límite quiral, $(\mu_E/T_c = 1.5, T_E/T_c = 0.54)$. Para el modelo de ICI el punto crítico final se localiza en $(\mu_E/T_c = 2.3, T_E/T_c = 0.5)$.

Estudiamos el efecto de un campo magnético externo eB en las temperaturas de transición de ruptura-restauración de simetría quiral y confinamiento-desconfinamiento usando un modelo de CI confinante para quarks. En la aproximación de campo medio, observamos el fenómeno de catálisis magnética, caracterizado por un comportamiento creciente de las temperaturas pseudocríticas para las transiciones al crecer eB. Considerando un acomplamiento que corre

inspirado por lattice, cuyo comportamiento es monotónicamente decreciente con eB, la catálisis magnética inversa toma lugar en nuestro modelo. Nuestros resultados están de acuerdo con predicciones de otros modelos de interacciones fuertes y estudios de lattice.

PALABRAS CLAVE: Cromodinámica cu'antica, diagrama de fase, ecuaciones de Schwinger-Dyson, simetría quiral, confinamiento.

Abstract

In this dissertation we study the quantum chromodynamics (QCD) phase diagram in the temperature T and chemical potential μ plane from the Schwinger-Dyson equations (SDE) framework implementing truncations that invoke constant quark masses. We truncate the gap equation for the fermion propagator in three different manners. First, we consider the constant mass approximation (CMA), where we use a momentum and temperature dependent effective coupling and gluon propagator inspired by recent lattice results within the so-called refined Gribov-Zwanziger scenario for confinement, but truncate the gap equation so as to render wavefunction renormalization trivial and have a dynamical quark mass independent of the momentum; Second, we consider a variant of the Nambu–Jona-Lasinio model, regularized within a proper time approach which in literature has been referred to as the the contact interaction (CI) model, where the strong coupling, gluon propagator and the dynamical quark mass are independent of momentum; Finally we improve the CI model, that we named ICI model, where we match our predictions for the quark-antiquark condensate with the lattice results. The critical temperature for the chiral symmetry breaking-restoration transition is obtained from the position of the maximum of the thermal gradient of the chiral condensate for all the three cases. For the confinement-deconfinement phase transition in the truncation of CMA, we use parameters related to the violation of the axiom of reflection positivity of the quark propagator (derived from the "spatially averaged quark propagator") and for the CI and ICI, we use the dual quark condensate and the confining length scale. The critical temperatures at zero μ for the chiral symmetry breaking-restoration and confinement-deconfinement transitions are coincidental for all the three cases, also in agreement with lattice. We extend our finite T calculations by including chemical potential μ and chart out the phase diagram in all cases. The transitions are cross-over in the presence of current quark mass and are of second-order in the chiral limit until the critical end point is reached. This point is defined as the point in the $T-\mu$ plane where the continuous phase transitions become of first-order. The critical end point for the truncation of CMA is located at ($\mu_E/T_c = 0.42,\ T_E/T_c = 0.8$), for CI at ($\mu_E/T_c = 1.68,\ T_E/T_c = 0.4$) with current quark mass and in the chiral limit at ($\mu_E/T_c = 1.5,\ T_E/T_c = 0.54$). For ICI model with current quark mass, the critical end point is located at ($\mu_E/T_c = 2.3,\ T_E/T_c = 0.5$).

We study the effect of an external magnetic field eB on the chiral symmetry breaking-restoration and the confinement-deconfinement transition temperatures by using a confining CI model for quarks. In the mean field approximation, we observe the magnetic catalysis phenomenon, characterised by a rising behavior of the pseudo-critical transition temperatures with growing eB. Considering a lattice inspired running coupling which monotonically decreases with eB, inverse magnetic catalysis takes place in our model. Our findings are in agreement with predictions from other models of strong interaction and lattice predictions.

KEYWORDS: Quantum chromodynamics, phase diagram, Schwinger-Dyson equations, chiral symmetry, confinement.

List of Figures

Chapter 1

Introduction

Quantum chromodynamics (QCD) is the theory of the strong color force among the quarks and gluons. It was developed by H. Fritzch and M. Gell-Mann in the 1970s. In 1973, a major breakthrough came, when the phenomenon of asymptotic freedom of non-Abelian gauge theory was discovered by G. 't Hooft, D. J. Gross, H. D. Politzer and F. Wilczek. For the discovery of asymptotic freedom in QCD, D. J. Gross, H. D. Politzer and F. Wilczek were awarded the 2004 Nobel Prize in Physics. Asymptotic freedom allows a perturbative treatment of strong interactions at high energies or short distances. It is successful in predicting the phenomena involving large momentum transfer by an electron on a proton target, where the coupling is small and the Feynman diagram-based perturbation theory becomes a reliable tool. This is what we call the perturbative QCD. Perturbation theory fails in the large distance domain, where the coupling becomes large. The theory does not provide answers to some key questions, for example, if like photons, the gluons are also massless, as they are assumed to be in QCD, why long-range strong interactions have never been detected? If the strong interaction is color dependent, why are only color singlets observed? This is the famous outstanding problem of the color confinement and hence the subject of non-perturbative QCD. Many methods have been devised to deal with this aspect of strong interactions, among which one of the most promising consists on the continuum approach i.e., the Schwinger-Dyson equations (SDE). Lattice gauge theory, introduced by K.G Wilson in 1974, on the other hand, describes strong interactions in a framework in which the continuum space-time is descretized.

Another important issue of non-perturbative QCD is the origin of the mass of the visible universe, roughly speaking, of protons and neutrons. Consider the mass of proton which is made up of three light quarks, two u and one d. It is around 1 GeV, and each quark mass is around $3 - 10$ MeV, according to the Higgs mechanism in the Standard Model of Particle Physics, which led to the discovery of Higgs particle in 2013 at CERN. The sum of all the three current quark masses inside the proton is approximately 99% less than the resultant mass of the proton. The question is now here, where does this mass come from? The answer is provided

in non-perturbative QCD through the phenomenon of "dynamical chiral symmetry breaking".

QCD at finite temperature and density plays an important role to understand transitions that took place in the early universe, after a few microseconds from the Big Bang. As it is known, the observable degrees of freedom of QCD at low temperature are the color-singlet hadrons, while at high temperature, the interaction between quarks and gluons becomes weaker, causing hadrons to split up in a new phase[1] where the dominant degrees of freedom are the quarks and gluons. This type of phase transition is referred to as confinement-deconfinement transition. The vanishing of dynamically generated quark mass at high temperature T and/or chemical potential μ corresponds to another type of transition i.e., chiral symmetry restoration, while at zero T and μ, chiral symmetry is broken. Thus, when the strength of the QCD interaction diminishes with increasing T and μ, only the current quark masses survive when these parameters exceed a set of critical values. This is the chiral symmetry breaking-restoration phase transition. As for experiment is concerned, implications of chiral symmetry breaking for the elastic and transition form factors of mesons and baryons form an integral part of the planned program at the 12 GeV upgrade of the Thomas Jefferson National Accelerator Facility in Virginia [**?**]. There are other experiments around the world that might help to understand the confinement and chiral transitions like RHIC in Brookhaven, LHC at CERN, and future experiment proposals like CBM at FAIR, in Germany.

The chart of the QCD phase diagram is shown in Fig. **??**. At $T = 0$ and $\mu = 0$, chiral symmetry is broken and quarks and gluons are confined inside hadrons (baryons and mesons), bound states and resonances. At sufficiently high T and μ, the hadronic matter undergoes a transition from the chiral symmetry broken phase to chiral symmetry restoration and from a confining to a deconfined phase, where the quarks and gluons exist freely in a state named quark-gluon plasma. The sketch also indicates the existence of other possible states (neutron stars and color super conducting phase) at low $T = 0$ and high μ. Perturbation theory fails to access to the description of these transitions and hence a non-perturbative treatment is necessary. Our aim in this thesis is to study these phase transitions using a non-perturabtive approach to QCD.

We use the SDE framework to study the above mentioned phase transitions from first principles. Though there is not enough experimental data available at finite T and μ, we consider the lattice results (which are only available at finite T and $\mu = 0$) as a guide and then consider a finite density situation to explore the phase diagram at finite T and μ. We consider two-flavors with physical up and down current quark masses assuming isospin symmetry and within the rainbow-ladder approximation and in Landau gauge through out this work. Chapter 2 is devoted to explore the QCD phase diagram from an effective kernel of the QCD gap equation based on the constant mass approximation (CMA), where the gap equation solution is independent of momentum. In Chapter 3, we study this chart through the confining vector-

[1]Here the word 'phase' mean to characterize regions with different dominant degrees of freedom.

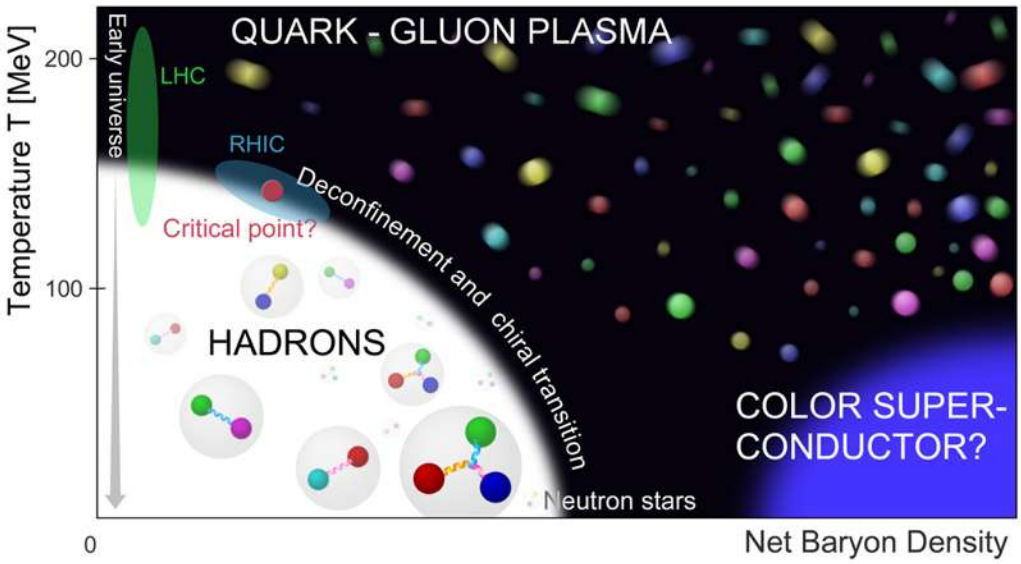

Figure 1.1: Chart of the QCD phase diagram sketched by Guido Cossu Post-doc researcher at KEK, Tsukuba.

vector contact interaction model (CI) for quarks and also it improved form i.e., ICI. In the past few years, the effect of an external magnetic field on the QCD phase transitions has opened an interesting area of research where phenomena such as Magnetic Catalysis (MC) and Inverse Magnetic Catalysis (IMC) could take place and modify the behavior of hadron matter. Experimental motivation behind this fact comes from peripheral heavy-ion collisions, since not all the nucleons are participants in the reaction, because they are electric charges in motion, they produce in the interaction region a very strong magnetic field which quickly weakens, but whose effects can be measured in experiments. Thus, our Chapter 4 is based on the study of the effect of external magnetic filed on the QCD phase transitions through CI model. We discuss our findings and conclude in Chapter 5. For complementarity, we added three appendices of some calculational details.

From this dissertation the following papers were published:

- E. Gutiérrez, A. Ahmad, A. Ayala, A. Bashir and A. Raya, *J. Phys. G* **41**, 075002 (2014),
- F. Márquez, A. Ahmad, M. Buballa and A. Raya, *Phys. Lett. B* **747**, 529 (2015),

along with the following proceedings:

- A. Ahmad and A. Raya, *J. Phys.: Conf. Ser.* **418**, 012009 (2013),

- A. Ahmad, A. Ayala, A. Bashir, E. Gutiérrez and A. Raya, *J. Phys.: Conf. Ser.* **651**, 012018 (2015).

The work

- A. Ahmad, A. Raya, *Inverse Magnetic Catalysis within a Confining Contact Interaction Model for Quarks*

is under consideration and the following manuscripts

- A. Ahmad, *et. al.*, *QCD phase diagram from Constant Mass Approximation*,
- A. Ahmad, *et. al.*, *QCD phase diagram from vector-vector Contact Interaction Model of Quarks*,

are in progress.

Chapter 2

QCD Phase Diagram from Constant Mass Approximation

In this Chapter we study the QCD phase diagram through the quark gap equation. Starting with $N_f = 2$ fermion flavors, we begin our discussion at zero temperature and solve the gap equation (in Landau gauge) with a kernel that includes a momentum dependent coupling [**?**] and a gluon propagator model [**?**] as discussed in [**?**], though here we use the flavor dependent version of RGZ model i.e., flavor dependent (FRGZ) [**?**]. We promote the same truncation at finite temperature and density. We introduce the Constant Mass Approximation (CMA) to the gap equation and study the QCD phase diagram. The CMA has been motivated in the field of magnetic catalysis of dynamical chiral symmetry breaking [**?**]. It is based on the observation that the kernel of the gap equation yields only significant contribution in the small momentum region, where the mass function is roughly constant. We use this idea to solve the gap equation. We use the rainbow-ladder truncation (bare vertex) through out in this work. At finite temperature we take available lattice results [**?**] for the quark-antiquark condensate as a guide, and fit our CMA based gap equation kernel quark-antiquark condensate at finite temperature. In order to identify the pseudo-critical temperature for the chiral transition, we use the thermal gradient of the quark condensate and confinement is explored through the parameters invoking of the axiom of reflection positivity. At the end, we introduce the chemical potential to sketch the QCD phase diagram. Part of this Chapter is based on our work [**?**].

2.1 Gap equation at zero temperature

SDEs form an infinite set of coupled integral relations among the Green functions and are the equations of motion of a given quantum field theory (QFT). The two point function is related to the three point function, the three point function is related also to the four point function and so on. In pictorial form the SDEs for the quark propagator, gluon propagator and quark-gluon

vertex respectively, are shown in Figs. **??** - **??**. Mathematically, the quark gap equation is given

Figure 2.1: SDE for the quark propagator.

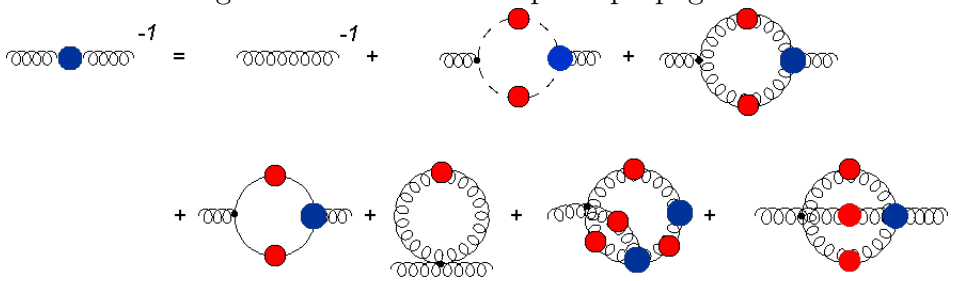

Figure 2.2: SDE for the gluon propagator.

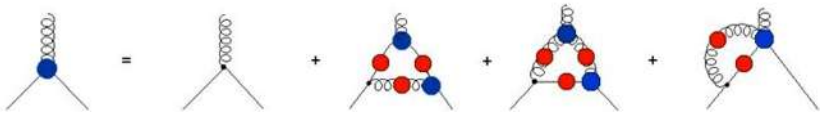

Figure 2.3: SDE for the quark-gluon vertex.

by

$$S(p)^{-1} = i\gamma \cdot p + m_c + \Sigma(p), \tag{2.1.1}$$

where $S(p)^{-1}$ is the full (inverse) quark propagator, m_c the current quark mass and

$$\Sigma(p) = \int \frac{d^4k}{(2\pi)^4} g^2 D_{\mu\nu}(q^2) \frac{\lambda^a}{2} \gamma_\mu S(k) \frac{\lambda^a}{2} \Gamma_\nu(k,p) \tag{2.1.2}$$

is the self energy, which involves $\Gamma_\nu(k,p)$, the dressed quark-gluon interaction vertex, $q = k - p$ is the gluon momentum and $D_{\mu\nu}(q^2)$, the dressed gluon propagator, which can be modeled or takes a form given by solving the coupled equations between gluon and ghost propagators or by parametrizing the data from lattice QCD simulations. g is the coupling constant and λ_s^a are the Gell-Mann matrices of the color group $SU(3)_c$. According to the Lorentz covariance of QCD, the inverse quark propagator decomposes as

$$S(p)^{-1} = i\gamma \cdot pA(p^2) + B(p^2), \tag{2.1.3}$$

and the quark propagator can be also be expressed

$$S(p) = i\gamma \cdot p\sigma_v(p^2) + \sigma_s(p^2), \tag{2.1.4}$$

where $A(p^2)$ and $B(p^2)$ are scalar functions, which can be written as

$$F(p^2) = \frac{1}{A(p^2)}, \qquad M(p^2) = \frac{B(p^2)}{A(p^2)}, \tag{2.1.5}$$

with $M(p^2)$ representing the quark mass function, $F(p^2)$ the quark wavefunction renormalization function. Furthermore,

$$\sigma_s(p^2) = \frac{F(p^2)M(p^2)}{p^2 + M^2(p^2)}, \qquad \sigma_v(p^2) = \frac{F(p^2)}{p^2 + M^2(p^2)}. \tag{2.1.6}$$

We can write the gap equation in the form of a coupled system of equations for $A(p^2)$ and $B(p^2)$, that is, from Eq. (**??**) and Eq. (**??**), we have

$$\begin{aligned} i\gamma \cdot pA(p^2) + B(p^2) &= i\gamma \cdot p + m_c \\ &+ \int \frac{d^4k}{(2\pi)^4}\left[g^2 D_{\mu\nu}(q^2)\frac{\lambda^a}{2}\gamma_\mu \frac{1}{i\gamma \cdot kA(k^2) + B(k^2)}\frac{\lambda^a}{2}\Gamma_\nu(k,p)\right]. \end{aligned} \tag{2.1.7}$$

Here $\sum \lambda_a\lambda_a = \frac{16}{3}I$, where I is the identity in color space. The gluon propagator in Landau gauge takes the form,

$$D_{\mu\nu}(q^2) = D(q^2)\left(\delta_{\mu\nu} - \frac{q_\mu q_\nu}{q^2}\right), \tag{2.1.8}$$

and in the rainbow-ladder truncation, we consider

$$\Gamma_\nu(k,p) = \gamma_\nu. \tag{2.1.9}$$

Inserting Eq. (**??**) and Eq. (**??**) in Eq. (**??**), we have

$$\begin{aligned} i\gamma \cdot pA(p^2) + B(p^2) &= i\gamma \cdot p + m_c \\ &+ \frac{1}{12\pi^4}\int d^4k\left[g^2 D(q^2)\left(\delta_{\mu\nu} - \frac{q_\mu q_\nu}{q^2}\right)\gamma^\mu\left(\frac{-i\gamma \cdot kA(k^2) + B(k^2)}{k^2A^2(k^2) + B^2(k^2)}\right)\gamma_\nu\right]. \end{aligned} \tag{2.1.10}$$

The equation for $A(p^2)$ is obtained by multiplying $-i\gamma \cdot p$ on both sides of Eq. (**??**) and taking the trace, which yields

$$\begin{aligned} 4p^2A(p^2) = 4p^2 - \frac{1}{12\pi^4}\int d^4k\Bigg[&g^2 D(q^2)\left(\delta_{\mu\nu} - \frac{q_\mu q_\nu}{q^2}\right) \\ &\times \frac{Tr\left[p_\alpha\gamma_\alpha\gamma_\mu\gamma_\beta k_\beta A(k^2)\gamma_\nu + p_\alpha\gamma_\mu\gamma_\alpha B(k^2)\gamma_\nu\right]}{k^2A^2(k^2) + B^2(k^2)}\Bigg]. \end{aligned} \tag{2.1.11}$$

Since

$$Tr[\gamma_\alpha\gamma_\mu\gamma_\beta\gamma_\nu] = 4[\delta_{\alpha\mu}\delta_{\beta\nu} - \delta_{\alpha\beta}\delta_{\mu\nu} + \delta_{\alpha\nu}\delta_{\mu\beta}], \qquad Tr[\gamma_\alpha\gamma_\mu\gamma_\nu] = 0,$$
$$\left(\delta_{\mu\nu} - \frac{q_\mu q_\nu}{q^2}\right) Tr[\gamma_\alpha p_\alpha \gamma_\mu \gamma_\beta k_\beta \gamma_\nu] = -4\left[(p\cdot k) + 2\frac{(p\cdot q)(q\cdot k)}{q^2}\right], \tag{2.1.12}$$

Eq. (**??**) becomes

$$\begin{aligned} A(p^2) &= 1 + \frac{1}{12p^2\pi^4}\int d^4k[g^2D(q^2)]\frac{A(k^2)}{k^2A^2(k^2)+B^2(k^2)}\left[(p\cdot k) + 2\frac{(p\cdot q)(q\cdot k)}{q^2}\right], \\ &= 1 + \frac{1}{12p^2\pi^4}\int d^4k[g^2D(q^2)]\sigma_v(k^2)\left[(p\cdot k) + 2\frac{(p\cdot q)(q\cdot k)}{q^2}\right]. \end{aligned} \tag{2.1.13}$$

Next, multiplying identity matrix I by Eq. (**??**) and taking the trace, we have

$$\begin{aligned} 4B(p^2) &= 4m_c \\ &+\frac{1}{12\pi^4}\int d^4k g^2 D(q^2)\left(\delta_{\mu\nu} - \frac{q_\mu q_\nu}{q^2}\right)\frac{Tr[-i\gamma_\mu\gamma_\beta k^\beta A(k^2)\gamma_\nu + \gamma_\mu B(k^2)\gamma_\nu]}{k^2A^2(k^2)+B^2(k^2)}, \end{aligned} \tag{2.1.14}$$

or

$$4B(p^2) = 4m_c + \frac{1}{12\pi^4}\int d^4k g^2 D(q^2)\left(\delta_{\mu\nu} - \frac{q_\mu q_\nu}{q^2}\right)\frac{Tr[\gamma_\mu\gamma_\nu]B(k^2)}{k^2A^2(k^2)+B^2(k^2)}. \tag{2.1.15}$$

As

$$Tr[\gamma_\mu\gamma_\nu] = 4\delta_{\mu\nu}, \qquad \left(\delta_{\mu\nu} - \frac{q_\mu q_\nu}{q^2}\right)\delta_{\mu\nu} = 3,$$

we have

$$4B(p^2) = 4m_c + \frac{4}{4\pi^4}\int d^4k[g^2D(q^2)]\frac{B(k^2)}{k^2A^2(k^2)+B^2(k^2)}, \tag{2.1.16}$$

or

$$B(p^2) = m_c + \frac{1}{4\pi^4}\int d^4k[g^2D(q^2)]\sigma_s(k^2). \tag{2.1.17}$$

A non trivial solution of Eq. (**??**) reveals dynamical chiral symmetry breaking (DCSB). Different models for $g^2D(q^2)$ have been tested in [**?**] to study the DCSB.

2.2 Gap equation kernel at zero temperature $T = 0$

In Ref. [**?**] we studied the gap equation with the so-called Refined Gribov-Zwanziger (RGZ) gluon propagator model [**?**] and used a momentum dependent effective interaction proposed in Ref. [**?**]. We further tune the support of the kernel to obtain the physical condensate in chiral limit and with current quark masses, which are approximated with well known phenomenological model of Maris-Tandy in Ref. [**?**]. We use the flavor dependent form of the RGZ gluon propagator (FRGZ) given in [**?**],

$$D(k^2) = \frac{k^2 + M_1^2}{k^4 + k^2(M_1^2 - \frac{13 g_1^2 < A_1^2 >}{24}) + M_1^2 m_0^2}, \tag{2.2.1}$$

where the parameters in this dressing function are the following: $M_1 = 4.85$ GeV^2 is related to the condensate of auxiliary fields emerging when incorporating the horizon condition to the action, $g_1^2 < A_1^2 >= 0.474(16.406 - N_f)$ GeV^2 is related to the dimension-two gluon condensate and $m_0 = 1.011(9.161 - N_f)^{-1/2}$ GeV^2. A plot of the dressing function in Eq. (**??**) for $N_f = 2$ is shown in Fig. **??**, *left panel*. We complete our kernel with the effective interaction $g_{eff}^2(k^2) =$

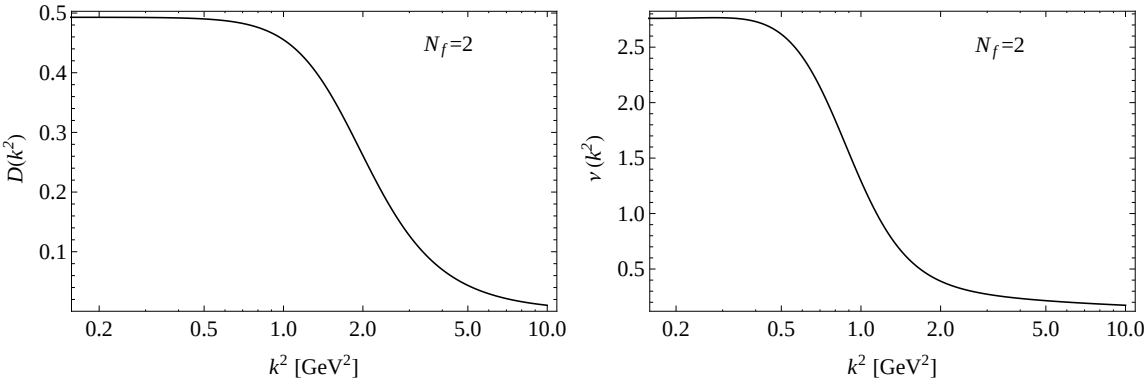

Figure 2.4: *Left panel*: FRGZ gluon propagator [**?**] as a function of momentum, Eq. (**??**). *Right panel*: Effective coupling [**?**], Eq. (**??**), as a function of momentum.

$4\pi a_2 \nu(k^2)$ where $\nu(k^2)$ is given by

$$\nu(k^2) = \left[\frac{a + b\left(\frac{k}{\Lambda}\right)^2}{1 + c\left(\frac{k}{\Lambda}\right)^2 + d\left(\frac{k}{\Lambda}\right)^4 + o\left(\frac{k}{\Lambda}\right)^6 + \frac{\pi\gamma}{\log\left[e + \left(\frac{k}{\Lambda}\right)^2\right]}} \right], \tag{2.2.2}$$

with $a = 1.47$, $b = 0.881$, $c = 0.314$, $d = 0.00986$, $o = 0.00168$, $\gamma = 12/25$, $\Lambda = 0.234$, $\nu(k^2)$ is shown in Fig. **??**, *right panel*, and $a_2 = 0.7$ is the parameter introduced in [**?**] to match the chiral condensate obtained from MT model [**?**].

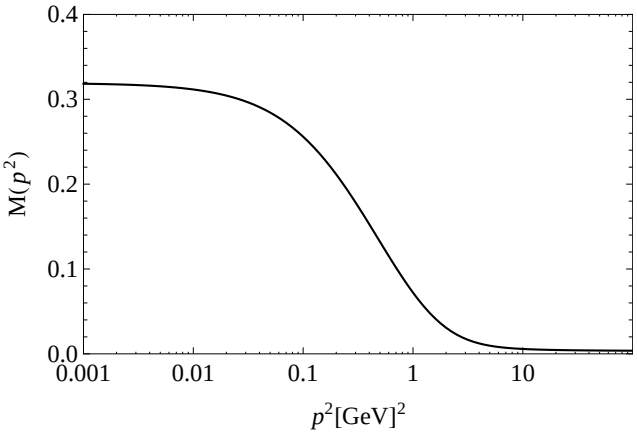

Figure 2.5: Mass function $M(p^2) = B(p^2)/A(p^2)$ as a function of momentum.

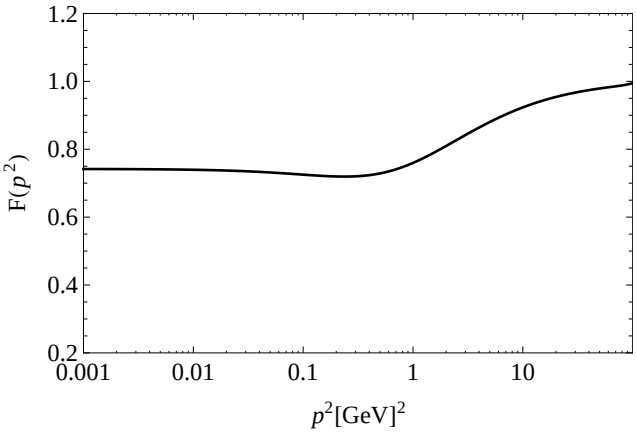

Figure 2.6: Wave function renormalization $F(p^2) = 1/A(p^2)$ as a function of momentum.

2.2.1 Chiral condensate

The order parameter for the dynamical chiral symmetry breaking is the chiral condensate (see Appendix A). It corresponds to the vacuum expectation value of the composite quark-antiquark operator. In the chiral limit (where the current quark mass is equal to zero), when the expectation value of this parameter is zero, then there is chiral symmetry, and if the value of this parameter is finite, then chiral symmetry is broken and quarks acquire masses. In the presence of current quark mass, it is an approximate order parameter. The chiral condensate

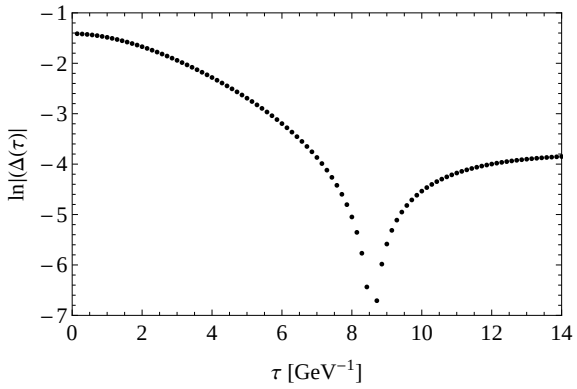

Figure 2.7: Confinement test.

is the trace of the propagator at the origin of the position co-ordinates (see Appendix A), that is

$$\begin{aligned} -\langle\bar{\psi}\psi\rangle = Tr[S(x=0)] = N_c Tr\int\frac{d^4p}{(2\pi)^4}[S(p^2)], \\ = 4N_c\int\frac{d^4p}{(2\pi)^4}\frac{F(p^2)M(p^2)}{p^2+M^2(p^2)}, \end{aligned} \tag{2.2.3}$$

where $N_c = 3$ is the numbers of colors.

2.2.2 Reflection positivity and confinement

Consider the "spatially averaged Schwinger function" (See Appendix A Chapter 6)

$$\Delta(t)_{v,s} = \frac{1}{2\pi}\int dp_4 e^{-ip_4 t}\sigma_{v,s}(p_4,\vec{0}) = \frac{1}{\pi}\int dp_4 \cos(p_4 t)\sigma_{v,s}(p_4,\vec{0}) \geqslant 0. \tag{2.2.4}$$

Thus, for the stable (free particle) $\Delta(t) \geq 0$, while for confined particle $\Delta(t) < 0$. In general, the fermion propagator in a quantum field theory has real poles and pairs of complex conjugate poles. In principle we could search for confinement by locating the poles of the propagator in the complex $p^2 - plane$. For real poles, $\Delta(t)_{v,s}$ decays exponentially,

$$\Delta(t)_{v,s} \sim e^{-Mt}, \tag{2.2.5}$$

and is positive definite. It corresponds to a stable asymptotic state. For complex conjugate pairs of poles: the dynamical masses develop an imaginary part "$M = a \pm ib$". The corresponding

propagator could describe a short lived excitation which decays exponentially at large time-like distances as

$$\Delta(t)_{v,s} \sim e^{-at}\cos(bt+\delta), \tag{2.2.6}$$

describes a confined particle due to the complex conjugate poles, which lead to the violation of the reflection positivity.

2.2.3 Solution of the gap equation at $T = 0$

With a particular choice of the mentioned kernel gap equation, we obtained the chiral condensate $-\langle\bar{\psi}\psi\rangle^{1/3} \sim 0.26$ GeV. The quark mass function $M(p^2)$ with current quark mass $(m_c = 3)$MeV and quark wave function renormalization function are shown in Fig. **??** and Fig. **??**, respectively. From Fig. **??**, it is obvious that their is confinement in the FRGZ model. It should be noted that we use $N_f = 2$ throughout this work. In the next section we study the gap equation at finite temperature and density.

2.3 Gap equation at finite temperature T and density μ

We use the imaginary time formalism [**?**], in which the temporal co-ordinate gets discretized. Fermions obey the anti-periodic boundary condition:

$$\psi(\vec{x},\tau=0) = -\psi(\vec{x},\tau=\beta), \tag{2.3.1}$$

where $\beta = 1/T$. Bosons obey the periodic boundary condition:

$$\phi(\vec{x},\tau=0) = \phi(\vec{x},\tau=\beta). \tag{2.3.2}$$

This difference causes fermions and bosons to have a different behavior in their Matsubara frequencies i.e., fermion Matsubara frequencies are given by $\omega_n = (2n+1)\pi T$ and boson Matusbara frequencies, $\Omega_n = 2n\pi T$. It is obvious that the Lorentz symmetry $O(4)$ of the theory is lost because the temporal dimension gets discretized and thus at finite temperature (and or chemical potential) the theory has only $O(3)$ symmetry, that corresponds to spatial rotations. In the Matsubara formalism, we adopt the prescription

$$\int \frac{d^4k}{(2\pi)^4} \to T\sum_n \int \frac{d^3k}{(2\pi)^3}, \tag{2.3.3}$$

the fermion four-momentum splits into

$$p_\mu \to P_\mu = (\vec{p},\omega_n), \tag{2.3.4}$$

and the boson four-momentum as

$$q_\mu \to Q_\mu = (\vec{q}, \Omega_n). \tag{2.3.5}$$

The inverse dressed quark propagator at finite temperature and density is given by

$$S^{-1}(\vec{p}, \widetilde{\omega}_n) = (i\vec{\gamma}\cdot\vec{p})A(\vec{p}^2, \widetilde{\omega}_n^2) + i\gamma_0\tilde{\omega}_n C(\vec{p}^2, \widetilde{\omega}_n^2) + B(\vec{p}^2, \widetilde{\omega}_n^2), \tag{2.3.6}$$

and quark propagator can be written as

$$S(\vec{p}, \widetilde{\omega}_n) = (i\vec{\gamma}\cdot\vec{p})\sigma_A(\vec{p}^2, \widetilde{\omega}_n^2) + i\gamma_0\tilde{\omega}_n \sigma_C(\vec{p}^2, \widetilde{\omega}_n^2) - \sigma_B(\vec{p}^2, \widetilde{\omega}_n^2), \tag{2.3.7}$$

where $\widetilde{\omega}_n = \omega_n + i\mu$, μ is the chemical potential. Here $A(\vec{p}^2, \widetilde{\omega}_n^2)$, $C(\vec{p}^2, \widetilde{\omega}_n^2)$ and $B(\vec{p}^2, \widetilde{\omega}_n^2)$ are complex scalar functions, which satisfy:

$$\begin{aligned} A(\vec{p}^2, \widetilde{\omega}_n^2)^* &= A(\vec{p}^2, \widetilde{\omega}_{-n-1}^2), \\ B(\vec{p}^2, \widetilde{\omega}_n^2)^* &= B(\vec{p}^2, \widetilde{\omega}_{-n-1}^2), \\ C(\vec{p}^2, \widetilde{\omega}_n^2)^* &= C(\vec{p}^2, \widetilde{\omega}_{-n-1}^2). \end{aligned} \tag{2.3.8}$$

With these conditions, complex functions yield the solution of gap equation equal in pairs for each $-n-1$ and n Matsubara frequencies i.e. the solution for -1 is paired with 0, -2 is paired with 1, and so on (see Appendix B), and hence yield a real value for the condensate at zero and finite chemical potential.

To find the expression for sigmas ($\sigma_{A,B,C}$), we first take the product of Eq. (**??**) and Eq. (**??**), i.e., $S^{-1}S$. Multiplying the identity matrix I by $S^{-1}S$ and taking the trace, we have

$$\begin{aligned} Tr\left[S^{-1}S\right] &= Tr\left[(i\vec{\gamma}\cdot\vec{p}A + i\gamma_0\tilde{\omega}_n C + B)(i\vec{\gamma}\cdot\vec{p}\sigma_A + i\gamma_0\tilde{\omega}_n\sigma_C - \sigma_B)\right] \\ 4 &= -4\vec{p}^2 A\sigma_A - 4\tilde{\omega}_n^2 C\sigma_C - 4B\sigma_B \\ 1 &= -\vec{p}^2 A\sigma_A - \tilde{\omega}_n^2 C\sigma_C - B\sigma_B. \end{aligned} \tag{2.3.9}$$

Now multiplying γ_0 with $S^{-1}S$ and taking the trace,

$$\begin{aligned} Tr\left[\gamma_0 S^{-1}S\right] &= Tr\left[\gamma_0(i\vec{\gamma}\cdot\vec{p}A + i\gamma_0\tilde{\omega}_n C + B)(i\vec{\gamma}\cdot\vec{p}\sigma_A + i\gamma_0\tilde{\omega}_n\sigma_C - \sigma_B)\right] \\ 0 &= -4i\tilde{\omega}_n C\sigma_B + 4i\tilde{\omega}_n B\sigma_C \\ &\Rightarrow C\sigma_B = B\sigma_C \\ \frac{B}{C} &= \frac{\sigma_B}{\sigma_C}. \end{aligned} \tag{2.3.10}$$

Finally, multiplying $\vec{\gamma}$ with $S^{-1}S$ and taking the trace gives

$$\begin{aligned} Tr\left[\vec{\gamma}S^{-1}S\right] &= Tr\left[\vec{\gamma}(i\vec{\gamma}\cdot\vec{p}A + i\gamma_0\tilde{\omega}_n C + B)(i\vec{\gamma}\cdot\vec{p}\sigma_A + i\gamma_0\tilde{\omega}_n\sigma_C - \sigma_B)\right] \\ 0 &= -4ip_\alpha A\sigma_B + 4ip_\alpha B\sigma_B \\ &\Rightarrow A\sigma_B = B\sigma_A \\ \frac{A}{B} &= \frac{\sigma_A}{\sigma_B}. \end{aligned} \tag{2.3.11}$$

From Eq. (**??**) and Eq. (**??**), we have

$$\frac{A}{C} = \frac{\sigma_A}{\sigma_C}. \tag{2.3.12}$$

Using Eq. (**??**) and Eq. (**??**) in Eq. (**??**), we have

$$1 = -\vec{p}^2 A\sigma_A - \tilde{\omega}_n^2 C\frac{C}{A}\sigma_A - B\frac{B}{A}\sigma_A. \tag{2.3.13}$$

After simplifying,

$$\sigma_A(\vec{p}^2, \widetilde{\omega}_n^2) = -\frac{A(\vec{p}^2, \widetilde{\omega}_n^2)}{\vec{p}^2 A^2(\vec{p}^2, \widetilde{\omega}_n^2) + \tilde{\omega}_n^2 C^2(\vec{p}^2, \widetilde{\omega}_n^2) + B^2(\vec{p}^2, \widetilde{\omega}_n^2)}. \tag{2.3.14}$$

Similarly,

$$\sigma_B(\vec{p}^2, \widetilde{\omega}_n^2) = -\frac{B(\vec{p}^2, \widetilde{\omega}_n^2)}{\vec{p}^2 A^2(\vec{p}^2, \widetilde{\omega}_n^2) + \tilde{\omega}_n^2 C^2(\vec{p}^2, \widetilde{\omega}_n^2) + B^2(\vec{p}^2, \widetilde{\omega}_n^2)}, \tag{2.3.15}$$

and

$$\sigma_C(\vec{p}^2, \widetilde{\omega}_n^2) = -\frac{C(\vec{p}^2, \widetilde{\omega}_n^2)}{\vec{p}^2 A^2(\vec{p}^2, \widetilde{\omega}_n^2) + \tilde{\omega}_n^2 C^2(\vec{p}^2, \widetilde{\omega}_n^2) + B^2(\vec{p}^2, \widetilde{\omega}_n^2)}. \tag{2.3.16}$$

The QCD gap equation at finite temperature and density reads

$$S^{-1}(\vec{p}, \widetilde{\omega}_n) = (i\vec{\gamma}\cdot\vec{p}) + i\gamma_0\widetilde{\omega}_n + m_c + \Sigma(\vec{p}, \widetilde{\omega}_n), \tag{2.3.17}$$

where now

$$\Sigma(\vec{p}, \widetilde{\omega}_n) = T\sum_{l=-\infty}^{\infty}\int \frac{d^3\vec{k}}{(2\pi)^3} g^2 D_{\mu\nu}(\vec{p}-\vec{k}, \Omega_{nl})\frac{\lambda^a}{2}\gamma_\mu S(\vec{k}, \widetilde{\omega}_l)\frac{\lambda^a}{2}\Gamma_\nu(\vec{k}, \vec{p}, \tilde{\omega}_l, \tilde{\omega}_n), \tag{2.3.18}$$

with $\Omega_{nl} = \tilde{\omega}_n - \tilde{\omega}_l$. At finite temperature, the gluon propagator[1] splits into transverse and longitudinal components due to heat bath, which in the rest frame is specified by the four velocity $v_\mu = (1, \vec{0})$. Longitudinal and transverse pieces of the gluon propagator are distinguished by the Debye mass m_D [**?**]. The propagator has the form

$$D_{\mu\nu}(\vec{q}^2, \Omega_{nl}^2) = P_{\mu\nu}^T D^T(\vec{q}^2, \Omega_{nl}^2) + P_{\mu\nu}^L D^L(\vec{q}^2, \Omega_{nl}^2, m_D^2), \tag{2.3.19}$$

where $m_D^2 = g^2(4/3)T^2$, a value that is obtained from the the lowest order hard thermal loop (HTL) result with $g = 1$ [**?**]. The operators $P_{\mu\nu}^T$ and $P_{\mu\nu}^L$ are the transverse and longitudinal projection operators, respectively, given as

$$\begin{aligned} P_{\mu\nu}^L &= \delta_{\mu\nu} - \frac{Q_\mu Q_\nu}{Q^2} - P_{\mu\nu}^T, \\ P_{44}^T = 0, \qquad P_{ij}^T &= \delta_{ij} - \frac{\vec{q}_i\vec{q}_j}{\vec{q}^2}. \end{aligned} \tag{2.3.20}$$

[1] We use the Langau gauge (where the gauge parameter equal to zero) in this thesis.

Re-writing Eq. (**??**) as

$$\begin{aligned}\Sigma(\vec{p},\widetilde{\omega}_n) &= \frac{4}{3}T\sum_{l=-\infty}^{\infty}\int\frac{d^3\vec{k}}{(2\pi)^3}g^2\Bigg[\left(\delta_{\mu\nu}-\frac{Q_\mu Q_\nu}{Q^2}\right)D^L(\vec{q}^2,\Omega_{nl}^2,m_D^2)\\ &\quad +P_{\mu\nu}^T\left(D^T(\vec{q}^2,\Omega_{nl}^2)-D^L(\vec{q}^2,\Omega_{nl}^2,m_D^2)\right)\Bigg]\\ &\quad\times\left[\gamma_\mu\left(i\vec{\gamma}\cdot\vec{k}\sigma_A(\vec{k}^2,\widetilde{\omega}_l^2)+i\gamma_0\widetilde{\omega}_n\sigma_C(\vec{k}^2,\widetilde{\omega}_l^2)-\sigma_B(\vec{k}^2,\widetilde{\omega}_l^2)\right)\gamma_\nu\right], \qquad (2.3.21)\end{aligned}$$

we can find the self-consistent expression for $B(\vec{p}^2,\widetilde{\omega}_n^2)$ and the rest of the unknown functions. First, multiplying Eq. (**??**) by I and then taking the trace, we get

$$\begin{aligned}Tr[I\Sigma(\vec{p},\widetilde{\omega}_n)] &= \frac{4}{3}T\sum_{l=-\infty}^{\infty}\int\frac{d^3\vec{k}}{(2\pi)^3}g^2\Bigg[\left(\delta_{\mu\nu}-\frac{Q_\mu Q_\nu}{Q^2}\right)D^L(\vec{q}^2,\Omega_{nl}^2,m_D^2)\\ &\quad +P_{\mu\nu}^T\left(D^T(\vec{q}^2,\Omega_{nl}^2)-D^L(\vec{q}^2,\Omega_{nl}^2,m_D^2)\right)\Bigg]\\ &\quad\times\Bigg[-4\delta_{\mu\nu}\sigma_B(\vec{k}^2,\widetilde{\omega}_l^2)\Bigg]. \qquad (2.3.22)\end{aligned}$$

As $\left(\delta_{\mu\nu}-\frac{Q_\mu Q_\nu}{Q^2}\right)\delta_{\mu\nu}=3$ and $P_{\mu\nu}^T\delta_{\mu\nu}=2$, Eq. (**??**) becomes

$$\begin{aligned}Tr[I\Sigma(\vec{p},\widetilde{\omega}_n)] &= -\frac{16}{3}T\sum_{l=-\infty}^{\infty}\int\frac{d^3k}{(2\pi)^3}g^2\sigma_B(\vec{k}^2,\widetilde{\omega}_l^2)\\ &\quad\times\left[D^L(\vec{q}^2,\Omega_{nl}^2,m_D^2)+2D^T(\vec{q}^2,\Omega_{nl}^2)\right]. \qquad (2.3.23)\end{aligned}$$

Also,

$$\begin{aligned}Tr[I\Sigma(\vec{p},\widetilde{\omega}_n)] &= Tr[S^-1(\vec{p},\widetilde{\omega}_n)-i\vec{\gamma}\cdot\vec{p}-i\gamma_0\widetilde{\omega}_n-m_c]\\ &= Tr[i\vec{\gamma}\cdot\vec{p}A+i\gamma_0\widetilde{\omega}_nC+B-m_c]\\ &= 4B-4m_c. \qquad (2.3.24)\end{aligned}$$

From Eq. (**??**) and Eq. (**??**), we have

$$\begin{aligned}B(\vec{p}^2,\widetilde{\omega}_n^2) &= m_c+\frac{4}{3}T\sum_{l=-\infty}^{\infty}\int\frac{d^3\vec{k}}{(2\pi)^3}g^2\frac{B(\vec{k}^2,\widetilde{\omega}_l^2)}{\vec{k}^2A^2(\vec{k}^2,\widetilde{\omega}_l^2)+\widetilde{\omega}_l^2C^2(\vec{k}^2,\widetilde{\omega}_l^2)+B^2(\vec{k}^2,\widetilde{\omega}_l^2)}\\ &\quad\times\left[D^L(\vec{q}^2,\Omega_{nl}^2,m_D^2)+2D^T(\vec{q}^2,\Omega_{nl}^2)\right]. \qquad (2.3.25)\end{aligned}$$

The corresponding expression for $A(\vec{p}^2,\widetilde{\omega}_n^2)$ is obtained by multiplying $-i\vec{\gamma}\cdot\vec{p}$ with Eq. (**??**) and taking the trace. We have

$$\begin{aligned} Tr[-i\vec{\gamma}\cdot\vec{p}\Sigma(\vec{p},\widetilde{\omega}_n)] &= \frac{4}{3}T\sum_{l=-\infty}^{\infty}\int\frac{d^3\vec{k}}{(2\pi)^3}g^2\Bigg[\left(\delta_{\mu\nu}-\frac{Q_\mu Q_\nu}{Q^2}\right)D^L(\vec{q}^2,\Omega_{nl}^2,m_D^2) \\ &\quad +P^T_{\mu\nu}(D^T(\vec{q}^2,\Omega_{nl}^2)-D^L(\vec{q},\Omega_{nl}^2,m_D^2))\Bigg] \\ &\quad\times Tr\Bigg[-i\vec{\gamma}\cdot\vec{p}\gamma_\mu\left(i\vec{\gamma}\cdot\vec{k}\sigma_A(\vec{k}^2,\widetilde{\omega}_l^2)+i\gamma_0\widetilde{\omega}_l\sigma_C(\vec{k}^2,\widetilde{\omega}_l^2)-\sigma_B(\vec{k}^2,\widetilde{\omega}_l^2)\right)\gamma_\nu\Bigg]. \end{aligned} \tag{2.3.26}$$

Simplifying Eq. (**??**), we have

$$\begin{aligned} Tr[-i\vec{\gamma}\cdot\vec{p}\Sigma(\vec{p},\widetilde{\omega}_n)] &= -\frac{16}{3}T\sum_{l=-\infty}^{\infty}\int\frac{d^3\vec{k}}{(2\pi)^3}g^2\Bigg[\Bigg[\sigma_A(\vec{k}^2,\widetilde{\omega}_l^2)\Bigg\{(\vec{p}\cdot\vec{k}) \\ &\quad +\frac{2(\vec{p}\cdot\vec{q})(\vec{q}\cdot\vec{k})}{Q^2}-\frac{2(\vec{p}\cdot\vec{q})(\vec{q}\cdot\vec{k})}{\vec{q}^2}\Bigg\} \\ &\quad +\frac{2\Omega_{nl}^2(\vec{p}\cdot\vec{q})}{Q^2}\widetilde{\omega}_l\sigma_C(\vec{k}^2,\widetilde{\omega}_l^2)\Bigg]D^L(\vec{q}^2,\Omega_{nl}^2,m_D^2) \\ &\quad +2\frac{(\vec{p}\cdot\vec{q})(\vec{q}\cdot\vec{k})}{\vec{q}^2}D^T(\vec{q}^2,\Omega_{nl}^2)\sigma_A(\vec{k}^2,\widetilde{\omega}_l^2)\Bigg]. \end{aligned} \tag{2.3.27}$$

As

$$A(\vec{p}^2,\widetilde{\omega}_n^2)=1+\frac{1}{4\vec{p}^2}Tr[-i\vec{\gamma}\cdot\vec{p}\Sigma(\vec{p},\widetilde{\omega}_n)], \tag{2.3.28}$$

using Eq. (**??**) in Eq. (**??**), we have

$$\begin{aligned} A(\vec{p}^2,\widetilde{\omega}_n^2) &= 1-\frac{4T}{3\vec{p}^2}\sum_{l=-\infty}^{\infty}\int\frac{d^3\vec{k}}{(2\pi)^3}g^2\Bigg[\Bigg[\sigma_A(\vec{k}^2,\widetilde{\omega}_l^2)\Bigg\{(\vec{p}\cdot\vec{k}) \\ &\quad +\frac{2(\vec{p}\cdot\vec{q})(\vec{q}\cdot\vec{k})}{Q^2}-\frac{2(\vec{p}\cdot\vec{q})(\vec{q}\cdot\vec{k})}{\vec{q}^2}\Bigg\} \\ &\quad +\frac{2\Omega_{nl}(\vec{p}\cdot\vec{q})}{Q^2}\widetilde{\omega}_l\sigma_C(\vec{k}^2,\widetilde{\omega}_l^2)\Bigg]D^L(\vec{q}^2,\Omega_{nl}^2,m_D^2) \\ &\quad +2\frac{(\vec{p}\cdot\vec{q})(\vec{q}\cdot\vec{k})}{\vec{q}^2}D^T(\vec{q}^2,\Omega_{nl}^2)\sigma_A(\vec{k}^2,\widetilde{\omega}_l^2)\Bigg]. \end{aligned} \tag{2.3.29}$$

The function $A(\vec{p}^2,\widetilde{\omega}_n^2)$ corresponds to the spatial part of the quark wavefunction renormalization function and $A(\vec{p}^2,\widetilde{\omega}_n^2)\to 1$ in the perturbative region. Next, multiplying $-i\gamma_0$ by Eq. (**??**) and taking trace,

$$\begin{aligned} Tr[-i\gamma_0\Sigma(\vec{p},\widetilde{\omega}_n)] &= \frac{4}{3}T\sum_{l=-\infty}^{\infty}\int\frac{d^3\vec{k}}{(2\pi)^3}g^2\Bigg[\left(\delta_{\mu\nu}-\frac{Q_\mu Q_\nu}{Q^2}\right)D^L(\vec{q},\Omega_{nl}^2,m_D^2) \\ &\quad +P_{\mu\nu}^T\left(D^T(\vec{q}^2,\Omega_{nl}^2)-D_L(\vec{q}^2,\Omega_{nl}^2,m_D^2)\right)\Bigg] \\ &\quad \times Tr\Bigg[-i\gamma_0\gamma_\mu\left(i\vec{\gamma}\cdot\vec{k}\sigma_A(\vec{k}^2,\widetilde{\omega}_l^2)+i\gamma_0\widetilde{\omega}_l\sigma_C(\vec{k}^2,\widetilde{\omega}_l^2)-\sigma_B(\vec{k}^2,\widetilde{\omega}_l^2)\right)\gamma_\nu\Bigg]. \end{aligned} \tag{2.3.30}$$

On simplifying, we get

$$\begin{aligned} Tr[-i\gamma_0\Sigma(\vec{p},\widetilde{\omega}_n)] &= -\frac{16}{3}T\sum_{l=-\infty}^{\infty}\int\frac{d^3\vec{k}}{(2\pi)^3}\frac{g^2}{Q^2}\Bigg[\Bigg\{2\sigma_A(\vec{k}^2,\widetilde{\omega}_l^2)(\vec{q}\cdot\vec{k})\Omega_{nl} \\ &\quad +\left(-Q^2+2\Omega_{nl}^2\right)\widetilde{\omega}_l\sigma_C(\vec{k}^2,\widetilde{\omega}_l^2)\Bigg\}D^L(\vec{q}^2,\Omega_{nl}^2,m_D^2) \\ &\quad +2Q^2\sigma_C(\vec{k}^2,\widetilde{\omega}_l^2)\widetilde{\omega}_l D^T(\vec{q}^2,\Omega_{nl}^2)\Bigg]. \end{aligned} \tag{2.3.31}$$

As

$$C(\vec{p}^2,\widetilde{\omega}_n^2)=1+\frac{1}{4\widetilde{\omega}_n}Tr[-i\gamma_0\Sigma(\vec{p},\widetilde{\omega}_n)], \tag{2.3.32}$$

inserting Eq. (**??**) into Eq. (**??**), we have

$$\begin{aligned} C(\vec{p}^2,\widetilde{\omega}_n^2) &= 1-\frac{4}{3\widetilde{\omega}_n}T\sum_{l=-\infty}^{\infty}\int\frac{d^3\vec{k}}{(2\pi)^3}\frac{g^2}{Q^2}\Bigg[\Bigg\{2\sigma_A(\vec{k}^2,\widetilde{\omega}_l^2)(\vec{q}\cdot\vec{k})\Omega_{nl}+ \\ &\quad (-Q^2+2\Omega_{nl}^2)\widetilde{\omega}_l\sigma_C(\vec{k}^2,\widetilde{\omega}_l^2)\Bigg\}D^L(\vec{q}^2,\Omega_{nl}^2,m_D^2) \\ &\quad +2Q^2\sigma_C(\vec{k}^2,\widetilde{\omega}_l^2)\widetilde{\omega}_l D^T(\vec{q}^2,\Omega_{nl}^2)\Bigg]. \end{aligned} \tag{2.3.33}$$

$C(\vec{p}^2,\widetilde{\omega}_n^2)$ corresponds to the temporal part of the quark wavefunction renormalization function and $C(\vec{p}^2,\widetilde{\omega}_n^2)\to 1$ at high momentum.

At finite temperature and density, the chiral quark condensate is defined as

$$\begin{aligned} -\langle\bar{\psi}\psi\rangle &= N_c T r T \sum_n \int \frac{d^3p}{(2\pi)^3}[S(\vec{p},\widetilde{\omega}_n)], \\ &= 4N_c T \sum_n \int \frac{d^3p}{(2\pi)^3}[-\sigma_B(\vec{p}^2,\widetilde{\omega}_n^2)]. \end{aligned} \tag{2.3.34}$$

Performing the angular integration,

$$-\langle\bar{\psi}\psi\rangle = \frac{2N_c T}{\pi^2} \sum_n \int_0^\infty dp p^2[-\sigma_B(\vec{p}^2,\widetilde{\omega}_n^2)]. \tag{2.3.35}$$

In the next section we use the constant mass approximation where we only take into account the B equation Eq. (**??**) to study the QCD phase diagram.

2.4 CMA and QCD Phase diagram

CMA is compatible with the observation that the kernel of the gap equation at finite temperature and density yields only a significant contribution from the small momentum region for every Matsubara frequency, where the scalar functions A, B and C are roughly constants. Furthermore, because the kernel is strongly suppressed at high momentum, we can approximate the solution to the gap equation by momentum independent functions for every $\tilde{\omega}_n$. Recalling that the mass function for the quark is

$$M(\vec{p}^2,\tilde{\omega}_n^2) = \frac{B(\vec{p}^2,\tilde{\omega}_n^2)}{A(\vec{p}^2,\tilde{\omega}_n^2)}, \tag{2.4.1}$$

our starting point is Eq. (**??**),

$$\begin{aligned} B(\vec{p}^2,\widetilde{\omega}_n^2) &= m_c + \frac{4}{3}T \sum_{l=-\infty}^{\infty} \int \frac{d^3\vec{k}}{(2\pi)^3} \frac{B(\vec{k}^2,\widetilde{\omega}_l^2)}{\vec{k}^2 A^2(\vec{k}^2,\widetilde{\omega}_l^2) + \tilde{\omega}_l^2 C^2(\vec{k}^2,\widetilde{\omega}_l^2) + B^2(\vec{k}^2,\widetilde{\omega}_l^2)} \\ &\quad \times \left[g^2 D^L(\vec{q}^2,\Omega_{nl}^2,m_D^2) + 2g^2 D^T(\vec{q}^2,\Omega_{nl}^2)\right]. \end{aligned} \tag{2.4.2}$$

The CMA consists of several steps, which we enlist below:

Step-1: We set $A(\vec{k}^2,\tilde{\omega}_l^2) = C(\vec{k}^2,\tilde{\omega}_l^2) = 1$ and $B(\vec{p}^2,\tilde{\omega}_n^2) = M(\vec{p}^2,\tilde{\omega}_n^2)$. Thus

$$\begin{aligned} M(\vec{p}^2,\widetilde{\omega}_n^2) &= m_c + \frac{4}{3}T \sum_{l=-\infty}^{\infty} \int \frac{d^3\vec{k}}{(2\pi)^3} \frac{M(\vec{k}^2,\widetilde{\omega}_l^2)}{\vec{k}^2 + \tilde{\omega}_l^2 + M^2(\vec{k}^2,\widetilde{\omega}_l^2)} \\ &\quad \times \left[g^2 D^L(\vec{q}^2,\Omega_{nl}^2,m_D^2) + 2g^2 D^T(\vec{q}^2,\Omega_{nl}^2)\right]. \end{aligned} \tag{2.4.3}$$

Step-2: We take $\vec{p}=0$, and in the kernel we also take $M(\vec{k}^2,\tilde{\omega}_l^2)=M(0,\tilde{\omega}_l^2)$. Then, replacing $M(0,\tilde{\omega}_n^2)=M(\tilde{w}_n^2)$, we have the following tower of relations of constant masses for every Matsubara frequency

$$\begin{aligned} M(\widetilde{\omega}_n^2) &= m_c+\frac{4}{3}T\sum_{l=-\infty}^{\infty}\int\frac{d^3\vec{k}}{(2\pi)^3}\frac{M(\widetilde{\omega}_l^2)}{\vec{k}^2+\tilde{\omega}_l^2+M^2(\widetilde{\omega}_l^2)} \\ &\quad\times\left[g^2D^L(\vec{k}^2,\Omega_{nl}^2,m_D^2)+2g^2D^T(\vec{k}^2,\Omega_{nl}^2)\right]. \end{aligned} \tag{2.4.4}$$

Performing the angular integration, we have

$$\begin{aligned} M(\tilde{\omega}_n^2) &= m_c+\frac{2T}{\pi^2}\sum_{l=-\infty}^{\infty}\int_0^{\Lambda^2}dk\vec{k}^2\frac{M(\tilde{\omega}_l^2)}{\vec{k}^2+\tilde{\omega}_l^2+M^2(\tilde{\omega}_l^2)} \\ &\quad\times\left[g^2D^L(\vec{k}^2,\Omega_{nl}^2,m_D^2)+2g^2D^T(\vec{k}^2,\Omega_{nl}^2)\right]. \end{aligned} \tag{2.4.5}$$

Step-3: We calculate the condensate, which in this case can be written as

$$-\langle\bar{\psi}\psi\rangle=\frac{2N_cT}{\pi^2}\sum_{l=-\infty}^{\infty}\int_0^{\Lambda^2}dk\vec{k}^2\frac{M(\tilde{\omega}_l^2)}{\vec{k}^2+\tilde{\omega}_l^2+M^2(\tilde{\omega}_l^2)}. \tag{2.4.6}$$

In all the above, Λ is the ultraviolet cut-off. We use $\Lambda=1$ GeV throughout of our calculation in this Chapter.

2.4.1 CMA gap equation kernel at finite T

We promote the same gap equation kernel (of Section 2.2) at finite temperature T. The only difference is the that the gluon propagator has now transverse and longitudinal parts due to the heat bath, which are given by

$$[g^2D^T(\vec{k}^2,\Omega_{nl}^2)]\Gamma_\nu(\vec{k},\tilde{\omega}_l,\tilde{\omega}_n)=\zeta(T)g_{eff}^2(\vec{k}^2,\Omega_{nl}^2)D^T(\vec{k}^2,\Omega_{nl}^2)\gamma_\nu,$$

$$[g^2D^L(\vec{k}^2,\Omega_{nl}^2)]\Gamma_\nu(\vec{k},\tilde{\omega}_l,\tilde{\omega}_n)=\zeta(T)g_{eff}^2(\vec{k}^2,\Omega_{nl}^2)D^L(\vec{k}^2,\Omega_{nl}^2,m_D^2)\gamma_\nu. \tag{2.4.7}$$

The parameter $\zeta(T)$ is deduced so as to reproduce the lattice results for the temperature dependent quark-antiquark condensate quoted by *Bazavov et. al.,* Ref. [**?**]. The self-consistent

solution of the coupled equations with a current quark mass $m_c = 3.5$ MeV, subsequently yields the quark propagator with the form of the function $\zeta(T)$,

$$\zeta(T) = \frac{a_1 + b_1 T + c_1 T^2}{1 + d_1 T + e_1 T^2 + f_1 T^3}, \tag{2.4.8}$$

where $a_1 = 0.355$, $b_1 = -2.83$, $c_1 = 6.627$, $d_1 = -6.74$, $e_1 = 4.45$ and $f_1 = 43.35$ with appropriate mass dimensions in GeV. Lattice data is sufficiently well reproduced at zero chemical potential as shown in Fig. **??**, *left panel*. From the behavior of the condensate, one can draw the curve corresponding thermal gradient of the condensate $-\partial_T \langle\bar{\psi}\psi\rangle^{1/3}$, for which its maximum yields a pseudo-critical temperature of $T_c \approx 0.164\,\text{GeV}$, see Fig. **??**, *right panel* (compare it with $T_c = 0.154\,\text{GeV}$ reported in Ref. [**?**] and also reported in [**?**].

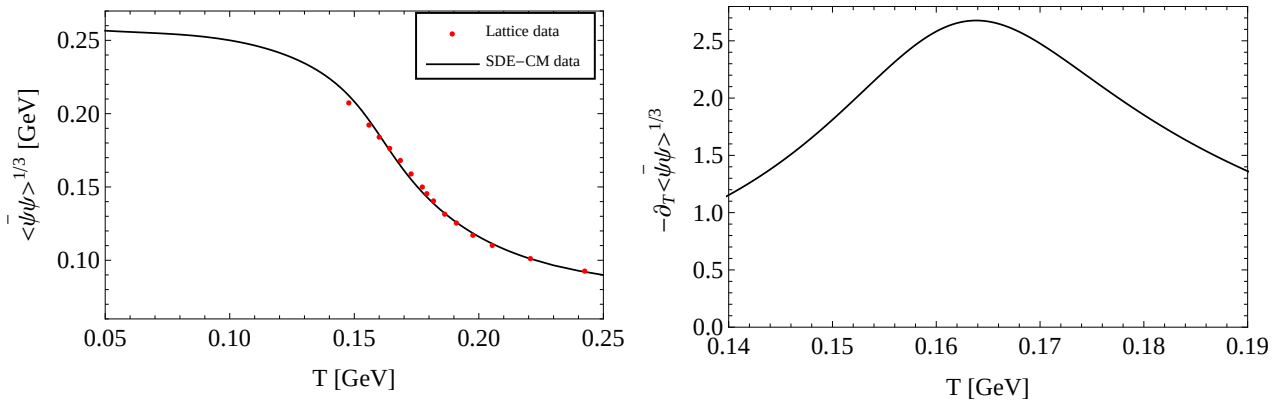

Figure 2.8: *Left panel*: Chiral condensate from CMA (solid black curve) fitted with the lattice data [**?**] (red dots). *Right panel*: Thermal gradient of the condensate -$\partial_T \langle\bar{\psi}\psi\rangle^{1/3}$ calculated from the CMA for $\zeta(T)$ given by Eq. (**??**) as a function of temperature. Its maximum is located at $T_c \sim 0.164$ GeV.

2.4.2 Finite temperature and density

Her we promote the gap equation at finite T and μ, it should be noted that we just taking into introduced chemical potential in the definition of the Debye mass in the longitudinal part of the gluon propagator i.e., $m_D^2 = g^2\left((4/3)T^2 + \mu^2/\pi^2\right)$, and leave the function $\zeta(T)$ and the vertex as an independent of μ. It is due to lack of information about the μ -dependent vertex in the literature. Though in the quark propagator the chemical potentail is included through the definition of Matsubara frequencies $\tilde{\omega}_n = (2n+1)\pi T + i\mu$. With the above mentioned assumption the gap equation solved numerically at finite T and μ. The chiral

condensate at finite temperature T and chemical potential μ is shown in Fig. **??**, *left panel*. When the chemical potential μ increases, a discontinuity starts around the region where the pseudo-critical temperature is located. The slope of the curve drops dramatically near chemical potential $\mu = 70.5$ MeV, as shown in Fig. **??** *left panel*–. This is an likely indicator of a physical effect. The thermal gradient of chiral condensate for different values of μ to locate the critical end point is plotted in Fig. **??**, *right panel*. It is obvious from Fig. **??**, *right panel*, that plots become narrower for increasing μ and suddenly tend to infinity approximately at $\mu = 0.705$ GeV. We identify the chemical potential corresponding to the position of the critical end point at $\mu_E = 0.0705$ GeV, and the corresponding critical end point temperature is $T_E = 0.124$ GeV . The transition is a cross-over before and after this point becomes first-order. The phase diagram plotted in $\mu - T$ plane is shown in Fig. **??**, *left panel* and a zoom is plotted Fig. **??**, *right panel*. We again used $T_c(\mu) = T_c(0) + a\mu^2$ fit near the $\mu = 0$ axis. In this case, our numerical accuracy allows us to extract results only until around μ =0.08-0.1 GeV. An extrapolation of our fit for intermediate values of μ to $T \sim 0$ region yields $\mu_E \sim 0.14$ GeV for chiral symmetry restoration. We again extrapolated the dots to achieve the Clausius-Clapeyron condition as already done in our previous Chapter.

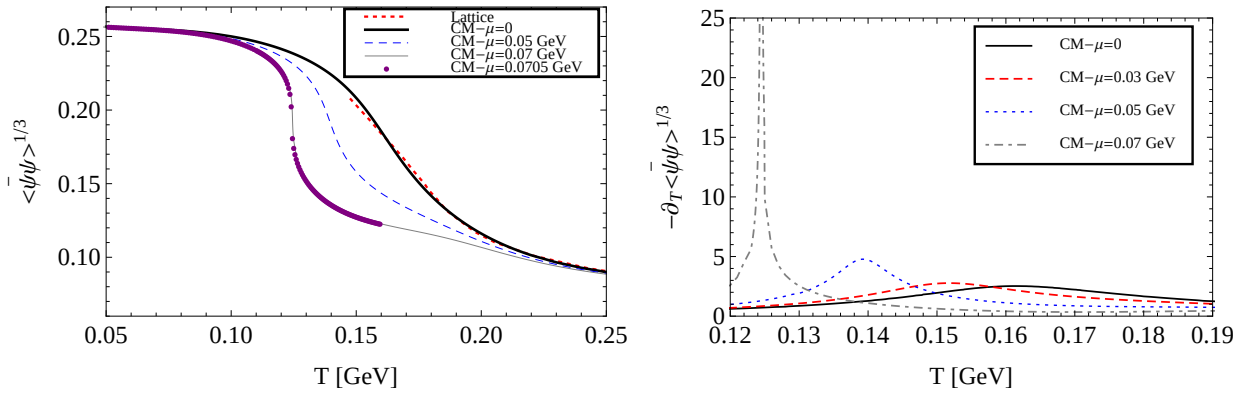

Figure 2.9: *Left panel*: Condensate for different values of μ as a function of temperature. For large μ, the curve develops a discontinuity which becomes more and more marked for increasing values of μ. *Right panel*: -$\partial_T \langle\bar{\psi}\psi\rangle^{1/3}$ as a function of temperature for different values of μ. The peak gives the critical point (μ_E, T_E). Note that the height of this thermodynamic variable shoots up to infinity for a sufficiently large μ, indicating a change in the order of phase transition.

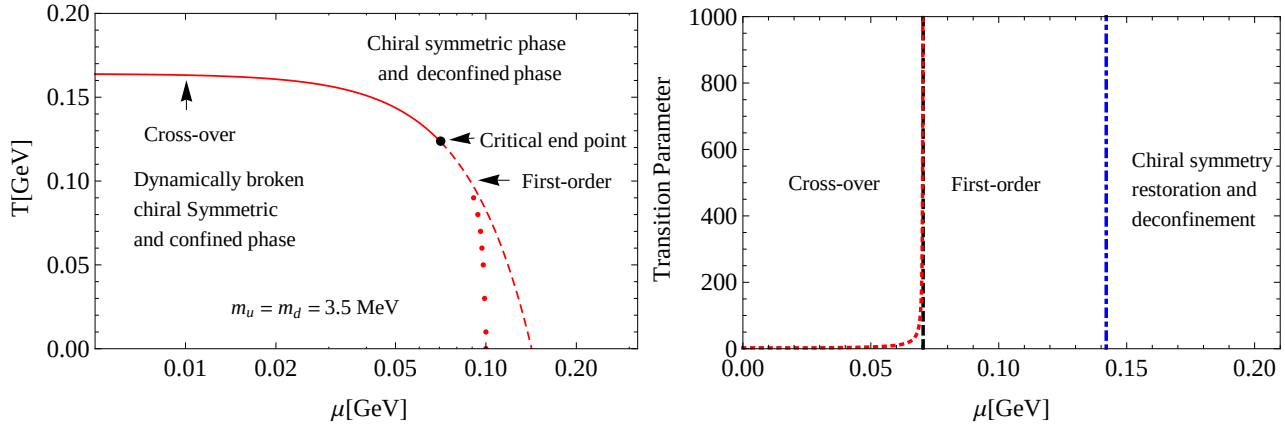

Figure 2.10: *Left panel*: QCD phase diagram for chiral symmetry breaking/restoration and confinement/deconfinement indicating the critical end point which corresponds to $\mu_E \approx 0.0705$ GeV and $T_E \approx 0.124$ GeV. Near $\mu = 0$, the curve corresponding to chiral symmetry restoration/deconfinement can be fitted with a quadratic expression $T_c(\mu) = T_c(0) + a\mu^2$, with $T_c(0) = 0.164$ GeV and $a = -8.133$ GeV^{-1}. *Right panel*: Behavior of transition parameters as a function of the chemical potential μ that shows where the different transitions occur. From $\mu = 0$ to the vertical black-dashed line at $\mu_E \approx 0.0705$ GeV, the transition is a cross-over. After the black-dashed line, phase transition is of first order. Chiral symmetry broken and confinement continues above $\mu_E \approx 0.0705$ GeV and appears to be restored at $\mu \approx$ 0.14 GeV, represented by a vertical blue-dot-dashed line.

2.5 Confinement

A special case of Schwinger function to test confinement (see Appendix A) with constant masses was considered in Ref. [**?**]. It is given by

$$\Delta(\tau) = T \sum_n e^{-i\tilde{\omega}_n \tau} \frac{M(\tilde{\omega}_n^2)}{\tilde{\omega}_n^2 + M^2(\tilde{\omega}_n^2)}. \tag{2.5.1}$$

According to the axiom of reflection positivity, if $\Delta(\tau)$ is positive for all τ i.e., $\Delta(\tau) \geq 0$, then the particle is stable, otherwise is confined. We use the above Schwinger function to define an order parameter for the confinement phase transition, which has been discussed in detail in Ref. [**?**]. $\Delta(\tau)$ as a function of τ at different T and $\mu = 0$ is shown in Fig. **??**, *left panel*. At low T, it oscillates with high amplitude, which is a signal of confinement, while with growing T, the amplitude becomes smaller and goes to zero approaching T_c, hence signalling deconfinement. The amplitude of $\Delta(\tau)$ at $\tau = 0$, that is $|\Delta(0)|$, at different T and $\mu = 0$ is plotted in Fig. **??**,

right panel. We observe the pseudo-critical temperature for the confinement-deconfinement phase transition around $T_c \sim 0.16$ GeV (which coincides with the chiral symmetry breaking temperature) by taking the thermal gradient $\partial_T|\Delta(0)|$. The inverse of the value of τ at which the first crossing occurs in $\Delta(\tau)$ from positive to negative value has been taken as the order parameter for confinement in Ref. [**?**]. The parameter we introduced here implies that the CMA gives a propagator with an analytic structure compatible with chiral symmetry breaking and confinement. Similar behavior of this parameter is valid for $\mu \neq 0$, and thus the phase diagram is basically the same as for chiral symmetry breaking as shown in Fig. **??**, *left panel*.

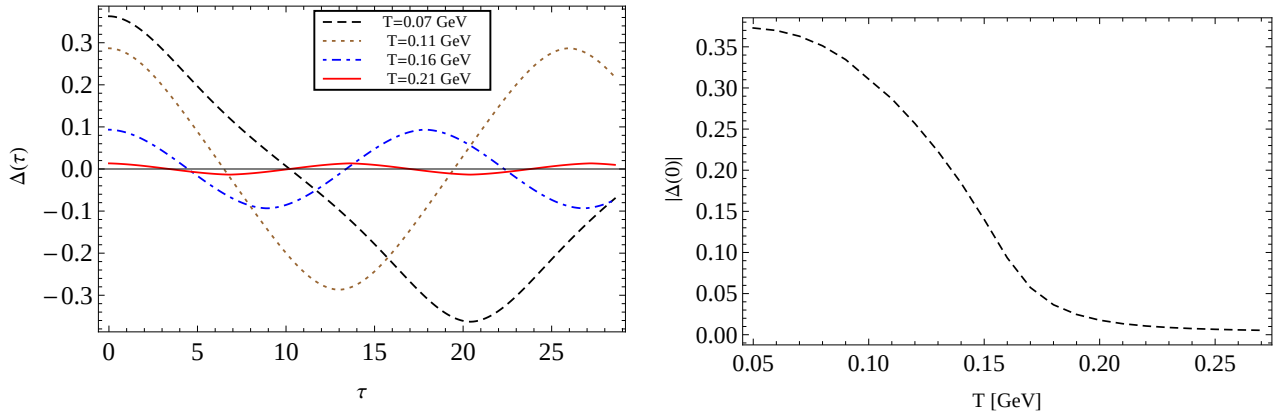

Figure 2.11: *Left panel*: $\Delta(\tau)$ at different temperatures T as a function of τ. At low T, it oscillates with high amplitude and hence signals confinement, while at high T, the amplitude becomes smaller and goes to zero, which implies deconfinement. *Right panel*: Amplitude of the $\Delta(0)$ as a function of T: At $T > T_c \approx 0.160$ GeV, the amplitude goes to zero.

2.6 Discussion

In this Chapter we used the CMA to study the QCD phase diagram. In this approximation, we took into account only the B-equation which is related to the quark mass function for the propagator and set $\vec{p} = 0$. Our kernel includes a thermal effective coupling and a flavor ($N_f = 2$) dependent thermal gluon propagator. The idea behind this approximation is to understand how the temperature and chemical potential affect the dynamical quark mass at zero momentum. We used the lattice results at finite temperature and fitted the quark-antiquark condensate accordingly [**?**]. We then took the thermal gradient of the chiral condensate to obtain the pseudo-critical temperature for the chiral symmetry breaking-restoration transition and it came out to be $T_c = 164$ MeV. The critical temperature for the confinement-deconfinement

phase transition was obtained from the "spatially averaged Schwinger function", where we took the thermal gradient of the amplitude of the oscillations of the said function at different temperatures, which coincides with the one we obtained for the chiral symmetry breaking-restoration phase transition. We included the chemical potential and observed that at $\mu = 70.5$ MeV, the chiral condensate shoot up to infinity where the first order phase transition started and finally sketched the phase diagram. The critical end point (from cross-over to first order) in this case is located at ($\mu_E/T_c = 0.42,\ T_E/T_c = 0.8$). Since along the $\mu = 0$ axis lattice results are regarded as a reliable representation of a theory in the continuum, it is natural to make comparisons between lattice and SDE approaches. Since our results agree with the lattice at $\mu = 0$-axis and as a consequence our CMA, $T_E/T_c = 0.8$ agrees with SDE–Maris-Tandy prediction [**?**, **?**] where I participated as co-author. At finite μ, ($\mu_E/T_c = 0.42$) is two times less than SDE prediction [**?**] and three times less than [**?**]. This may be due to the the fact our function $\zeta(T)$ in Eq. (**??**) and the full quark-gluon vertex $\Gamma_\nu(\vec{q}, \tilde{w}_l, \vec{p}, \tilde{w}_n)$ were taken to be independent of μ, but they surely depend on this parameter and a different choice of these quantities may change the position of the critical end point. On the other hand, the C equation Eq. (**??**) may be effect the position of the critical end point. An important feature of the CMA is that we are dealing with static (in momentum) quarks, but the virtual gluons are momentum and temperature dependent. Thus the thermal fluctuations dress the valence quarks and make them behave as massive and confined inside the hadrons.

In the next Chapter we use the confining vector-vector contact interaction model [**?**, **?**], which is based on the proper-time regularization [**?**] of the Nambu–Jona-Lasinio (NJL) model to study the gap equation at zero and finite temperature and density. The gluon dressing function and the coupling are taken to be independent of momentum, which ensures that the gap equation solution exhibits this feature too. We use the dual quark condensate [**?**] and the confining scale to test the confinement-deconfinement phase transition.

Chapter 3

QCD Phase Diagram from Contact Interaction Model for quarks

In this Chapter, we use a confining variant of the NJL model regularized within a proper-time scheme [**?**] to study QCD phase transitions at finite temperature and density. This vector-vector contact interaction (CI) model has been successfully used to reproduce hadronic static properties of pions and other low energy mesons and baryons in vacuum [**?**, **?**]. Extensions of this model at finite temperature [**?**] or density [**?**] have already been considered. We proceed to embed this interaction in a rainbow-ladder truncation of the gap equation with two considerations: in a first case, we use the ratio of the coupling constant to the gluon mass scale as independent of the temperature, and in a second case, as a function of T. Confinement in this model is implemented through a proper-time regularization with two cut-offs, infra-red and ultra-violet. This procedure ensures the absence of real as well as complex poles in the quark propagator. The infra-red cut-off corresponds to the confinement scale whereas the ultra-violet cut-off plays a dynamical role due to the non-renormalizability of the model. The pole-less structure of the quark propagator corresponds to the absence of quark production thresholds and it is another analytic form consistent with quark confinement [**?**]; an excitation described by a pole-less propagator would never reach its mass-shell.
We use the thermal gradient of the chiral condensate to observe the transition temperature for chiral symmetry breaking-restoration. For the confinement-deconfinement phase transition, we use the dual condensate [**?**], which is the Fourier transform of the conventional chiral quark condensate evaluated at a dual angle (see discussion below) and the confining length scale, which we consider as temperature dependent and slightly different to the one proposed in [**?**]. We solve the gap equation with a temperature dependent effective coupling and infra-red cut-off. In previous Chapters we discussed only the single and stable solution of the gap equation which supports dynamical chiral symmetry breaking. Here we also discuss multiple solutions to the gap equation [**?**, **?**], though we focus on the stable one to explore the chiral symmetry

breaking-restoration and confinement-deconfinement phase transitions. At the end we discuss the QCD phase diagram. Part of this Chapter is based on our work published in Ref. [**?**]. The rest will be presented elsewhere [**?**].

3.1 Gap equation and CI at zero temperature

It has been shown in a series of articles at zero temperature that the static properties of low energy mesons and baryons can be faithfully reproduced by assuming that quarks interact not via massless vector-boson exchange but instead through the following contact interaction [**?**, **?**] as shown in Fig.**??**:

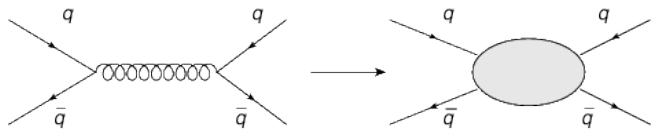

Figure 3.1: *Left side*: One gluon exchange four fermion interaction. *Right side*: Four fermion contact interaction.

Mathematically,

$$g^2\Delta_{\mu\nu}(q) = \delta_{\mu\nu}\frac{4\pi\alpha_{\rm IR}}{m_G^2} \equiv \delta_{\mu\nu}\alpha_{\rm eff}(0), \tag{3.1.1}$$

where $m_G = 800$ MeV is a gluon mass scale which is in fact generated dynamically in QCD [**?**] and $\alpha_{\rm IR} = 0.93\pi$ specifies the interaction strength in the infra-red. We then proceed to embed this interaction in a rainbow-ladder truncation of the gap equation, Eq. (**??**), and solve it consistently through the simultaneous equations

$$B(p^2) = m_c + \frac{16\alpha_{\rm eff}(0)}{3}\int\frac{d^4k}{(2\pi)^4}\frac{B(k^2)}{k^2A^2(k^2)+B^2(k^2)} \tag{3.1.2}$$

and

$$A(p^2) \;=\; 1 + \frac{4\alpha_{\rm eff}(0)}{3p^2}\int\frac{d^4k}{(2\pi)^4}\frac{(p\cdot k)A(k^2)}{k^2A^2(k^2)+B^2(k^2)}. \tag{3.1.3}$$

Performing the angular integration,

$$\int d^4k \;=\; \frac{1}{2}\int_0^\infty k^2dk^2\int_0^{2\pi}d\psi(=2\pi)\int_0^\pi d\theta\sin^2\theta\int_0^\pi d\phi\sin\phi(=2) \tag{3.1.4}$$

$$\;=\; 2\pi\int_0^{\Lambda^2}k^2dk^2\int_0^\pi d\theta\sin^2\theta, \tag{3.1.5}$$

we notice that

$$\int d^4k(p\cdot k) = 0. \tag{3.1.6}$$

Thus, the wavefunction renormalization $A(p^2) = 1$, and the quark mass function become momentum independent, i.e., $B(p^2) = M$, a constant which we determine self-consistently through

$$M = m_c + \frac{\alpha_{\rm eff}(0)M}{3\pi^2}\int_0^\infty ds \frac{s}{s+M^2}\,, \tag{3.1.7}$$

with $s = k^2$. We now exponentiate the denominator inside the integral and employ the confining proper-time regularization,

$$\frac{1}{s+M^2} = \int_0^\infty d\tau {\rm e}^{-\tau(s+M^2)} \to \int_{\tau_{uv}^2}^{\tau_{ir}^2} d\tau {\rm e}^{-\tau(s+M^2)} = \frac{{\rm e}^{-\tau_{uv}^2(s+M^2)} - {\rm e}^{-\tau_{ir}^2(s+M^2)}}{s+M^2}\,. \tag{3.1.8}$$

Here, $\tau_{ir,uv}^{-1} = \Lambda_{ir,uv}$ are respectively, the infra-red and ultra-violet regulators. This procedure ensures the absence of real as well as complex poles in the quark propagator. The gap equation can now be written as

$$M \;\; = \;\; m_c + \frac{M^3\alpha_{\rm eff}(0)}{3\pi^2}\left[\Gamma(-1, M^2\tau_{uv}^2) - \Gamma(-1, M^2\tau_{ir}^2)\right]\,, \tag{3.1.9}$$

where

$$\Gamma(\alpha, x) = \int_x^\infty t^{\alpha-1}{\rm e}^{-t}dt$$

is the incomplete Gamma function. We use the parameters of Ref. [**?**], namely,

$$\alpha_{\rm eff}(0) = 5.739\times 10^{-5}\ {\rm MeV}^{-2}\,, \tag{3.1.10}$$

$$\tau_{ir} = (240\ {\rm MeV})^{-1}\,, \tag{3.1.11}$$

$$\tau_{uv} = (905\ {\rm MeV})^{-1}\,, \tag{3.1.12}$$

which have been fitted to vacuum properties in the pion and rho-meson sector. With these parameters, considering a current quark mass $m_c = 7$ MeV, the constituent quark mass and the chiral condensate per flavor are calculated to be $M = 367$ MeV and $\langle\bar{u}u\rangle^{1/3} = \langle\bar{d}d\rangle^{1/3} = -243$ MeV, respectively.

3.2 Finite temperature

At finite temperature, the gap equation in the CI-model becomes[1]

$$M = m + \frac{16\alpha_{\rm eff}(0)}{3} T \sum_{l=-\infty}^{\infty} \int \frac{d^3\vec{k}}{(2\pi)^3} \frac{M}{\vec{k}^2 + \omega_l^2 + M^2}, \tag{3.2.1}$$

where $\omega_l = (2l+1)\pi T$ are the fermionic Matsubara frequencies. This equation and some of its variants have been discussed in several works [**?**]. For our purposes, we regularize the integrals by exponentiating the denominator for each ω_l, i.e.,

$$\frac{1}{\vec{k}^2 + \omega_l^2 + M^2} \longrightarrow \int_{\tau_{uv}^2}^{\tau_{ir}^2} d\tau {\rm e}^{-\tau(\vec{k}^2+\omega_l^2+M^2)}. \tag{3.2.2}$$

Inserting Eq.(**??**) in Eq.(**??**) and performing the angular integrations, we have

$$M = m_c + \frac{8M\alpha_{\rm eff}(0)}{3\pi^2} T \sum_{l=-\infty}^{\infty} \int_{\tau_{uv}^2}^{\tau_{ir}^2} d\tau \int_0^{\infty} d\vec{k}\vec{k}^2 {\rm e}^{-\tau(\vec{k}^2+\omega_l^2+M^2)}. \tag{3.2.3}$$

We use that

$$\int_0^{\infty} d\vec{k}\vec{k}^2 e^{-\tau\vec{k}^2} = \frac{\sqrt{\pi}}{4\tau^{3/2}}, \qquad \sum_{l=-\infty}^{\infty} e^{-\tau\omega_l^2} = \Theta_2(0, e^{-4\pi^2\tau T^2}). \tag{3.2.4}$$

We introduce a temperature dependent infra-red cut-off (confinig length scale) in the gap equation in the form

$$M \;\; = \;\; m_c + \frac{2M\alpha_{eff}(0)T}{3\pi^{3/2}} \int_{\tau_{uv}^2}^{\tilde{\tau}_{ir}} d\tau \frac{{\rm e}^{-M^2\tau}\Theta_2(0, {\rm e}^{-4\pi^2T^2\tau})}{\tau^{3/2}}, \tag{3.2.5}$$

where

$$\tilde{\tau}_{ir} = \tau_{ir}(T) = \tau_{ir}\frac{M(0)}{M(T)}, \tag{3.2.6}$$

with $M(0)$ the dynamical mass at $T = 0$, and $M(T)$ the dynamical mass at finite temperature. In the chiral limit, at the critical temperature T_c, $M(T) = 0$ and $\tilde{\tau}_{ir} \to \infty$. This ensures that

[1]The self-consistent solution of the gap equation yields $A = 1$ (odd integrand) and $C = 1$ after proper time regularization when $\sum_{l=-\infty}^{\infty} \omega_l e^{-\tau\omega_l^2} = \frac{-1}{2\tau}\Theta_2'(0, e^{-4\pi^2\tau T^2}) = 0$. Here $\Theta_2(x, y)$ is the second Jacobi theta function. The prime on it represent the first derivative w.r.t. y.

the chiral symmetry restoration and deconfinement take place at the same T_c. Once the quark propagator is known, one can calculate the order parameter for dynamical chiral symmetry breaking, namely, the quark-antiquark condensate that comes from the trace of the quark propagator,

$$-\langle\psi\bar{\psi}\rangle = \frac{3MT}{2\pi^{3/2}}\int_{\tau_{uv}^2}^{\tilde{\tau}_{ir}} d\tau \frac{\mathrm{e}^{-M^2\tau}\Theta_2(0,\mathrm{e}^{-4\pi^2T^2\tau})}{\tau^{3/2}}. \tag{3.2.7}$$

In the next sections we the solve gap equation, Eq. (**??**), and derive the condensate, Eq. (**??**) numerically.

3.3 Chiral symmetry breaking-restoration

In previous Chapters, we only referred to the stable solutions of the gap equation to find the critical temperature for the chiral symmetry breaking-restoration transition. Here we also discuss some other solutions of the gap equation at finite temperature. In literature [**?**], these solutions have been named positive Nambu mode N^+, negative Nambu mode N^- and Wigner mode W. The multiple solutions of the gap equation Eq. (**??**) at finite T are shown in Fig. **??**, *left panel*, in chiral the limit and in Fig.**??**, *right panel*, with a current quark mass $m_c = 7$ MeV. The quark-antiquark condensate $\langle\bar{\psi}\psi\rangle_{N^+}^{1/3}$ in the chiral limit is shown in Fig. **??**, *left panel*, and its thermal gradient $-\partial_T\langle\bar{\psi}\psi\rangle_{N^+}^{1/3}$ is depicted in Fig. **??**, *right panel*. The temperature at which the thermal gradient of the chiral condensate diverges is the critical temperature for the chiral symmetry restoration, which occurs at $T_c \approx 216$ MeV. At low temperatures, the quark condensate has a finite value for both positive-mode N^+ and negative-mode N^- solutions, which are related to the chiral symmetry breaking. For the W-mode solution, that corresponds to chirally symmetric phase, the chiral condensate has zero value from low to high temperatures. All the three solutions vanish at the temperature $T_c \approx 216$ MeV, and the phase transition in this case is of second order.

However, for a finite light bare quark mass $m_c = 7$ MeV, the second order phase transition changes to a smooth cross-over as depicted in Fig. **??**, *left panel*. Current quark mass causes to break explicitly the chiral symmetry, which can be viewed from the W-mode solution; it is now negative as compared to case of the chiral limit. The W and N^- solutions combine at $T \approx 197$ MeV and then merge to N^+ to become a single solution. The temperature at which all the three modes merge to one can be obtained through the thermal gradient of the chiral condensate $-\partial_T\langle\bar{\psi}\psi\rangle_{N^+}^{1/3}$ as shown in Fig. **??**, *right panel*, which peaks at $T_c \approx 225$ MeV, pointing out the critical temperature for the chiral symmetry restoration in agreement with Ref. [**?**].

Though this value is about 30% higher than the one reported by the lattice-regularized QCD studies [**?**], it is easily understandable because we work with a constant interaction

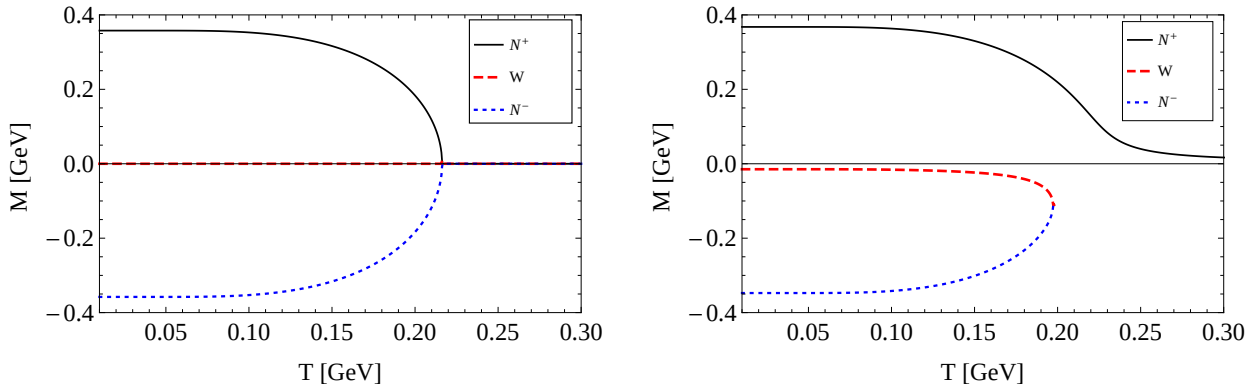

Figure 3.2: *Left panel*: Solutions of the gap equation Eq. (**??**) for the dynamical mass in the chiral limit. *Right panel*: With a current quark mass $m_c = 7$ MeV.

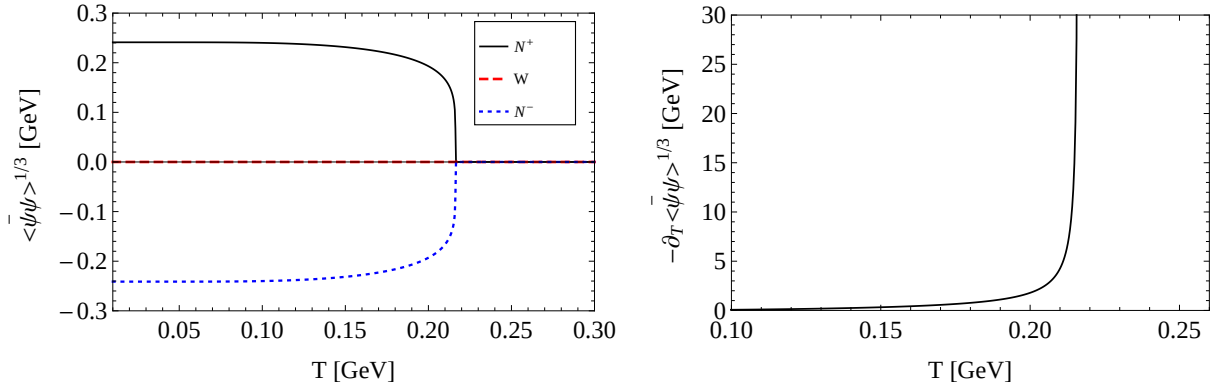

Figure 3.3: *Left panel*: Multiple-modes of the chiral condensate Eq.(**??**) $\langle\bar{\psi}\psi\rangle^{1/3}_{N^+,N^-,W}$ in the chiral limit. *Right panel*: Thermal gradient of the condensate $-\partial_T\langle\bar{\psi}\psi\rangle^{1/3}_{N^+}$, which diverges at $T_c \approx 216$ MeV.

strength $\alpha_{\rm IR}$ and gluon mass scale m_G. In fact, as the temperature increases, interactions are screened, a phenomenon which effectively presents itself as a decrease in $\alpha_{\rm IR}$ and increase in m_G with temperature. This deficiency of the model can be remedied by a simple proposal for the temperature dependence of $\alpha_{\rm IR}/m_G^2$ as we shall see in a subsequent section. For the the confinement-deconfimenet phase transition, we use the confining length scale as a function of temperature and the dual condensate or dressed Polykov loop, which we discuss next.

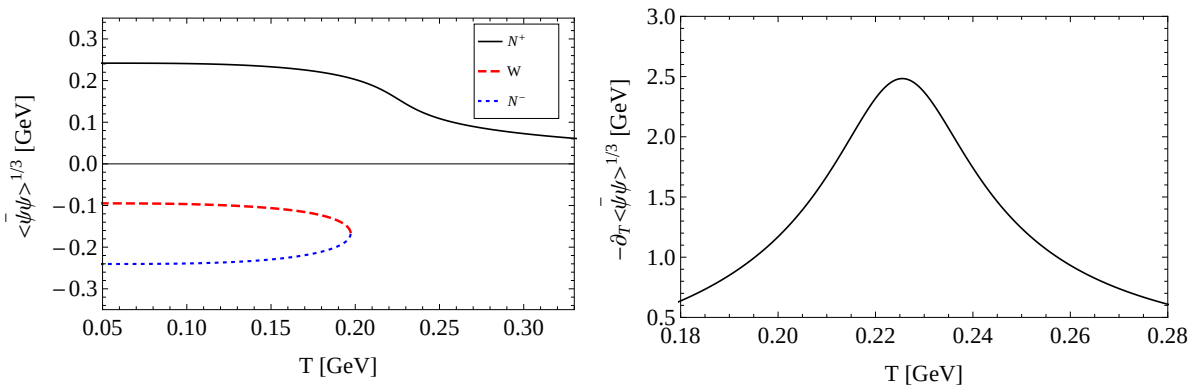

Figure 3.4: *Left panel*: $\langle\bar{\psi}\psi\rangle^{1/3}_{N^+,N^-,W}$ with a current quark mass $m_c = 7$ MeV. *Right panel*: Thermal gradient $-\partial_T\langle\bar{\psi}\psi\rangle^{1/3}_{N^+}$, which peaks at $T \approx 225$ MeV.

3.4 Confinement-deconfinement: Infra-red cut-off as a function of temperature

The confining length scale $\tilde{\tau}_{ir}^{-1}$ for different temperatures is shown in Fig. **??**, *left panel* and its thermal gradient $\partial_T\tilde{\tau}_{ir}^{-1}$ is depicted in Fig. **??**, *right panel*, respectively, in chiral limit. The temperature at which $M(T) \to 0$ (i.e., when chiral symmetry is restored), $\tilde{\tau}_{ir}$ diverges (or $\tilde{\tau}_{ir}^{-1} \to 0$), is the critical temperature $T_c = 216$ MeV, for the confinement-deconfinement phase transition.[2] When a finite quark mass $m_c = 7$ MeV is considered into the gap equation, the critical temperature for the confinement-deconfinement phase transition can be obtained by the maximum of $\partial_T\tilde{\tau}_{ir}^{-1}$ which is located at $T_c \approx 220$ MeV as shown in Fig. **??**, *right panel*. The confining length scale $\tilde{\tau}_{ir}^{-1}$ with a current quark mass is depicted in Fig. **??**, *left panel*.

3.5 Confinement-deconfinement: The dual condensate or dressed Polyakov loop

Analytical properties of the quark propagator have been studied in literature at zero and finite temperature to determine whether such propagator supports confinement. The formal statement comes from the axiomatic field theory, particularly the axiom of reflection positivity which states that for any field correlator in coordinate space to be a part of the Hilbert space of physically realizable states, the Fourier transform to momentum space of the said correlator

[2] A different temperature dependent infra-red cut-off was considered in Ref. [**?**], and used as an order parameter for the deconfinement phase transition.

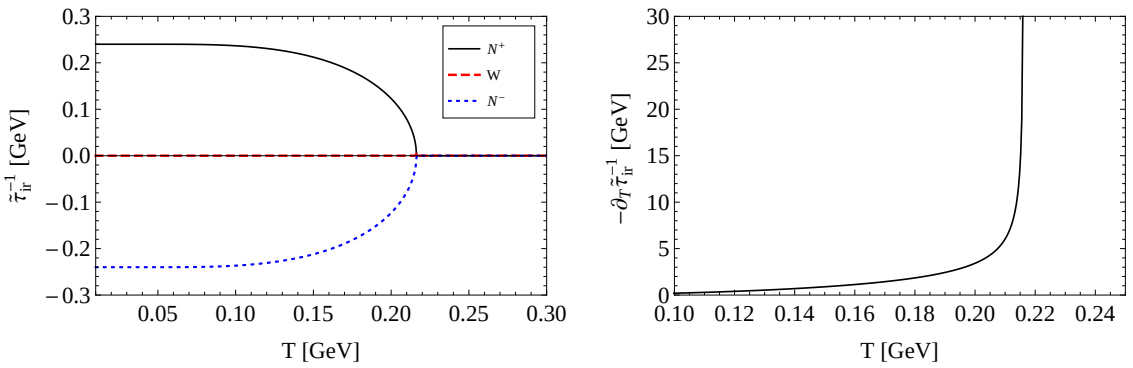

Figure 3.5: *Left panel*: Confining length scale $\tilde{\tau}_{ir}^{-1}$ Eq. (**??**) in the chiral limit. *Right panel*: Thermal gradient of the confining length scale $\partial_T \tilde{\tau}_{ir}^{-1}$ in the chiral limit, which diverges at $T \approx 216$ MeV.

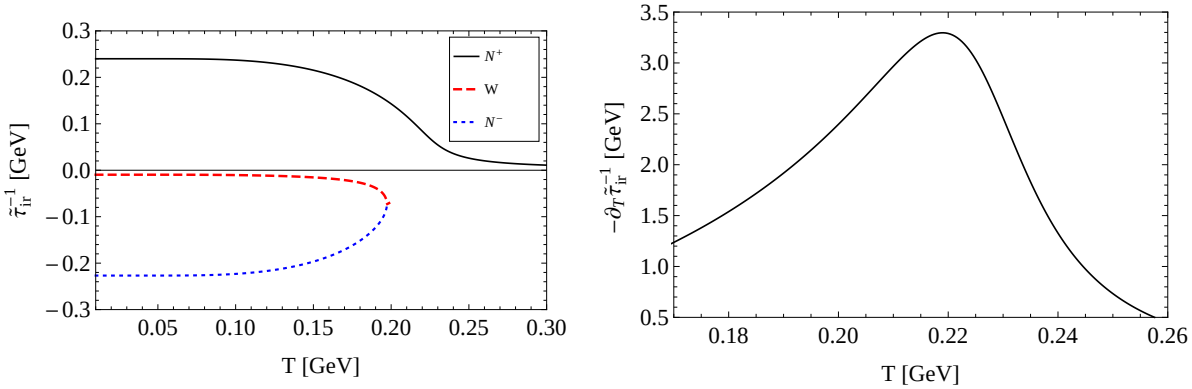

Figure 3.6: *Left panel*: Confining length scale $\tilde{\tau}_{ir}^{-1}$, with a current quark mass $m_c = 7$ MeV. *Right panel*: Thermal gradient of the confining length scale $\partial_T \tilde{\tau}_{ir}^{-1}$, whose maximum is located at $T \approx 220$ MeV.

should be positive definite [**?**]. Thus, violation of this axiom is verified on the basis of a non trivial momentum dependence of the quark mass function and as such, it cannot be implemented in our present model. At zero temperature, it is constructed such that the quark propagator has neither real nor complex poles. The implementation of quark confinement is through the lack of quark production thresholds.

Therefore, we resort to the dressed Polyakov loop (dPl) to explore confinement in our model. Recall that for infinitely massive quarks, the Polyakov loop (Pl) [**?**] is an order parameter for the

center symmetry[3] breaking and hence confinement in pure SU(3) gauge theory. In the past few years, another order parameter, i.e., the dPl or the dual quark condensate has been suggested to be associated with the confinement-deconfinement phase transition in lattice [**?**], SDE studies [**?**, **?**, **?**] and in variants of NJL model [**?**] (see Refs. [**?**, **?**, **?**]). It generalizes the ordinary Pl by considering spatial fluctuations. Both Pl and dPl correspond to the same equivalence class regarding the winding properties of the respective loops. It reduces to the Pl in the infinite quark mass limit. This fact is what motivates the consideration of dual condensate or dressed polykov loop dPl as an order parameter for the deconfinement phase transition, which has been explored within the SDE formalism extensively Refs. [**?**, **?**, **?**]. Starting point is the generalized quark condensate $\langle\bar{\psi}\psi\rangle_\phi$, which is the analogue of the usual quark condensate, but evaluated for quark fields with twisted boundary conditions

$$\psi(1/T,\vec{x}) = \mathrm{e}^{-i\phi}\psi(0,\vec{x}), \tag{3.5.1}$$

in the imaginary time direction, where $\phi \in [0, 2\pi]$. When $\phi = \pi$, we recover the standard anti-periodic boundary condition for the quark field. These U(1)-valued boundary conditions in momentum space correspond to generalized ϕ- dependent Matsubara frequencies that can be obtained from a slight modification of the usual fermionic Matsubara frequencies $\omega_n = (2n+1)\pi T$, as

$$\omega_n \to \omega_n^\phi = \left(2n + \frac{\phi}{\pi}\right)\pi T, \tag{3.5.2}$$

The ϕ-dependent condensate can be obtained from the ϕ-dependent quark propagator as

$$\langle\bar{\psi}\psi\rangle_\phi = N_c \sum_n \int \frac{d^3\vec{k}}{(2\pi)^3} Tr[S(\vec{k},\omega_n^\phi)] \tag{3.5.3}$$

The conventional condensate $\langle\bar{\psi}\psi\rangle$ is obtained for the special case when $\phi = \pi$. The dual condensate $\Sigma_{\tilde{n}}$ is then defined as the Fourier-transform of the $\langle\bar{\psi}\psi\rangle_\phi$ with respect ϕ, is given by

$$\Sigma_{\tilde{n}} = -\int_0^{2\pi} \frac{d\phi}{2\pi} e^{-i\tilde{n}\phi}\langle\bar{\psi}\psi\rangle_\phi, \tag{3.5.4}$$

where $\tilde{n}$ is an integer and $\Sigma_{\tilde{n}}$ is the projection of $\langle\bar{\psi}\psi\rangle_\phi$ onto the loops $\tilde{n}$-times around the temporal direction. In lattice representation this can be written as a sum of Wilson loops winding $\tilde{n}$ times around the temporal boundary [**?**]. In particular, since the PL is the shortest loop with winding number 1, the case $\tilde{n} = 1$ may be viewed as a collection of generalized

[3]Is the symmetry of the pure $SU(3)$ gauge theory, whose gauge group correspond to Z(N) (the Abelian group of the Nth-roots of unity) is the center of the group, namely, the subgroup whose elements commute with all group elements.

Polyakov loops with spatial fluctuations, and has been termed "dressed Polyakov loop" [**?**],

$$\Sigma_1 = -\int_0^{2\pi} \frac{d\phi}{2\pi} e^{-i\phi} \langle \bar{\psi}\psi \rangle_\phi. \tag{3.5.5}$$

Dressed Polyakov loop Σ_1 and the ordinary (thin) PL transform in the same manner under center transformations, which motivates the consideration of Σ_1 as an order parameter for the deconfinement phase transition. Moreover, since the spatial fluctuations are suppressed for infinite quark masses, Σ_1 reduces to the thin PL in this limit. On the other hand, as seen from its definition, it is also related to the quark condensate, albeit with unphysical boundary conditions. This hints for a possible connection between chiral and deconfinement phase transition, explaining why both transitions occur in the same temperature region [**?**, **?**]. Another important feature of Σ_1 is that it could be calculated directly lattice and SDE studies. This view has been challenged in Refs. [**?**, **?**, **?**] and [**?**]. The latter reference is particularly interesting because the dPl has been explored in three-dimensional quantum electrodynamics, a confining theory which, however, possesses a trivial center symmetry. Although the behavior is qualitatively the same as reported in [**?**] for QCD, it cannot be directly linked to the confinement transition. In our work [**?**] we extend on these lines in what follows.
Generalizing the Matsubara frequencies is formally equivalent to considering a theory with a purely imaginary chemical potential $\mu_I = \phi T$. This can be seen from the observation that $\langle \bar{\psi}\psi \rangle_\phi$ is symmetric around $\phi = \pi$, i.e., $\langle \bar{\psi}\psi \rangle_{\phi-\pi} = \langle \bar{\psi}\psi \rangle_{\phi+\pi}$, where $\langle \bar{\psi}\psi \rangle_{\phi=\pi}$ corresponds to the conventional quark condensate. Then, we prefer to write Eq. (**??**) as

$$\Sigma_1 = -\int_0^{\pi} \frac{d\varphi}{\pi} \cos(\varphi) \langle \bar{\psi}\psi \rangle_{\varphi+\pi}. \tag{3.5.6}$$

We now define the normalized φ-dependent dual quark condensate as $\sigma = \langle \bar{\psi}\psi \rangle_{\varphi+\pi,T} / \langle \bar{\psi}\psi \rangle_0$, where $\langle \bar{\psi}\psi \rangle_0$ is the conventional chiral condensate at zero temperature. We plot σ in the chiral limit in Fig. **??**, *left panel*, as a function of dual angle φ at different temperatures. At low temperatures, σ behaves practically as a constant for varying φ. As we approach the critical temperature, the variation becomes more pronounced and approaches a second order phase transition at $T_c \approx 216$ MeV. In the presence of a finite current quark mass $m_c = 7$ MeV, the plot of σ as a function of the dual angle φ at different temperatures is shown in Fig. **??**, *right panel*. Because of a finite current quark mass, no derivative singularity appears. The pseudo-critical temperature in this case is $T_c \approx 220$ MeV. Our plots compare well with the ones shown in [**?**].

The normalized dPl $\Sigma_1(T)/\langle \bar{\psi}\psi \rangle(0)$ is shown in Fig.**??**, *left panel*, in chiral limit and the *right panel*, corresponds to a finite current quark mass. Note that the chiral symmetry restoration curve as well as the deconfinement curve cross each other at the same temperature $T = T_c$ illustrating the simultaneity of both the transitions. Now the question is whether the dual

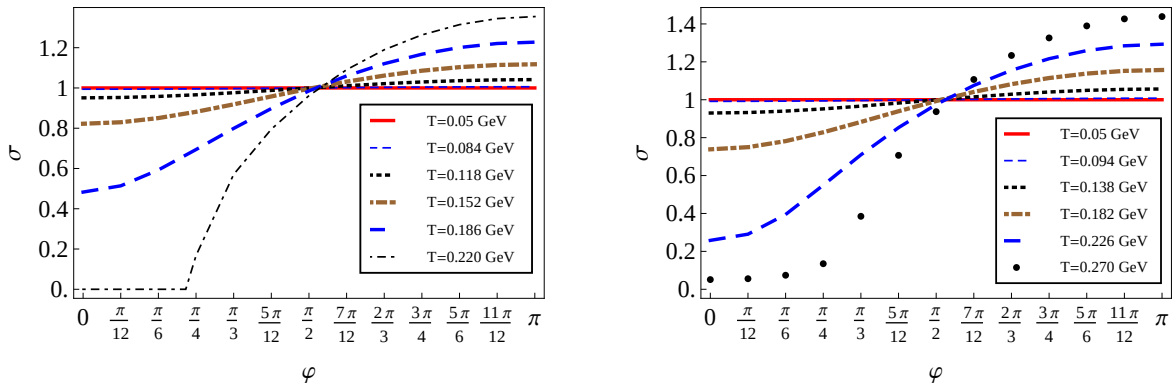

Figure 3.7: Normalized chiral condensate as a function of the dual angle φ for the CI. *Left panel:* Chiral limit. *Right panel*: With a finite current quark mass $m_c = 7$ MeV. Here, $\sigma = \langle\bar{\psi}\psi\rangle_{\varphi+\pi,T}/\langle\bar{\psi}\psi\rangle_0$. Chiral symmetry breaking-restoration transition takes place at $T_c \approx 216$ MeV and $T_c \approx 220$ MeV, respectively for the chirally symmetric and asymmetric cases.

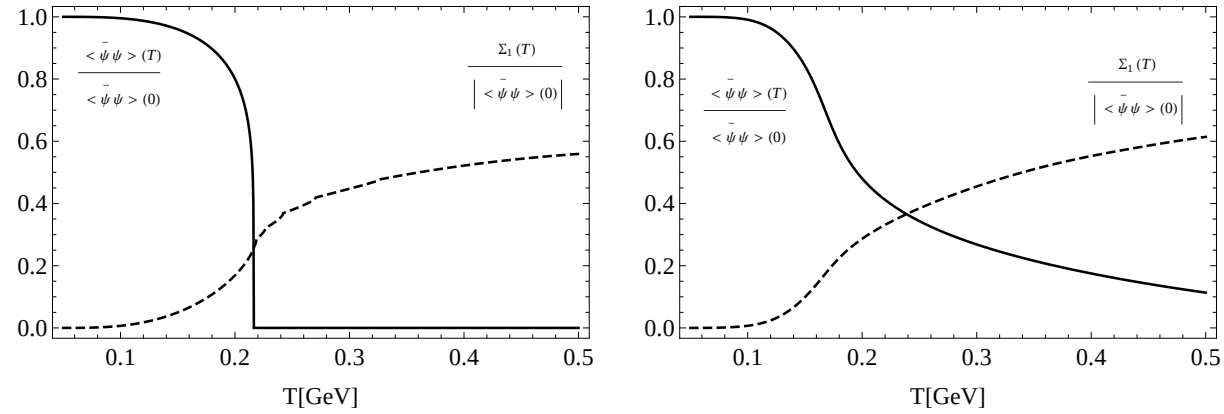

Figure 3.8: Normalized chiral condensate $\langle\bar{\psi}\psi\rangle(T)/\langle\bar{\psi}\psi\rangle(0)$ and dPl $\Sigma_1(T)/\langle\bar{\psi}\psi\rangle(0)$: *Left panel:* Chirally symmetric case. *Right panel:* Chirally asymmetric case with a finite seed mass $m_c = 7$ MeV.

quark condensate is the true parameter for the confinement-deconfinement phase transition? The answer is given in Ref. [**?**], where we studied some other confining nonlocal NJL models and concluded that the dPl is not a clear order parameter for the confinement-deconfinement phase transition because it has the same behavior in both confining and non-confining theories and it cannot be linked to center symmetry in these models. In the next section we use the

infra-red cut-off in as a function of temperature which is related to the QCD confining length to study the confinement-deconfinement phase transition.

3.6 Improved Contact Interaction (ICI) Model

That the simple CI model of Eq. (**??**), constructed primarily for the zero temperature description of QCD and hadron physics, cannot be the complete story at finite temperature. As temperature increases from its zero value, due to screening effects, the coupling $\alpha_{\rm IR}$ decreases and the gluon mass scale m_G increases and thus the ratio of these two, the effective coupling $\alpha_{\rm eff}(0)$ Eq. (**??**), decreases. We can effectively mimic this behavior by assuming a temperature dependent $\alpha_{\rm eff}$ i.e.,

$$\alpha_{\rm eff}(0) \quad \Rightarrow \quad \alpha_{\rm eff}(T). \tag{3.6.1}$$

Following the lead from modern computations of the gluon propagator at finite temperature [**?**] and the temperature dependence of the quark-antiquark condensate for two light degenerate quark flavors [**?**], we can model this temperature dependence as plotted in Fig. **??**, *left panel*. It can be parametrized as the following Padé approximation

$$\alpha_{\rm eff}(T) = \left(\frac{1 + aT + bT^2}{c + dT + eT^2 + fT^3} \right)^2 , \tag{3.6.2}$$

where $a = -14.1$ GeV, $c = 60.8$ GeV^2, $c = 0.132$ GeV, $d = -1.86$ GeV^{-1}, $e = 7.6$ GeV^{-2} and $f = 3.24$ GeV^{-3}. We now repeat our calculation for the explicit chiral symmetry breaking case, solving for the gap equation with the temperature dependent cut-off in Eq. (**??**) and then evaluating the quark-antiquark condensate, plotted in Fig. **??**, *right panel*, which reproduces lattice data at high temperature. Avoiding repeating the calculational details, we present the plot for the multiple-mode dynamical quark condensate in Fig. **??**, *left panel*. Its inflection point, calculated through the thermal gradient of the chiral condensate is shown in Fig. **??** *right panel*, which now reveals the pseudo-critical temperature $T_c \approx 165$ MeV in accordance with lattice results [**?**]. This should be compared with our previous result of $T_c \approx 220$ MeV computed for a temperature independent effective coupling $\alpha_{\rm eff}(0)$. The temperature dependent confining length scale τ_{ir}^{-1} is plotted in Fig. **??**, *left panel*, and its thermal gradient is shown in Fig. **??**, *right panel*. Within the numerical accuracy available, we find that the chiral symmetry restoration and confinement-deconfinement phase transitions are coincidental at $T_c^{\chi,c} \approx 165$ MeV. Thus $T_c^{\chi,c} \approx 165$ MeV obtained from the ICI model agrees with lattice QCD [**?**].

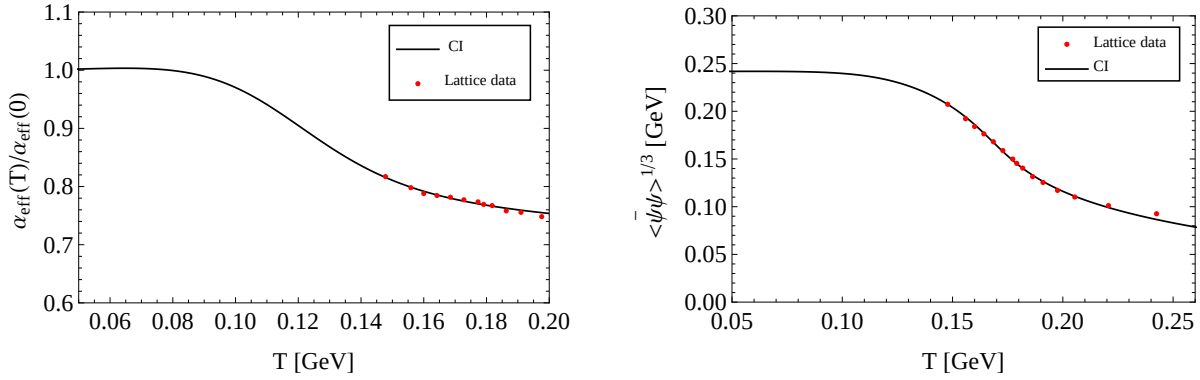

Figure 3.9: *Left panel*: Solid curve shows the temperature dependent normalized effective coupling $\alpha_{\rm eff}(T)/\alpha_{\rm eff}(0)$. Within the ICI-model, this curve is fitted to the dots which reproduce lattice results [**?**] in the appropriate temperature range $[150, 220]$ MeV. *Right panel*: Chiral condenste obtained from the ICI-model, with a current quark mass $m_c = 7$ MeV and a temperature dependent infra-red cut-off fitted with lattice data points [**?**].

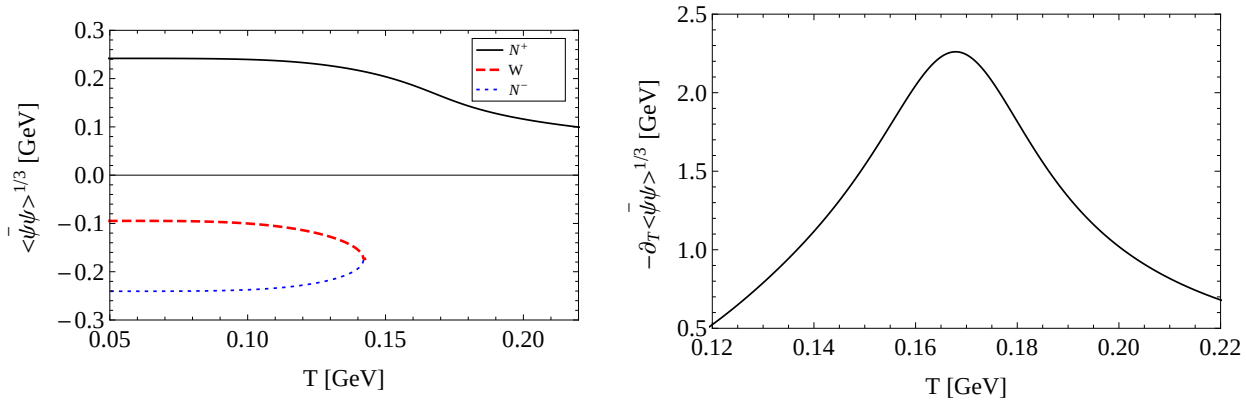

Figure 3.10: *Left panel*: Multiple-modes of chiral quark condensate with a current quark mass $m_c = 7$ MeV for with a temperature dependent infra-red cut-off $\tilde{\tau}_{ir}$ and temperature dependent effective coupling $\alpha_{\rm eff}(T)$. *Right panel*: Thermal gradient of the chiral quark condensate $-\partial_T\langle\bar{\psi}\psi\rangle$ which peaks at $T_c \approx 165$ MeV in the N^+-mode.

3.7 Finite temperature and density: QCD phase diagram

The gap equation at finite temperature and density can be obtained by shifting $\omega_n \to \omega_n + i\mu$ in Eq. (**??**), and is of the form[4]

$$M \;=\; m_c + \frac{M\alpha_{eff}(0)}{3\pi^2}\int_{\tau_{uv}^2}^{\tilde{\tau}_{ir,\mu}} d\tau \frac{\mathrm{e}^{-M^2\tau}\Theta_3(\frac{\pi T+i\mu}{2T}, \mathrm{e}^{-\frac{1}{4T^2\tau}})}{\tau^2}, \tag{3.7.1}$$

[4]At $T = 0$ and $T \neq 0$, $A = C = 1$. In case of finite quark chemical potential μ, $A = 1$ but $C \neq 1$ and can be considered as a renormalization of μ [**?**], though we perform the calculation assuming $A = C = 1$ at finite T

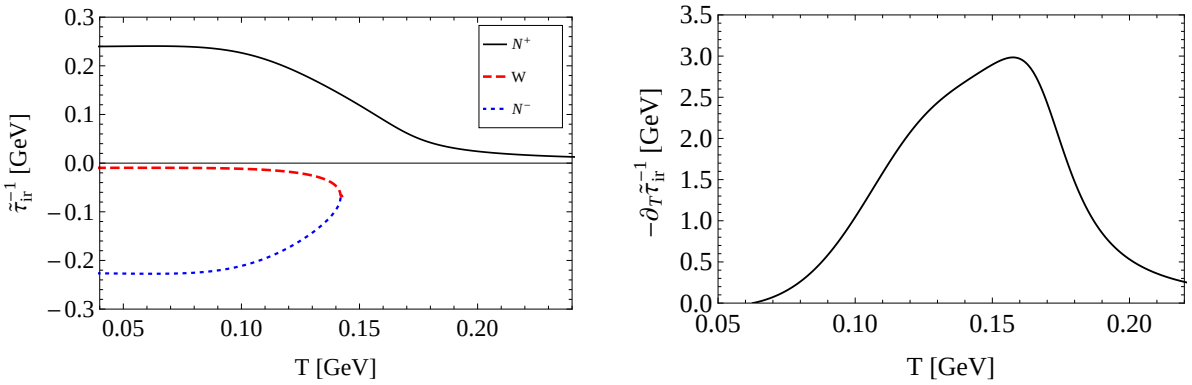

Figure 3.11: *Left panel*: Confining length scale $\tilde{\tau}_{ir}^{-1}$ from the ICI- model with a current quark mass $m_c = 7$ MeV. *Right panel*: Thermal gradient of the confining length scale $-\partial_T\tilde{\tau}_{ir}^{-1}$ in the N^+-mode, which peaks at $T \approx 165$ MeV.

where $\Theta_3(x, y)$ is the third Jacobi theta function and

$$\tilde{\tau}_{ir,\mu} = \tau_{ir}(T) = \tau_{ir}\frac{M(0)}{M(T,\mu)}, \tag{3.7.2}$$

with μ is the chemical potential. The chiral quark condensate is given by

$$-\langle\psi\bar{\psi}\rangle \;=\; \frac{3M}{4\pi^2}\int_{\tau_{uv}^2}^{\tilde{\tau}_{ir,\mu}} d\tau \frac{\mathrm{e}^{-M^2\tau}\Theta_3(\frac{\pi T+i\mu}{2T}, \mathrm{e}^{-\frac{1}{4T^2\tau}})}{\tau^2}. \tag{3.7.3}$$

We solve the gap equation numerically at finite T and μ in the chiral limit and with a finite current quark mass $m_c = 7$ MeV with the CI-model and ICI-model. The critical temperatures for chiral symmetry breaking-restoration and confinement-deconfinement phase transitions are obtained by the thermal gradients $-\partial_T\langle\bar{\psi}\psi\rangle$ and $-\partial_T\tilde{\tau}_{ir}^{-1}$ for different μ. Finally, we plot the QCD phase diagram in $T-\mu$-plane with the CI-model in the chiral limit in Fig. **??**, *left panel*, and with a current quark mass in Fig. **??**, *right panel*. We again used a $T_c(\mu) = T_c(0)+a\mu^2$ fit as in the previous Chapters, near the $\mu = 0$ axis, where for the CI-model, $a = -0.94$ in the chiral limit and with a quark current mass $a = -0.93$ and for the ICI-model, $a = -0.59$. The critical end point with the CI-model in the chiral limit is located at $(\mu_E/T_c = 1.5,\ T_E/T_c = 0.54)$. The critical end point for the CI-model with a current quark mass $m_c = 7$ MeV is located at $(\mu_E/T_c = 1.68,\ T_E/T_c = 0.4)$. The phase diagram for the ICI-model with current quark mass $m_c = 7$ MeV is shown in Fig. **??**, the critical end point is located at $(\mu_E/T_c = 2,\ T_E/T_c = 0.5)$.

and μ.

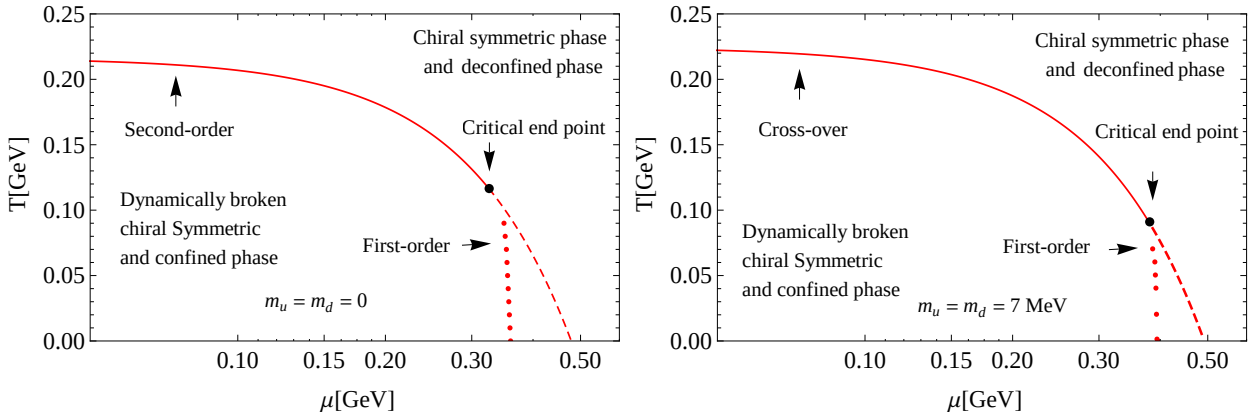

Figure 3.12: QCD phase diagram from the CI-model: *Left panel*, in the chiral limit. *Right panel*, with a current quark mass $m_c = 7$ MeV.

3.8 Discussion

In this Chapter we studied the gap equation at finite temperature with a confining vector-vector CI model for quarks. We discussed multiple solutions of the gap equation namely, positive-mode (N^+), negative-mode (N^-) and Wigner-mode (W). In the chiral limit, the critical temperature $T_c^\chi \approx 216$ MeV for chiral symmetry restoration is obtained by taking the thermal gradient of the chiral condensate in N^+-mode. For a finite current quark mass $m_c = 7$ MeV, we obtained the pseudo-critical temperature through the thermal gradient of the chiral condensate peaked at $T_c^{\chi,m} \approx 225$ MeV in N^+-mode. We used an infra-red cut-off as temperature dependent i.e, $\tilde{\tau}_{ir}$, and solve the gap equation. The thermal gradient $\partial_T \tilde{\tau}_{ir}^{-1}$ diverges where the chiral symmetry is restored in the chiral limit at $T_c \approx 216$ MeV and hence deconfinement takes place, while for a finite current quark mass, the position of its maximum gives as the pseudo-critical temperature $T_c^{c,m} \approx 220$ MeV in the N^+-mode. Next, we used the dual quark condensate to calculate the critical temperature for the confinement-deconfinement phase transition in the standard N^+-mode in chiral limit as well as with a finite current quark mass and obtained the critical temperature through its thermal gradient. The pseudo-critical temperature for this case comes out exactly the same as we obtained through the gradient of the confining length scale. The pseudo-critical temperature for the confinement-deconfinement transition is similar to that for chiral symmetry breaking-restoration $T_c^{\chi,0} = T_c^{c,0} \approx 216$ MeV, in the chiral limit as well as with a finite current quark mass i.e., $T_c^{\chi,m} = T_c^{c,m} \approx 220$ MeV. Thus the chiral symmetry breaking-restoration and confinement-deconfinement phase transitions take place simultaneously in the CI-model. As the critical temperatures in this case are higher than the lattice results [**?**], we took step forward to take the effective coupling as a temperature dependent $\alpha_{\rm eff}(T)$, the

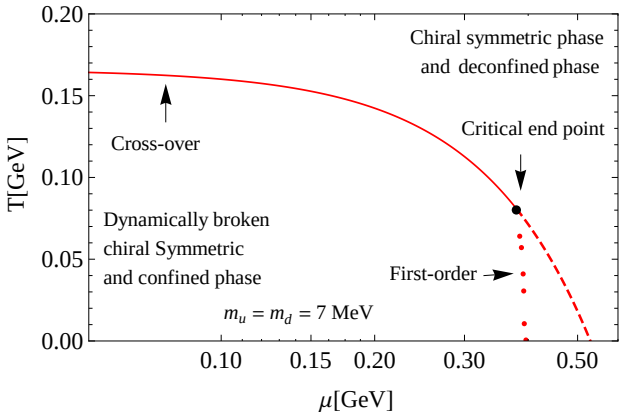

Figure 3.13: QCD phase diagram from the ICI-model with a current quark mass $m_c = 7$ MeV.

ICI-model, from which we reproduced lattice results [**?**] for the chiral condensate. The critical temperature for the chiral symmetry breaking restoration and confinement-confinement transitions remain the same i.e., $T_c^{\chi,m} = T_c^{c,m} \approx 165$ MeV. In Ref. [**?**], we checked whether the dual condensate is a true order parameter for confinement-deconfinement phase transition in local and non local versions of the NJL model. We conclude that it has the same behavior in confining and non-confining theories, which gives us no clear picture about the deconfinement phase transitions when it is not connected directly to center symmetry.
Finally, we included a finite chemical potential in the gap equation and drawn the phase diagrams for the CI-model (where the we took constant effective coupling but our infra-red cut-off as T and μ dependent) in chiral limit and with a current quark mass $m_c = 7$ MeV and for the ICI-model with a current quark mass $m_c = 7$ MeV. The critical end points for the CI-model in the chiral limit and with a current quark mass $m_c = 7$ MeV are located at $(\mu_E/T_c = 1.5,\ T_E/T_c = 0.54)$ and $(\mu_E/T_c = 1.68,\ T_E/T_c = 0.4)$, respectively. We improved our CI model with effective coupling as a function of temperature but not a function of chemical potential i.e. $\alpha_{eff}(T)$ that we named ICI-model, with a current quark mass $m_c = 7$ MeV. Though our results at zero density are agree with CMA (Chapter 2), SDE [**?**] and with Lattice[**?**], at finite density the position of the critical end point is $(\mu_E/T_c = 2,\ T_E/T_c = 0.5)$ higher than that of CMA (Chapter 2), SDE [**?**]. This may be due to the fact in this case we are not taking into account the effective coupling as a function of density or the C-equation (Eq. (**??**) of Chapter 2) with renoramlized chemical potential. Work in this regard is in progress.

In the next Chapter, we use the CI model under the influence of external magnetic field to understand how the magnetic field affects the critical temperature for the chiral symmetry breaking-restoration and confinement-deconfinement phase transitions.

Chapter 4

Inverse magnetic catalysis from CI model for the quarks

In the previous Chapter, we studied the gap equation for the CI model at zero and finite temperature, where entanglement between dynamical chiral symmetry breaking and confinement is expressed through an explicit temperature dependent infra-red regulator. We studied two cases; the simple CI model, where $\alpha_{\rm eff}$ is temperature independent and the ICI model, with a temperature dependent $\alpha_{\rm eff}(T)$. In this Chapter, based on Ref. [**?**], we study the effect of a magnetic filed on the chiral condensate and the confining scale, in both CI and ICI models. It is well known that strong magnetic fields have a tremendous impact in various physical systems. A typical example in astrophysics is a magnetar, in which the magnetic field might reaches intensities of the order of $B \sim 10^{10}$ Tesla [**?**]. In the early universe, it has been estimated that there could have been magnetic fields as strong as $B \sim 10^{14}$ and $B \sim 10^{19}$ Tesla [**?**, **?**] during the QCD and electroweak phase transitions, respectively. On more terrestrial grounds, in non-central heavy ion collisions at RHIC and LHC, the generated magnetic fields are approximately of the order of $B \sim 10^{14}$ to 10^{16} Tesla [**?**] in intensity. A number of interesting effects are triggered by strong magnetic fields in QCD. Among others, the chiral magnetic effect [**?**] has attracted attention to explore topological features of vacuum and the strong CP problem. Moreover, intense magnetic fields are of direct relevance to understand the chiral and confinement phase transitions, because in one hand a strong magnetic field catalizes the formation of chiral condensate, the so-called *magnetic catalysis* effect (see [**?**] and references therein), hence increasing the pseudo-critical transition temperatures as the strength of the magnetic field grows bigger [**?**]. At the same time, such a field produces a screening effect on gluon interactions in the infra-red, as can be accounted for from lattice [**?**] and suggested by effective model calculations [**?**, **?**, **?**, **?**]. This phenomenon has been dubbed as *inverse magnetic catalysis* and is responsible for a decreasing behavior of $T_c^{\chi,c}$ with stronger magnetic fields. We use lattice [**?**] as guide to study the effect of magnetic field on the critical temperature of the

QCD phase transitions.

4.1 Gap equation in a magnetic field

We consider a background homogeneous magnetic field directed along the z-axis, with magnitude B and defined through the symmetric gauge vector potential

$$A_\mu^{ext} = \left(0, -\frac{By}{2}, \frac{Bx}{2}, 0\right). \tag{4.1.1}$$

Within the Schwinger proper-time framework, the representation of the quark propagator in a magnetic field and in Euclidean space is of the form

$$\begin{aligned} S(k) &= \int_0^\infty d\tau \frac{\mathrm{e}^{-\tau(k_\parallel^2 + k_\perp^2 \frac{\tanh(|q_f B\tau|)}{|q_f B\tau|} + M^2)}}{\cosh(|q_f B\tau|)} \Big[\Big(\cosh(|q_f B\tau|) - i\gamma^1\gamma^2 \sinh(|q_f B\tau|)\Big) \\ &\quad \times (M - \not{k}_\parallel) - \frac{\not{k}_\perp}{\cosh(|q_f B\tau|)}\Big], \end{aligned} \tag{4.1.2}$$

where $k_\parallel^2 = k_0^2 + k_3^2$ and $k_\perp^2 = k_0^2 + k_3^2$, respectively, are parallel and transverse splitting of the quark momenta, in reference to the magnetic field direction, as usual, and $q_f = (+2e/3, -e/3)$ refers to the electric charges of up and down quarks. With these ingredients, adopting the regularization procedure of the previous Chapter, the corresponding gap equation for the dynamical mass at zero temperature under the influence of magnetic field (see Appendix C) becomes

$$M = m_c + \frac{\alpha_{\rm eff}(0)}{6\pi^2} \sum_{f=u,d} |q_f B| \int_{\tau_{uv}^2}^{\tau_{ir}^2} d\tau \frac{M \mathrm{e}^{-M^2\tau}}{\tau \tanh(|q_f B|\tau)}, \tag{4.1.3}$$

and the chiral condensate at zero temperature under the influence of magnetic field is given by

$$-\langle \bar{\psi}\psi \rangle = \frac{3}{8\pi^2} \sum_{f=u,d} |q_f B| \int_{\tau_{uv}^2}^{\tau_{ir}^2} d\tau \frac{M \mathrm{e}^{-M^2\tau}}{\tau \tanh(|q_f B|\tau)}. \tag{4.1.4}$$

The numerical solution of the gap equation and the chiral condensate are shown in Fig. **??**, *left panel*, and *right panel*, respectively. The dynamical mass and chiral quark condensate increase with the increase of the magnetic field strength.

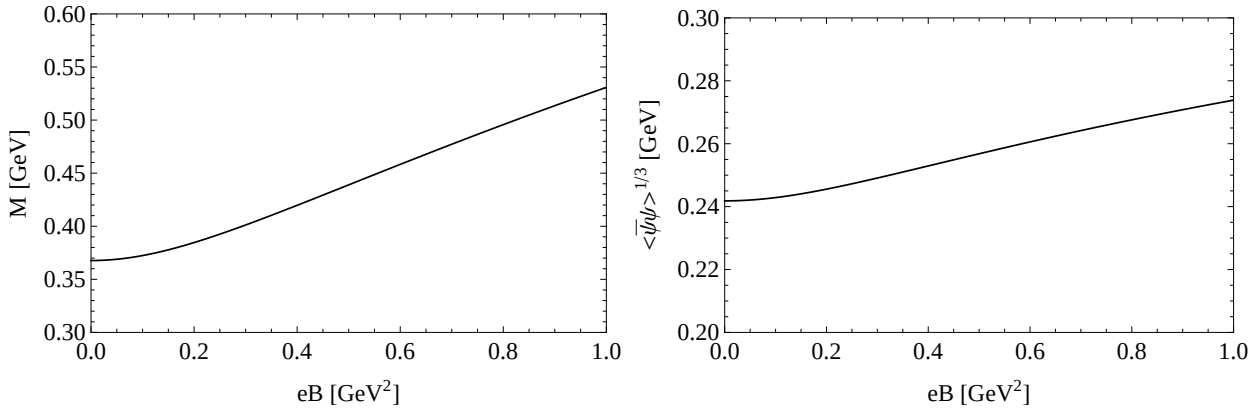

Figure 4.1: *Left panel*: Dynamical quark mass at zero temperature as a function of the magnetic field strength eB, with a current quark mass $m_c = 7$ MeV; *Right panel*: Chiral condensate as a function of eB.

4.2 Finite temperature T and Magnetic field B

The Schwinger propagator at finite temperature and in the presence of external magnetic field B is

$$S(k) = \int_0^\infty d\tau \frac{\mathrm{e}^{-\tau(\omega_n^2+k_3^2+k_\perp^2\frac{\tanh(|q_fB\tau|)}{|q_fB\tau|}+M^2)}}{\cosh(|q_fB\tau|)}\Big[\Big(\cosh(|q_fB\tau|) - i\gamma^1\gamma^2\sinh(|q_fB\tau|)\Big) \times(M - \not{k}_\parallel) - \frac{\not{k}_\perp}{\cosh(|q_fB\tau|)}\Big], \quad (4.2.1)$$

where ω_n stands for the fermion Matsubara frequencies. Using the above Eq. (**??**) in the gap equation, performing the momentum integration and summing over Matsubara frequencies, we reach at the following form of the gap equation for the dynamical mass (see Appendix C) at finite temperature T and magnetic field B

$$M = m_c + \frac{M\alpha_{\rm eff}(0)T}{3\pi^{3/2}}\sum_{f=u,d}|q_fB|\int_{\tau_{uv}^2}^{\bar{\tau}_{ir}^2} d\tau \frac{\mathrm{e}^{-M^2\tau}\Theta_2(0,\mathrm{e}^{-4\pi^2T^2\tau^2})}{\tau^{1/2}\,\tanh(|q_fB|\tau)}. \quad (4.2.2)$$

Here $\bar{\tau}_{ir} = \tau_{ir}M(0,0)/M(T,eB)$. The chiral quark condensate at finite temperature and in the presence of magnetic field is

$$-\langle\bar{\psi}\psi\rangle = \frac{3TM}{4\pi^{3/2}}\sum_{f=u,d}|q_fB|\int_{\tau_{uv}^2}^{\bar{\tau}_{ir}^2} d\tau \frac{\mathrm{e}^{-M^2\tau}\Theta_2(0,\mathrm{e}^{-4\pi^2T^2\tau^2})}{\tau^{1/2}\,\tanh(|q_fB|\tau)}. \quad (4.2.3)$$

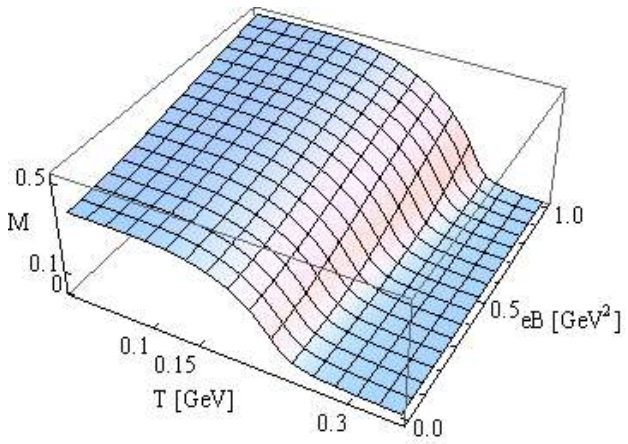

Figure 4.2: Dynamical quark mass M for CI-model as a function of temperature and magnetic field strength with a current quark mass $m_c = 7$ MeV.

The numerical solution to the above gap equation with the CI-model is shown in Fig. **??**. The chiral quark condensate $\langle\bar{\psi}\psi\rangle^{1/3}$ and the confining scale $\bar{\tau}_{ir}^{-1}$ are depicted in Fig. **??** and Fig. **??**, respectively. Dynamical mass for the quarks M, chiral quark condensate $-\langle\bar{\psi}\psi\rangle^{1/3}$ and confining scale $\bar{\tau}_{ir}^{-1}$ at finite temperature increase with the magnetic field strength. The critical temperatures for the chiral symmetry breaking-restoration and confinement-deconfinement phase transitions can be obtained by the position of the maximum of the peaks of thermal gradients of the chiral quark condensate $-\partial_T\langle\bar{\psi}\psi\rangle^{1/3}$ and the confining length scale $-\partial_T\bar{\tau}_{ir}^{-1}$. The maximum of the thermal gradients $-\partial_T\langle\bar{\psi}\psi\rangle^{1/3}$ and $-\partial_T\bar{\tau}_{ir}^{-1}$ are shown in Fig. **??**, *left panel* and *right panel*, respectively. The peaks shift toward the high temperature region with the increase of eB. We specify the temperature at which the maximum of the peaks of $-\partial_T\langle\bar{\psi}\psi\rangle^{1/3}$ by $T_{c,B}^{\chi}$ to be the critical temperature for the chiral symmetry breaking-restoration and for the confinement-deconfinement by $T_{c,B}^{c}$. Our scheme ensures that $T_{c,B}^{\chi} \simeq T_{c,B}^{c} \equiv T_{c,B}$. In the next section we discuss the gap equation ICI-model at finite temperature and in the presence of magnetic field. We also draw the phase digram in the T-eB plane for both the CI and ICI models.

4.3 Improved contact interaction model and the magnetic field

In the previous section, we discussed the CI-model at finite temperature and in external magnetic field. We observed that the critical temperatures for the chiral symmetry breaking-

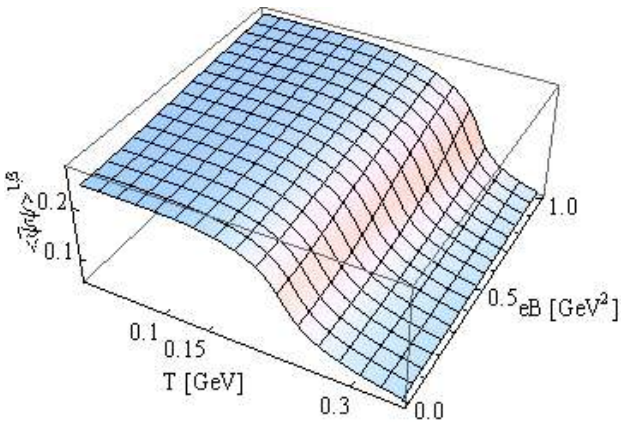

Figure 4.3: Chiral condensate for CI-model as a function of temperature and magnetic field strength.

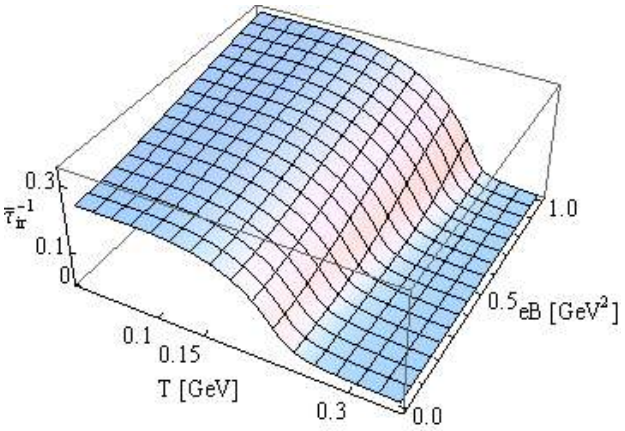

Figure 4.4: Confining scale $\bar{\tau}_{ir}$ for CI-model, as a function of temperature and magnetic field strength for a current quark mass $m_c = 7$ MeV.

restoration and confinement-deconfinement transitions increase with the increase of eB. Here we want to discuss the effect of external magnetic field with the ICI-model, in which $\alpha_{\rm eff}(0) \Rightarrow \alpha_{\rm eff}(T)$ is defined in Eq.(**??**). The chiral quark condensate is shown in Fig. **??** as a function of temperature and magnetic field and the confining scale is depicted in Fig. **??**. Thermal gradients $-\partial_T \langle\bar{\psi}\psi\rangle^{1/3}$ and $-\partial_T \bar{\tau}_{ir}^{-1}$, respectively are shown in Fig. **??**. The phase diagram in T-eB plane is depicted in Fig. **??** for both CI and ICI models. The normalized critical temperatures for both the models are plotted in Fig. **??**, which support the magnetic catalysis of the

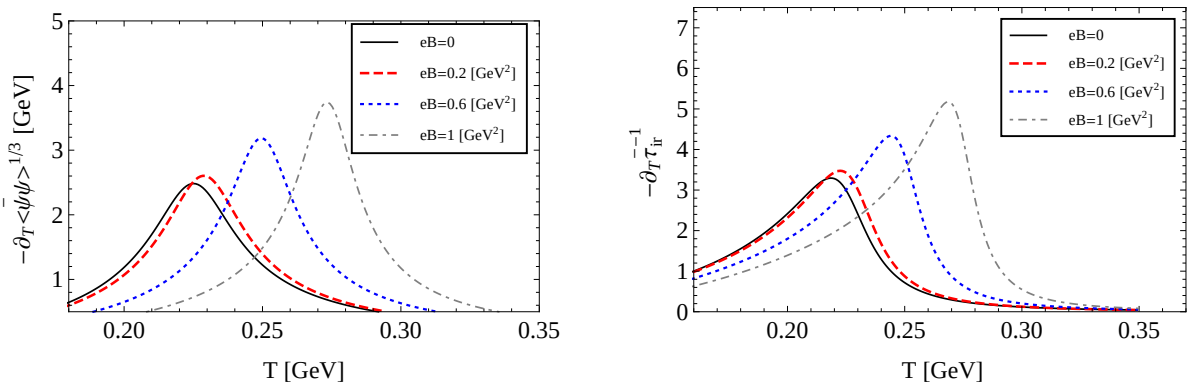

Figure 4.5: *Left panel*: Thermal gradient of the chiral condensate $-\partial_T \langle\bar{\psi}\psi\rangle^{1/3}$ at finite temperature and magnetic filed eB for CI-model. *Right panel*: Thermal gradient of the confining scale $-\partial_T \bar{\tau}_{ir}^{-1}$ for the CI-model. From the above plots, it is obvious that the critical temperature for the chiral phase transitions increase when the magnetic field strength gets stronger, which supports the phenomenon of magnetic catalysis.

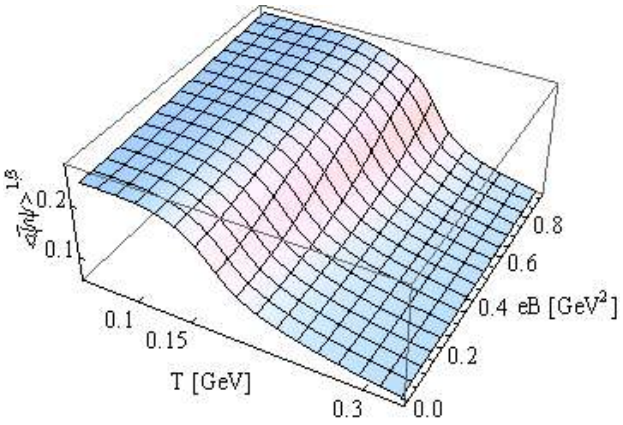

Figure 4.6: Chiral condensate as a function of temperature and magnetic field strength for a current quark mass $m_c = 7$ MeV for the ICI-model.

dynamical symmetry breaking-restoration and confinement-deconfinement transitions. In the next section we use the model for α_{eff} as a function of the magnetic field strength in the gap equation and check its effect in the transition temperatures.

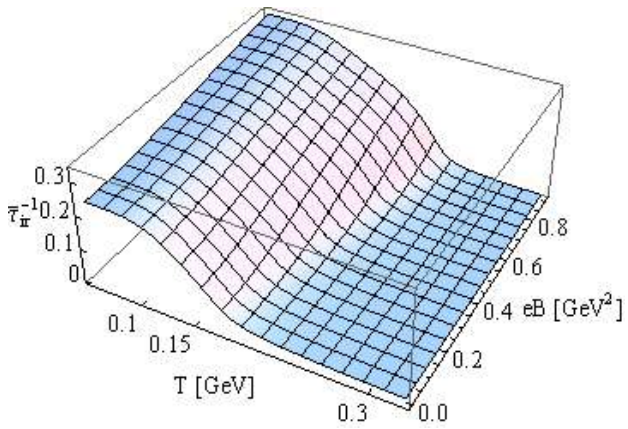

Figure 4.7: Confining length scale for the ICI-model as a function of temperature and magnetic field strength with a current quark mass $m_c = 7$ MeV.

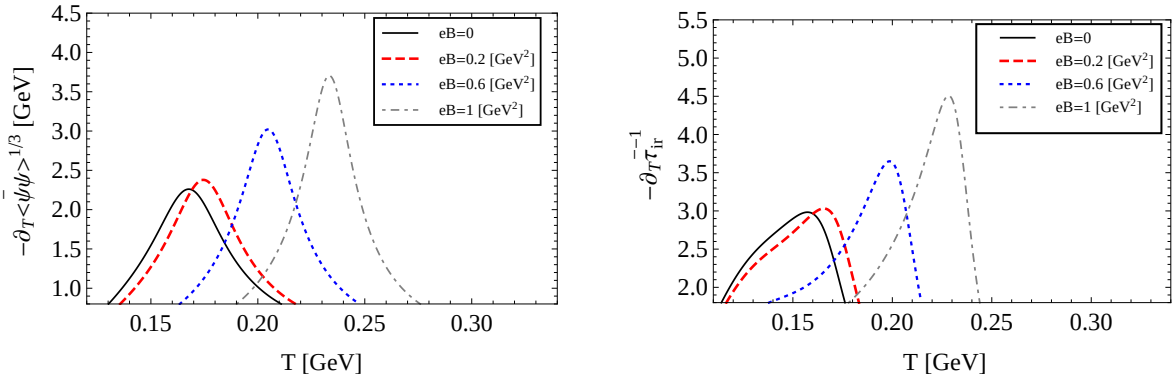

Figure 4.8: *Left panel*: Thermal gradient of the chiral condensate $-\partial_T \langle \bar{\psi}\psi \rangle^{1/3}$ at finite temperature and magnetic filed for the ICI-model. *Right panel*: Thermal gradient of the confining scale $\partial_T \bar{\tau}_{ir}^{-1}$ for the ICI-model.

4.4 Inverse Magnetic Catalysis (IMC)

In the previous section, we observed the phenomenon of magnetic catalysis (MC) i.e., the chiral quark condensate and pseudo-critical temperature for the chiral symmetry breaking-restoration and confinement-deconfinement transitions become enhanced as we increase the magnetic field strength eB, which also has been observed in low-energy effective models and NJL-type models [**?**]. This is due to the opening of the gap between the Landau states which leads to low

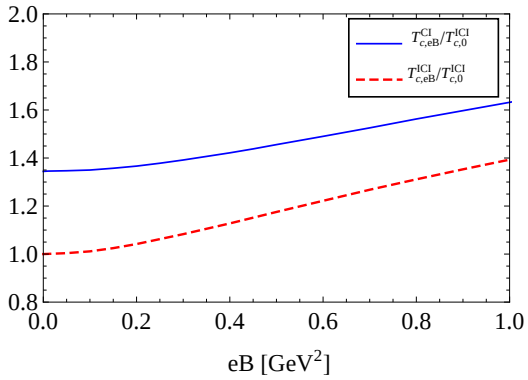

Figure 4.9: Effective phase diagram in the $T - eB$ plane. Dashed curve corresponds to the CI-model, whereas the solid curve is obtained with the ICI-model. From the above plot, it is obvious that the critical temperatures for the chiral symmetry restoration and deconfinement phase transitions increase with the increase of magnetic field strength, which support the phenomenon of magnetic catalysis.

energy contributions in the formation of chiral condensate. Recent lattice studies [**?**] and some effective model based approaches [**?**, **?**, **?**, **?**, **?**, **?**] show that the chiral condensate and the pseudo-critical temperature decrease with the increase of magnetic field i.e., Inverse magnetic catalysis (IMC). It has been argued in [**?**, **?**] that the phenomenon of IMC is due to the partial restoration of chiral symmetry. In the low momentum domain, where the chiral symmetry is broken, there is a strong screening effect of the gluon interactions, which suppresses the formation of the chiral quark condensate. In this zone, a gluon mass $m_G \propto \sqrt{N_f \alpha_s \mid eB \mid}$ [**?**] develops, which is due to fact that gluon fields couple to a quark-antiquark interacting state. Thus m_G increases and the strong coupling α_s decreases with increasing eB as $\alpha_s = b\ \ln(|eB|/\Lambda^2_{QCD})^{-1}$ with $b = (11N_c - 2N_f)/6\pi$ [**?**, **?**]. Therefore the effect of external magnetic field is that it increases the gluon mass and decreases the coupling between the quarks and as a result, the chiral condensate is damped, which causes to decrease the pseudo-critical temperature. In Ref. [**?**] the effect of external magnetic field is taken into account in the effective coupling in NJL and PNJL models and fitted to the lattice data [**?**] for the case of $N_f = 2 + 1$, where IMC has been observed. In Ref. [**?**], the vacuum one-loop quark-gluon vertex correction at zero temperature in the presence of a magnetic field studied where inverse magnetic catalysis from the properties of the QCD coupling in a magnetic field discussed.

Since our approach is based on the contact interaction similar to the NJL, so in this case particularly, as an initial step, we follow Ref.[**?**, **?**] as a guide to improve our mean field result by considering the functional form of the magnetic field dependent coupling by fitting the normalized critical temperature of our model to the normalized critical temperature as a function

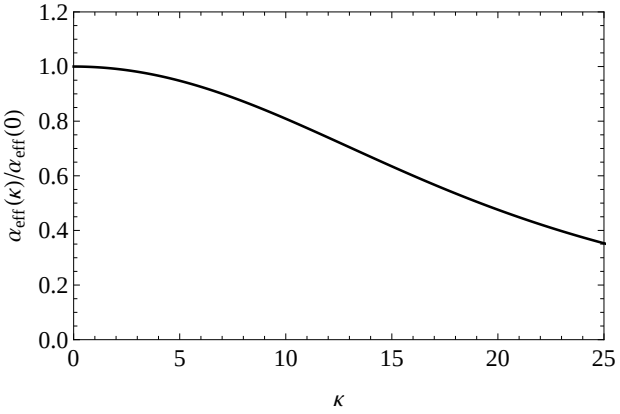

Figure 4.10: Effective coupling $\alpha_{\rm eff}(\kappa)$ in Eq. (**??**) normalized to the constant value of $\alpha_{\rm eff}(0)$ in Eq. (**??**).

of eB of lattice [**?**] of the form

$$\alpha_{\rm eff}(\kappa) = \alpha_{\rm eff}(0)\left(\frac{1+a\kappa^2+b\kappa^3}{1+c\kappa^2+d\kappa^4}\right), \tag{4.4.1}$$

with $\kappa = eB/\Lambda_{QCD}^2$, $a = 0.002$, $b = -8.06\times10^{-6}$, $c = 0.004\times10^{-4}$, $d = 0.06\times10^{-4}$ and we take $\Lambda_{QCD} = 240$ MeV. It should be noted that our coupling fit is taken at $T = 0$. The behavior of the magnetic effective coupling Eq. (**??**), normalized by $\alpha_{\rm eff}(0)$, Eq. (**??**), is depicted in Fig. **??**. The corresponding chiral condensate is shown in Fig. **??**. Again, we identify $T_{c,B}^{\chi,c}$ from the thermal gradient of the condensate and the confining length scale respectively. The corresponding phase diagram is shown in Fig. **??**.

Pseudo-critical temperature obtained with $\alpha_{eff}(0)$ increases as eB grows bigger, whereas for $\alpha_{\rm eff}(\kappa)$, $T_{c,B}$ monotonically decreases for higher magnetic fields. This behavior strongly resembles lattice [**?**] and other effective models approaches [**?**, **?**, **?**, **?**] with no "turn over" effect at intermediate eB [**?**].

4.5 Discussion

We have studied the effective QCD phase diagram in the $T - eB$ plane within a CI model. Such a model differs from the standard NJL theory by considering an infra-red cut-off which in addition to the dynamical ultra-violet scale, renders the quark propagator pole-less, hence supporting confinement. At finite temperature, we regularize the gap equation ensuring the coincidence of the chiral and confinement transitions at the same pseudo-critical temperature

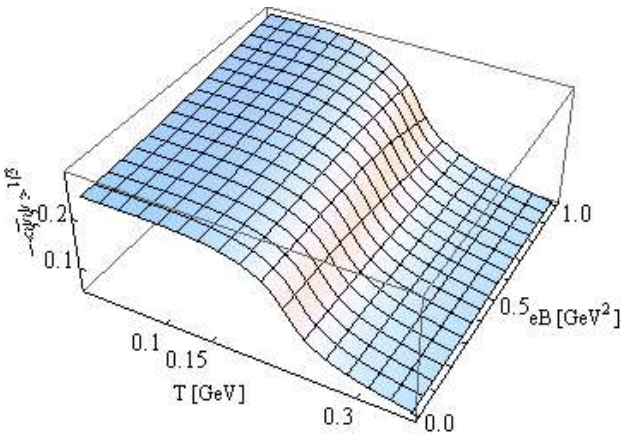

Figure 4.11: Chiral condensate as a function of temperature and magnetic field strength eB. Plot is generated with $\alpha_{\text{eff}}(\kappa)$ in Eq. (**??**).

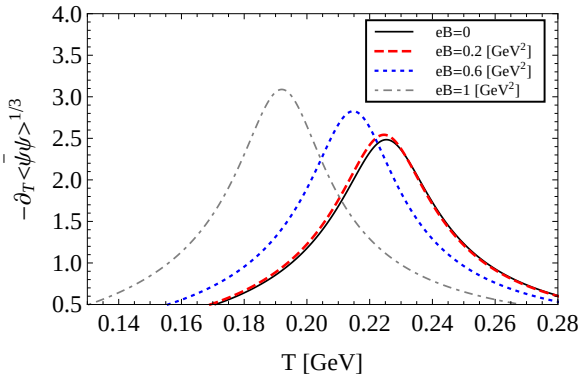

Figure 4.12: Thermal gradient of the chiral condensate $-\partial_T\langle\bar{\psi}\psi\rangle^{1/3}$. The pseudo-critical temperature decreases with the increase of the magnetic field strength eB.

$T_c^\chi \simeq T_c^c \equiv T_c \approx 225$ MeV. We then include the influence of a uniform magnetic field in the Schwinger proper-time formalism.

In the mean field limit, our effective phase diagram shows an increasing of $T_{c,B}$ for strong magnetic fields. This picture is in agreement with the appearance of magnetic catalysis in our model. The rising of $T_{c,eB}$ might be understood because a constant $\alpha_{eff}(0)$ is fully oblivious to any reminiscent back reaction effect of gluon interacting with magnetic fields which later would have been integrated out to define in our model. On the contrary, the magnetic field dependent coupling $\alpha_{\text{eff}}(\kappa)$ of Eq. (**??**) mimics the screening of gluon interactions in the infra-red

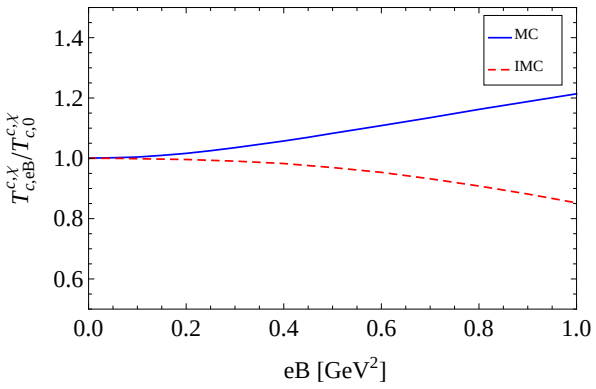

Figure 4.13: Effective phase diagram in the $T - eB$ plane IMC: Solid curve corresponds to the constant $\alpha_{\text{eff}}(0)$ in Eq. (**??**), whereas the dashed curve is obtained with $\alpha_{\text{eff}}(\kappa)$ in Eq. (**??**).

that occurs in QCD and triggers the appearance of the inverse magnetic catalysis effect. Our findings provide support to models in which the effective coupling, which may be considered proportional to the running coupling of QCD, behave as monotonically decreasing functions of the strength of the external magnetic field [**?**]. The running coupling model that we used in this Chapter must be improved by including the effect of the temperature and eventually the baryon chemical potential for the more realistic description of the phase diagram. Furthermore, the entanglement between the chiral and confinement pseudo-critical temperatures already hints that the back reaction effect also modifies the mechanism for confinement in a non trivial way still worth to explore in further detail.
In the next Chapter we present the final remarks and conclusions of the thesis.

Chapter 5

Final remarks and conclusion

Schwinger-Dyson equations (SDE) is one of the prominent tool to understand non-perturbative aspects of QCD. SDE at finite temperature and density play and important role to explore phase transitions that took place a few microsecond after the Big-Bang. This thesis is based on the SDE for the quark propagator at finite temperature and density. We studied different kernel models of the gap equation in Landau gauge and used the bare-vertex approximation to explore the QCD phase diagram in $T-\mu$ plane under extreme conditions of temperature and density. Lattice QCD provides reliable results at finite T and $\mu = 0$. According to this framework, the transitions from chiral symmetry breaking-restoration and confinement-deconfinement are cross-over for finite current quark masses. The critical temperature is $T_c = 155 \pm 15$ MeV for $N_f = 2$ quark flavors. At finite μ, lattice simulations suffer of the so-called sign problem and hence are unable to provide satisfactory results beyond the $\mu \simeq 0$ region. SDE have the advantage of not exhibiting the sign problem. In parallel, SDE and some other effective models of QCD have shown that at large μ and at $T = 0$, the transitions we are discussing are of first-order. When both finite T and μ are taken into account, a point in the middle of the phase diagram should be reached where the cross-over (with finite current quark mass) or second-order (in the chiral limit) phase transitions end and the first-order phase transition starts. According to the Clasious-Clapeyron condition, the first-order line in the phase diagram hits vertically the μ-axis and at finite μ when $T \to 0$. Similarly, at small μ, the phase diagram hits the vertical axis with a very small inclination. Though the exact location of the critical end point is less known as for as the experiment and lattice is concerned, other non-perturbative approaches provide the coordinates of such a point in the vicinity of ($\mu_E/T_c \approx 1$,$T_E/T_c \approx 1$). We took a step in this regard and studied three distinct (CMA, ICI and CI) kernel models of the gap equation from which we observed the existence of the critical end point in the phase diagram. Our results agree with lattice for finite T and full momentum dependent SDE-MT [**?**], at $\mu = 0$ as well as with experimental prediction in Heavy Ion Collision [**?**]. Our findings are summarized in Fig. **??**.

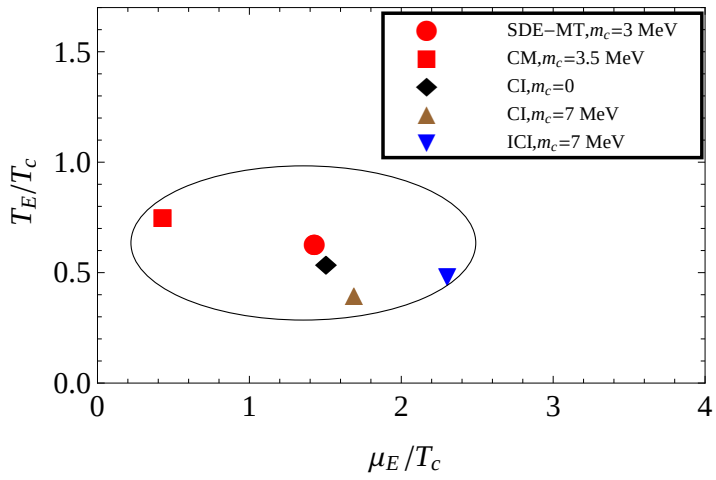

Figure 5.1: *QCD phase diagram*: The critical end points from cross-over to first-order for all the phase diagrams i.e., the SDE-MT [**?**] with $m_c = 3$ MeV, the CMA with $m_c = 3.5$ MeV, the CI with $m_c = 7$ MeV, the ICI with $m_c = 7$ MeV and from second-order to first-order for CI model in the chiral limit.

We notice that $3(\mu_E/T_c)_{CMA} \simeq (\mu_E/T_c)_{SDE}$, while $(T_E/T_c)_{CMA} \approx (T_E/T_c)_{SDE}$. We interpret this in the following terms: At $\mu = 0$, the phase transitions are purely due to the thermal fluctuations of sea quarks and gluons, that equally effect the static and the dynamical valence quarks. When a finite chemical is taken into account, it affects on the phase transitions, three times stronger on the static quarks (CMA) than on dynamical quarks (full momentum dependent SDE-MT [**?**]). Although the transitions that we are studying in this thesis took place in the early universe, their consequences leave prints in experimental signals of heavy ion collisions, for instance. In these experiments, the strongest magnetic field in the universe are created for a brief instant of time. Nevertheless, its effect on the chiral and deconfinement transitions have called the attention of a sector of the high energy physics community. In this connection, within the CI model, we consider the effect of an external magnetic field on the $T_c^{\chi,c}$. Magnetic catalysis appears in our model when the coupling does not include the influence of the magnetic field. But considering that the magnetic field brings quarks closer together as its strength increases, rendering quarks faster into the asymptotically free domain, by considering coupling [**?**] that runs weaker with an increasing magnetic field, which is also introduced in slightly different form in [**?**, **?**], we found the phenomenon of inverse magnetic catalysis [**?**], which agrees well with recent lattice results [**?**] and some effective models i.e., NJL-PNJL models [**?**] linear sigma model [**?**] and other predictions.

In the future, we pretend to extend our work with a more refined kernel of the QCD gap

equation to explore other areas of current interest such as Roberge Wiess-periodicity, the effect of magnetic field on the QCD phase diagram at finite density with full momentum dependent SDE, CMA and CI. We are also planing to extend this work to study neutron stars and the color-flavor-locked phase (CFL) of the QCD phase diagram.

Appendix A

QCD Essentials

A.1 QCD Lagrangian

The QCD Lagrangian density is given by

$$\mathcal{L}_{QCD} = -\frac{1}{4}F^{s}_{\mu\nu}F^{s\mu\nu} + \sum_{a=1}^{3}\sum_{A=1}^{N_f}\bar{\psi}^{A}_{a}\left(i\gamma^{\mu}D_{\mu} - m_{A}\right)\psi^{A}_{a}. \tag{A.1.1}$$

The first term in Eq. (**??**) is the gauge field part and the second term represents the Dirac part. ψ and $\bar{\psi}$ are the quark and an antiquark filed, respectively, and m_f is the current quark mass corresponding to each flavor. Here,

$$F^{s}_{\mu\nu} = \partial_{\mu}G^{s}_{\nu} - \partial_{\nu}G^{s}_{\mu} - g_{s}f_{stu}G^{t}_{\mu}G^{u}_{\nu} \tag{A.1.2}$$

is the gauge filed strength tensor,

$$D_{\mu}\psi^{A}_{b} = \partial_{\mu}\psi^{A}_{a} + \frac{ig_{s}}{2}G^{t}_{\mu}(\lambda^{t})_{ab}\psi^{A}_{b} \tag{A.1.3}$$

is the covariant derivative of the fermionic field and g_s is the strong coupling. The matrices λ^{α} are the Gell-Mann matrices with $s, t, u = 1, ..., 8$ as an internal symmetry index, that satisfy the $SU(3)$ Lie algebra

$$[\lambda_{s}, \lambda_{t}] = 2if_{stu}\lambda_{u}. \tag{A.1.4}$$

The f_{stu} are the $SU(3)$ structure constant. There are 8 gluon fields G^{t}_{μ} and $N_f = 6$ flavors of quarks in the present world. Each quark exist in three color states (red, green, blue) that is the reason the index $a = 1, 2, 3$ stands for the colors in the Lagrangian density. Gluons are bi-colored (color and anti-color) object. The QCD Lagrangian posses all the flavor symmetries of

a free quark model, which are only broken by a lack of degeneracy in the quark masses. It also have the well-known strong interaction symmetries, such as invariance under charge conjugation and space inversion. The Lagrangian contains $N_f + 1$ parameters: the quark masses, one for each flavor, plus one dimensionless coupling constant, g_s. There is another parameter hidden, a vacuum angle related to the possibility of strong CP violation, which is however experimentally found consistent with zero.

The quark-gluon coupling contained in the Dirac part of Eq. (**??**) is given by

$$\mathcal{L}_{qgc} = \frac{g_s}{2}\gamma_\mu \bar{\psi} G_t^\mu \lambda_t \psi, \tag{A.1.5}$$

which contribute $\int d^4x L_{qgc}$ to the action, which leads to the quark-gluon vertex

$$\frac{g_s}{2}\gamma_\mu (\lambda_t)_{ab}\delta_{AB}. \tag{A.1.6}$$

The quark propagator that can be obtained from the free Dirac part of Eq. (**??**) is of the form

$$S(p) = \frac{i\delta_{ab}\delta_{AB}}{\not{p} - m_A}, \tag{A.1.7}$$

with $\not{p} = \gamma_\mu p^\mu$. Gluon propagator can be obtained from the pure gauge sector (from the first term of Eq. (**??**)) and is given by

$$iD^{ab}_{\mu\nu}(q) = \frac{i\delta^{ab}}{q^2}\left(\delta_{\mu\nu} - (1-\xi)\frac{q_\mu q_\nu}{q^2}\right), \tag{A.1.8}$$

where ξ is the gauge parameter. In Landau gauge $\xi = 0$, the gluon propagator is of the form

$$iD^{ab}_{\mu\nu}(q) = \frac{i\delta^{ab}}{q^2}\left(\delta_{\mu\nu} - \frac{q_\mu q_\nu}{q^2}\right), \tag{A.1.9}$$

whereas in Feynman gauge $\xi = 1$, it is of the form

$$iD^{ab}_{\mu\nu}(q) = \frac{i\delta^{ab}\delta_{\mu\nu}}{q^2}. \tag{A.1.10}$$

The above mentioned propagators are free or bare.

A.2 QCD running coupling

The interaction among the quarks and gluons can also be represented by the running coupling constant. In QCD the gauge coupling constant g_s of the local $SU(3)_c$ appears, playing the

role similar to e, electric charge in QED. The "strong" fine structure constant is defined as $\alpha_s = g_s^2/4\pi$ and momentum dependence is given by [**?**]

$$\alpha_s(|q^2|) = \frac{\alpha_s(\mu^2)}{1 + \frac{\alpha_s(\mu^2)}{12\pi}(11N_c - 2N_f)\ln(|q^2|/\mu^2)}, \tag{A.2.1}$$

where $N_f = 6$ represents the number of quark flavors and $N_c = 3$ is the number of colors. Since $11N_c > 2N_f$, as a result, the strength of $\alpha_s(|q^2|)$ decreases at small distances or high energies ($\alpha_s(|q^2|) \to 0$ as $|q^2| \to \infty$). This property of QCD is called "asymptotic freedom". The parameter μ, with the dimensions of mass, remains as a relic of the renormalization. At sufficiently low $|q^2|$, the effective coupling becomes large. It is customary to denote the $|q^2|$ scale at which this happens by Λ^2_{QCD}, namely

$$\Lambda^2_{QCD} = \mu^2 \exp\left[\frac{-12\pi}{(11N_c - 2N_f)\,\alpha_s(\mu^2)}\right]. \tag{A.2.2}$$

Thus Eq. (**??**) implies that

$$\alpha_s(|q^2|) = \frac{12\pi}{(11N_c - 2N_f)\ln(|q^2|/\Lambda^2_{QCD})}. \tag{A.2.3}$$

For $|q^2| \gg \Lambda^2$, the effective coupling $\alpha_s(|q^2|)$ is small and hence quarks and gluons interact weakly, and therefore a perturbative description makes sense. For $|q^2| \leq \Lambda^2_{QCD}$, the quarks and gluons will arrange themselves into strongly bound, clusters, namely hadrons and a non-perturbative treatment is necessary. Λ_{QCD} is a free parameter, whose value is determined from the experiment. It is found to be in the range of 0.1 GeV to 0.5 GeV.

A.3 Confinement

In QCD, the strong coupling vanishes ($\alpha_s(|q^2|) \to 0$) asymptotically at infinitely high energy ($|q^2| \to \infty$) and quarks are non interacting and free inside hadrons. On the other hand, at low energy ($|q^2| \leq \Lambda^2_{QCD}$) and for sufficiently large $\alpha_s(|q^2|)$, quarks interact strongly and are confined inside the hadrons. Thus, QCD exhibits confinement of color. The only finite-energy asymptotic states of QCD are color-singlets. If one attempts to separate a color-singlet state into its color constituents, for instance by breaking a meson into a quark and an antiquark, a tube of gluons would form between these two color sources. With sufficiently strong coupling, this tube has fixed radius. So the energy cost of separating color sources would grow proportionally with the separation distance, i.e.,

$$V(r) = -\frac{\alpha_s}{r} + \sigma r. \tag{A.3.1}$$

When $r \to 0$, the first term dominates and hence quarks behave as free particles, while for $r \to \infty$, the second term plays a leading role and hence quarks are strongly confined inside the hadrons.

A.4 Chirality

A chiral (Greek word for hand) phenomenon is one that is not identical to its mirror image. The relative orientation of the spin ($\vec{s}$) of a particle and its momentum $\vec{p}$ can be used to define a "handedness", or helicity $h = \vec{s} \cdot \vec{p} / |\vec{p}|$. For massless particles, it is a Lorentz invariant quantity. The helicity of a particle is right-handed if the direction of its spin is the same as the direction of its motion and it is left-handed if the directions of spin and motion are opposite, as shown in Fig. **??**.

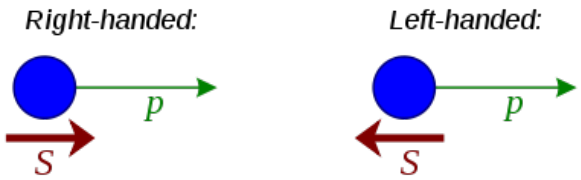

Figure A.1: Helicity states of the particle.

Massless particles (photons, gluons and gravitons) have a definite helicity, either positive or negative and it is Lorentz invariant. For massive particles (electrons, quarks and neutrinos) the helicity is a frame dependent quantity; it is possible for an observer to change to a reference frame that overtakes the spinning particle, in which case the particle will then appear to move backwards, and its helicity (which may be thought of as "apparent chirality") will be reversed. Chirality for a Dirac fermion ψ is defined through the operator γ^5, which has eigenvalues ± 1. Any Dirac field can thus be projected into its left-handed or right-handed component by acting with the projection operators:

$$\psi_L = \frac{1-\gamma^5}{2}\psi, \qquad \psi_R = \frac{1+\gamma^5}{2}\psi. \tag{A.4.1}$$

A theory that is asymmetric with respect to chiralities is called a chiral theory, while a non-chiral (i.e., parity-symmetric) theory is sometimes called a vector theory. Many pieces of the Standard Model of Particle Physics are non-chiral, which is traceable to anomaly cancellations in chiral theories. QCD is an example of a vector theory, since both chiralities of all quarks appear in the theory, and couple to gluons in the same way.

Symmetries of the QCD Lagrangian: According to Noether's theorem "each continuous

symmetry[1] of the Lagrangian density is associated with a conserved current current J_μ that satisfy $\partial^\mu J_\mu = 0$ and a conserved charge $Q = \int d^3x J_0$ that is constant in time".
The global symmetries of the above Lagrangian are following
$\mathbf{U_V(1)}$ symmetry (conservation of baryon number): If the Lagrangian is invariant under the $U_V(1)$ transformation

$$\psi \to e^{-i\alpha}\psi \tag{A.4.2}$$

where the parameter α is independent of space time coordinates. The associated conserved current is $J^k_\mu = \bar{\psi}\gamma_\mu\psi$ and the conserved charge is the conservation of baryon number. This symmetry is an exact symmetry in nature.
$\mathbf{SU_V(2)}$ symmetry (Isospin): When $m_u = m_d$ (up quark mass=down quark mass), the Lagrangian is invariant under rotation in space. The transformation in this case are

$$\psi \to e^{-i\frac{\vec{\sigma}\cdot\vec{\theta}}{2}}\psi \tag{A.4.3}$$

which leads to the conserved current $J^k_\mu = \bar{\psi}\gamma_\mu\sigma^k\psi$, $k = 1, 2, 3$. Here $\vec{\sigma}$ are the generator of the rotation (which are Pauli spin matrices in this case) and $\vec{\theta}$ are the rotation parameters. In general the mass of up and down quark are not exactly equal and thus isospin symmetry is only approximate symmetry of nature.
$\mathbf{SU_A(2)}$ symmetry: In the chiral limit, when the current quark mass $m_0 = 0$, the $SU_A(2)$ transformation are

$$\psi \to e^{-i\frac{\vec{\sigma}\cdot\vec{\theta}\gamma_5}{2}}\psi \tag{A.4.4}$$

is a symmetry and the corresponding conserved current is $J^k_{\mu 5} = \bar{\psi}\gamma_\mu\gamma_5\sigma^k\psi$. When $m_0 \neq 0$, this symmetry is explicitly broken by the part $m_0\bar{\psi}\psi$ in the Lagrangian density. This symmetry also broken spontaneously in the vacuum even in the chiral limit. According to the Goldstone theorem the spontaneous braking of a symmetry leads to the appearance of massless bosons, that are the massless bosons in the chiral limit.
$\mathbf{U_A(1)}$ symmetry (Axial): The $U_V(1)$ transformation are

$$\psi \to e^{-i\beta\gamma_5}\psi \tag{A.4.5}$$

where β is parameter of the transformation. The associated current is this case $J^k_{\mu 5} = \bar{\psi}\gamma_\mu\gamma_5\psi$. The $U_V(1)$ is explicitly violated due to quantum anomaly[2].
The above global symmetries summarize below in the table.

[1]Transformation of the fields under which the Lagrangian density of the system remain invariant.

[2]A chiral anomaly is the anomalous nonconservation of a chiral current. In some theories of fermions with chiral symmetry, the quantization may lead to the breaking of this (global) chiral symmetry. In that case, the charge associated with the chiral symmetry is not conserved. The non-conservation happens in a tunneling process from one vacuum to another. Such a process is called an instanton.

Group	Symmetry	Transformation	Current
$SU(2)_V$	Isospin	$\psi \to e^{i\vec{\sigma}.\vec{\theta}/2}\psi$	$J^k_\mu = \bar{\psi}\gamma_\mu\sigma^k\psi$
$U(1)_V$	Baryonic	$\psi \to e^{i\alpha}\psi$	$J^k_\mu = \bar{\psi}\gamma_\mu\psi$
$SU(2)_A$	Chiral	$\psi \to e^{i\vec{\sigma}.\vec{\theta}\gamma_5/2}\psi$	$J^k_{\mu 5} = \bar{\psi}\gamma_\mu\gamma_5\sigma^k\psi$
$U(1)_A$	Axial	$\psi \to e^{-i\beta\gamma_5}\psi$	$J^k_{\mu 5} = \bar{\psi}\gamma_\mu\gamma_5\psi$

Table A.1: Symmetries of QCD Lagrangian with $N_f = 2$ for massless quarks.

Chiral Symmetry: Chiral symmetries are symmetries under which the left-handed and right-handed parts of the field transform independently, i.e.,

$$\psi_L = \frac{1-\gamma^5}{2}\psi, \qquad \psi_R = \frac{1+\gamma^5}{2}\psi. \tag{A.4.6}$$

The Dirac part of the QCD Lagrangian Eq. (**??**) with $N_f = 2$, can be decomposed in terms of left-handed and right-handed as

$$\mathcal{L}_{qcd} = \bar{\psi}_L^{u,d}\left(i\not{D}\right)\psi_L^{u,d} + \bar{\psi}_R^{u,d}\left(i\not{D}\right)\psi_R^{u,d} - \bar{\psi}_L^{u,d}\left(m_{u,d}\right)\psi_R^{u,d} - \bar{\psi}_R^{u,d}\left(m_{u,d}\right)\psi_L^{u,d}. \tag{A.4.7}$$
$$\tag{A.4.8}$$

For massless quarks $m_u = m_d = m_0 = 0$, the left and right-handed components decouple and so the Lagrangian has bigger symmetry. It has $SU(2)_V \otimes SU(2)_A$[3] chiral symmetry which can be written as

$$SU(2)_V \otimes SU(2)_A \cong SU(2)_L \otimes SU(2)_R, \tag{A.4.9}$$

and the Lagrangian is invariant under the transformation

$$\psi_R \to e^{-i\vec{\sigma}\cdot\vec{\theta}_R}\psi_R, \qquad \psi_L \to e^{-i\vec{\sigma}\cdot\vec{\theta}_L}\psi_L. \tag{A.4.10}$$

This chiral symmetry can equally well regarded as vector–axial-vector symmetry [**?**]. Let us define

$$\theta_V = \frac{\theta_L + \theta_R}{2}, \qquad \theta_A = \frac{\theta_L - \theta_R}{2}. \tag{A.4.11}$$

Then, the Lagrangian is invariant under the transformation

$$\psi \to e^{-i\vec{\sigma}\cdot\vec{\theta}_V}\psi, \qquad \psi \to e^{-i\vec{\sigma}\cdot\vec{\theta}_A\gamma_5}\psi. \tag{A.4.12}$$

[3]The chiral symmetry transformation can be divided into a component that treats the left-handed and the right-handed parts equally, known as vector symmetry (V), and a component that actually treats them differently, known as axial symmetry (A).

A rotation through an equal angle to left and right corresponds to the vector transformation, while a rotation by equal and opposite angles to right and left gives an axial transformation.

When $m_u = m_d \neq 0$, the QCD Lagrangian does not posses the chiral symmetry, because the mass term in the Lagrangian, $\bar{\psi} m_{u,d} \psi$ breaks it explicitly. The chiral symmetry $SU(2)_L \otimes SU(2)_R$ breaking also take place spontaneously in the vacuum by a quark-atiquark condensate $\langle \bar{\psi}\psi \rangle \neq 0$ formed through non-perturbative interactions of quarks and gluons, into the diagonal vector subgroup $SU(2)_V$ known as isospin. The Goldstone bosons that correspond to the three broken generators are the pions. As a consequence, the effective theory of QCD bound states like the baryons, must now include mass terms for the constituent quarks, ostensibly disallowed by unbroken chiral symmetry. Thus, this chiral symmetry breaking induces the bulk of hadron masses, such as those for the nucleon, i.e., the bulk of the mass of all visible matter. The spontaneous breaking of chiral symmetry takes place for both with a current quark mass and in the chiral limit (massless quark).

A.4.1 The order parameter for the chiral symmetry breaking

Above, we discussed the patterns of chiral symmetry breaking. Now we discuss the corresponding order parameter. The Fourier transform of the quark propagator in position space is given by

$$S(x) = \int \frac{d^4p}{(2\pi)^4} e^{-ip.x} S(p). \tag{A.4.13}$$

At the origin of the co-ordinate space $x \to 0$, we have

$$S(x \to 0) = \int \frac{d^4p}{(2\pi)^4} S(p). \tag{A.4.14}$$

The chiral quark condensate is defined as

$$-\langle \bar{\psi}\psi \rangle = N_c Tr[S(x \to 0)] = N_c \int \frac{d^4p}{(2\pi)^4} Tr[S(p)]. \tag{A.4.15}$$

In the Schwinger-Dyson equations framework (discussed in Chapter 2) the dressed quark propagator is given by

$$S(p) = i\gamma \cdot p \sigma_v(p^2) + \sigma_s(p^2). \tag{A.4.16}$$

Thus the final expression for the chiral condensate is

$$-\langle \bar{\psi}\psi \rangle = 4N_c \int \frac{d^4p}{(2\pi)^4} \sigma_s(p^2), \tag{A.4.17}$$

where

$$\sigma_s(p^2) = \frac{F(p^2)M(p^2)}{p^2 + M^2(p^2)}, \qquad \sigma_v(p^2)\frac{F(p^2)}{p^2 + M^2(p^2)}, \tag{A.4.18}$$

with M the dynamically generated mass and $F(p^2)$ the quark wavefunction renormalization function. In the chiral limit, when $-\langle\bar{\psi}\psi\rangle \neq 0$, chiral symmetry is said to be dynamically broken and the chiral condensate is an exact order parameter, while $-\langle\bar{\psi}\psi\rangle = 0$, corresponds to the chirally symmetric phase. In the presence of the current quark mass, it is considered to be an approximate order parameter. Quark condensate satisfies the Gell-Mann-Oakes-Renner (GMOR) formula

$$-\langle\bar{\psi}\psi\rangle = \frac{1}{2}\frac{m_\pi^2 f_\pi^2}{(m_u + m_d)}, \tag{A.4.19}$$

with

$$f_\pi^2 = 4N_c \int \frac{d^4p}{(2\pi)^4}\sigma_s(p^2)\left[M(p^2) - \frac{p^2}{2}\frac{dM}{dp^2}\right] \tag{A.4.20}$$

is the pion decay constant and m_π is the mass of the pion, which can easily be calculated once we know the value of $\langle\bar{\psi}\psi\rangle$ and f_π. For example with $m_u + m_d = 13$ MeV, $\langle\bar{\psi}\psi\rangle = -(0.23\text{ GeV})^3$, and $f_\pi = 92$ MeV, the mass of the pion is found to be $m_\pi = 137$ MeV.

A.4.2 Reflection positivity and confinement

According to the axiom of violation of positivity, "if a certain degree of freedom has negative norm contributions in its propagator, it cannot describe a physical asymptotic state, i.e. absence of Kallen-Lehmann spectral representation for its propagator" [**?**]. In Euclidean quantum field theory, positivity is formulated in terms of the Osterwalder-Schrader axiom of reflection positivity [**?**]. In the special case of a two-point correlation function $\Delta(x - y)$, this condition can be written as

$$\int d^4x d^4y\ \bar{g}(\vec{x}, x_4)\Delta(x - y)g(\vec{y}, y_4) \geq 0, \tag{A.4.21}$$

where $g(\vec{x}, x_4)$ is a complex valued test function with support in $\{(\vec{x}, x_4) : x_4 = t > 0\}$. On applying the three dimensional Fourier transformation as argued in [**?**], this condition implies

$$\int_0^\infty dt \int_0^\infty dt' \int d^3p\ \tilde{\bar{g}}(t, \vec{p})\Delta\left(-(t + t'), \vec{p}\right)\tilde{g}(t', \vec{p}) \geq 0. \tag{A.4.22}$$

The above condition is valid only in a region around $t_0 = (t + t')$ where $\Delta(-t_0, \vec{p}) < 0$. One can choose a real test function $g(t)$ which peaks at t and t', and could immediately lead to a violation of reflection positivity. Thus the condition Eq. (**??**), for a special case of $\vec{p} = 0$, yield the "spatially averaged Schwinger function"

$$\Delta(t)_{v,s} = \frac{1}{2\pi}\int dp_4 e^{-ip_4 t}\sigma_{v,s}(p_4, \vec{0}) = \frac{1}{\pi}\int dp_4 \cos(p_4 t)\sigma_{v,s}(p_4, \vec{0}) \geqslant 0. \tag{A.4.23}$$

Form the above equation, one can write the Schwinger function as

$$\Delta(t)_{v,s} = \int d^3x \int \frac{d^4p}{(2\pi)^4} e^{-i(\vec{p}.\vec{x}+p_4 t)}\sigma_{v,s}(p^2), \tag{A.4.24}$$

where $\sigma_{v,s}$ were defined in Chapter 2. Thus, for the stable (free particle) $\Delta(t) \geq 0$, On setting $x = p^2 > 0$, the order parameter for confinement is defined as the inflection point x_c, i.e., the point at which

$$\left.\frac{d^2\sigma_v(x)}{dx^2}\right|_{x=x_c} = 0, \tag{A.4.25}$$

provided $x_c > 0$. The non existence of inflection points means the absence of confinement in the propagator.

A.4.3 QCD phase transitions

After the discovery of the asymptotic freedom and confinement, another question arose: What happens when a heat bath at finite temperature is taken into account? In response to this question, Collins [**?**] and Cabibo [**?**] in 1975 predicted the existence of a deconfined state of quarks and gluons at high temperature and/or high pressures. At sufficiently high temperatures, quarks and gluons interact weakly and the system behaves as an ideal ultra-relativistic gas. The degrees of freedom are then determined by the flavor numbers, spin states, color and charge states of quarks and gluons. Later, such deconfinened state was named *quark gluon plasma* (QGP)[4]. When colorless particle dissociate to create deconfined matter, one open question, after the discovery of asymptotic freedom, concerned with the properties of the transition from the hadron gas to the QGP: Does it take place smoothly or via a phase transition and exhibiting critical behavior? Another question was whether the QGP phase transition exists? Indeed, the chiral symmetry of the QCD Lagrangian with massless quark is spontaneously broken at low temperatures and this symmetry should be restored at high temperatures. This represents a valid condition to predict the existence of a QCD phase transition. It remained, however, an

[4]The word plasma is used to describe the state of matter when ions and electrons are dissociated in atoms.

open question if the chiral symmetry transition and the deconfinement transition are or not the same one. The answer is provided by SDE (that we studied in this dissertation) and Lattice QCD among other approaches.

Hadronic matter to quark gluon plasma: The bag model

According to the bag model: "hadrons are like little bubbles of (perturbative) vacuum or bags in which the quarks are to be treated as free particles (asymptotic freedom). Outside of the bag, quarks and gluons can not appear as free particles i.e., they are confined. The above mentioned feature can be achieved by considering a constant energy density B, (the bag constant) for the vacuum, which keeps quarks and gluons confined" [**?**]. The total energy of the hadrons is given by

$$E_H = \frac{4\pi}{3}R^3 + \frac{C}{R}, \tag{A.4.26}$$

where the first term represent the finite energy density of the vacuum associated with the volume of the bag, while the second term is the kinetic energy of the quark (in accordance with the uncertainty principle) inside the bag in the form of sphere with radius R. The value of R can be obtained by minimizing Eq. (**??**) with respect to R, which yields

$$R = \left(\frac{C}{4\pi B}\right)^{1/4}, \tag{A.4.27}$$

and

$$C = 4\pi B R^4. \tag{A.4.28}$$

Using Eq. (**??**) in Eq. (**??**) and setting $E_H = M_H$, the mass of the hadron is given by

$$M_H = \frac{16\pi}{3}R^3 B. \tag{A.4.29}$$

For $M_H = 1$ GeV, the bag constant $B^{1/4} = 200$ MeV. On the other hand, pressure P is given by

$$P = -\frac{\partial E_H}{\partial V} = -B + \frac{C}{4\pi}. \tag{A.4.30}$$

In case of two light quark and at zero density, the transition temperature from hadronic gas to the QGP can be calculated through balancing of the pressure of the ideal gas of massless hadrons (three states of pion) and the pressure of plasma phase. The pressure for ideal hadron (boson) gas is defined through the Stefan-Boltzmann law

$$P_{HG} = f_b \frac{\pi^2 T^4}{90}, \tag{A.4.31}$$

with $f_b = 3$, are the boson degrees of freedom. The pressure of the QGP is defined as

$$P_{QGP} = \left(f_{gb} + \frac{7}{8} f_{qf} \right) \frac{\pi^2 T^4}{90} - B, \tag{A.4.32}$$

where $f_{gb} = 2$ (spin states) $\times 8$ (no. of gluons), represents the gluon degrees of freedom and $f_{qf} = 3$ (three color)$\times 2$ (flavor) $\times 2$ (spin states) $\times 2$ (charge states corresponding to quarks and antiquarks), denote the quarks degrees of freedom. The factor 7/8 in Eq. (**??**) is introduced to obtain the correct statistics. Thus, setting $P_{HG} = P_{QGP}$, we have

$$T_c = \left(\frac{45B}{17\pi^2} \right)^{1/4}. \tag{A.4.33}$$

With $B^{1/4} = 200$ MeV, the critical temperature is found to be $T_c = 144$ MeV, (Recall 100 MeV $= 166 \times 10^9$ K) and the transition is of first order. Which is controversial because some recent effective models and SDE study, shows that the transition are second order in the chiral limit and cross-over in the presence of current quark mass. Lattice QCD with $N_f = 2$ with current quark mass also supported the smooth cross-over.

Hadronic matter to quark gluon plasma: SDE

The transition temperature for chiral symmetry breaking-restoration in the framework of SDE can be calculated through the chiral condensate. In the chiral limit, the temperature at which $-\partial_T \langle \bar{\psi}\psi \rangle^{1/3}$ diverges is the critical temperature of the chiral symmetry restoration. The transition is supposed to be of second order. In the presence of a current quark mass, the temperature at which $-\partial_T \langle \bar{\psi}\psi \rangle^{1/3}$ peaks is the pseudo-critical temperature and the transition in this case will be smooth cross-over.
The deconfinement temperature in the SDE can be calculated from the "Spatially Averaged propagator" (see section 7.4.2). At finite temperature (discussed in Chapter. 3), it is given by

$$\Delta(\tau) = T \sum_n e^{-i\omega_n \tau} \frac{M(0, \omega_n^2)}{\omega_n^2 + M^2(0, \omega_n^2)}. \tag{A.4.34}$$

At low temperature, the function $\Delta(\tau)$ oscillates with high amplitude and hence describes confinement. At sufficiently high temperature when $\Delta(\tau) \geqslant 0$, the amplitude of oscillations vanishes, and the temperature at which it happens is regarded as the pseudo-critical temperature for deconfinement.

Hadronic matter to quark gluon plasma: Lattice

The critical temperature for chiral symmetry breaking-restoration in lattice also studied through the quark-antiquark condensate. The transition temperature for confinment-deconfinement is

obtained from the expectation value of the Polyakov loop $\mathcal{P}$ [**?**].
Polakov loop: is a Wilson loop closed around the periodic Euclidean time direction, and is defined as a matrix in color space

$$\Phi(\vec{x}) = \Pi\text{exp}\left[i\int_0^{1/T} d\tau A_4\left(\vec{x},\tau\right)\right], \tag{A.4.35}$$

where Π denote the path ordering of the exponential and $A_4 = iA_0$. In Polaykov gauge, the matrix in diagonal form is given by

$$\Phi = \exp\left[i\left(\phi_3\lambda_3 + \phi_8\lambda_8\right)\right], \tag{A.4.36}$$

where the $\lambda' s$ are the Gell-Mann matrices and the $\phi' s$ are constant parameters. The expectation value of the trace of Eq. (**??**) is denoted by $\mathcal{P}$, and is given by

$$\mathcal{P} = \frac{1}{N_c}\left\langle \text{Tr}\Phi\right\rangle, \tag{A.4.37}$$

with $N_c = 3$ representing the number of colors. In pure gauge theory, with guage group $SU(N)$ the action S has a global $Z(N)$ symmetry. At finite temperature, this symmetry is spontaneously broken at the phase transition and the corresponding order parameter is the Polyakov loop expectation value $\mathcal{P}$, which is related to the free energy $E_q(T)$ induced by the static quark source in the gluonic heat bath i.e.,

$$\mathcal{P} = e^{-E_q(T)/T}. \tag{A.4.38}$$

When $E_q(T) \to \infty$, $\langle\mathcal{P}\rangle = 0$ and quarks are confined. For finite $E_q(T)$, when $\langle\mathcal{P}\rangle \neq 0$, it corresponds to the deconfined phase. Dual quark condensate (see Chapter 3) is another order parameter for the confinment-deconfinement phase transition introduced in lattice [**?**].

Appendix B

Gap equation at finite temperature

This Appendix is based on some mathematical steps of Chapter 2.

B.1 Traces and tensor contraction

$$\left(\delta_{\mu\nu} - \frac{Q_\mu Q_\nu}{Q^2}\right)\delta_{\mu\nu} = \left(\delta_{\mu\nu}\delta_{\mu\nu} - \frac{Q^2}{Q^2}\right) = 4 - 1 = 3. \tag{B.1.1}$$

$$\begin{aligned} P^T_{\mu\nu}\delta_{\mu\nu} &= P^T_{00}\delta_{00} + P^T_{i0}\delta_{i0} + P^T_{0j}\delta_{0j} + P^T_{ij}\delta_{ij} \\ = 0 + 0 + 0 + P^T_{ij}\delta_{ij} &= \left(\delta_{ij} - \frac{q_i q_j}{q^2}\right)\delta_{ij} = 3 - 1 = 2. \end{aligned} \tag{B.1.2}$$

$$Tr[\gamma_i p^i \gamma_\mu \gamma_j k^j \gamma_\nu] = 4p^i[\delta_{i\mu}\delta_{j\nu} - \delta_{ij}\delta_{\mu\nu} + \delta_{i\nu}\delta_{\mu\nu}]k^j. \tag{B.1.3}$$

$$\begin{aligned} Tr[\gamma_i p^i \gamma_\mu \gamma_0 \gamma_\nu] &= 4p^i[\delta_{i\mu}\delta_{0\nu} - \delta_{i0}\delta_{\mu\nu} + \delta_{i\nu}\delta_{\mu 0}] \\ &= 4p^i[\delta_{i\mu}\delta_{0\nu} + \delta_{i\nu}\delta_{\mu 0}]. \end{aligned} \tag{B.1.4}$$

$$
\begin{aligned}
P^T_{\mu\nu} Tr[\gamma_i p^i \gamma_\mu \gamma_j k^j \gamma_\nu] &= 4 P^T_{\mu\nu} p^i [\delta_{i\mu}\delta_{j\nu} - \delta_{ij}\delta_{\mu\nu} + \delta_{i\nu}\delta_{\mu\nu}] k^j \\
&= 4 p^i [P^T_{ij} - \delta_{ij} P^T_{\mu\nu}\delta_{\mu\nu} + P^T_{ij}] k^j \\
&= 4 p^i [2P^T_{ij} - 2\delta_{ij}] k^j \\
&= 4 p^i \left[2\left(\delta_{ij} - \frac{q_i q_j}{q^2}\right) - 2\delta_{ij} \right] k^j \\
&= 4 p^i \left(-2 \frac{q_i q_j}{q^2} \right) k^j \\
&= -8 \frac{(\vec{p}\cdot\vec{q})(\vec{q}\cdot\vec{k})}{q^2}.
\end{aligned} \tag{B.1.5}
$$

$$
P^T_{\mu\nu} Tr[\gamma_i p^i \gamma_\mu \gamma_0 \gamma_\nu] = 4 p^i P^T_{\mu\nu} [\delta_{i\mu}\delta_{0\nu} + \delta_{i\nu}\delta_{\mu 0}] = 4 p^i [P^T_{i0} + P^T_{0i}] = 0. \tag{B.1.6}
$$

$$
\begin{aligned}
\left(\delta_{\mu\nu} - \frac{Q_\mu Q_\nu}{Q^2}\right) Tr[\gamma_i p^i \gamma_\mu \gamma_j k^j \gamma_\nu] &= 4 p^i \left(\delta_{\mu\nu} - \frac{Q_\mu Q_\nu}{Q^2}\right) [\delta_{i\mu}\delta_{j\nu} - \delta_{ij}\delta_{\mu\nu} + \delta_{i\nu}\delta_{\mu\nu}] k^j \\
&= 4 \left[p^i (\delta_{ij} - 4\delta_{ij} + \delta_{ij}) k^j - \frac{p^i}{Q^2} (Q_i Q_j - \delta_{ij} Q^2 + Q_j Q_i) k^j \right] \\
&= 4 \left[-2(\vec{p}\cdot\vec{k}) - \frac{1}{Q^2} \left((\vec{p}\cdot\vec{q})(\vec{q}\cdot\vec{k}) - (\vec{p}\cdot\vec{k}) Q^2 + (\vec{k}\cdot\vec{q})(\vec{p}\cdot\vec{q}) \right) \right] \\
&= 4 \left[-2(\vec{p}\cdot\vec{k}) - 2\frac{(\vec{p}\cdot\vec{q})(\vec{q}\cdot\vec{k})}{Q^2} + \frac{(\vec{p}\cdot\vec{k}) Q^2}{Q^2} \right] \\
&= -4 \left[(\vec{p}\cdot\vec{k}) + 2\frac{(\vec{p}\cdot\vec{q})(\vec{q}\cdot\vec{k})}{Q^2} \right].
\end{aligned} \tag{B.1.7}
$$

$$
\begin{aligned}
\left(\delta_{\mu\nu} - \frac{Q_\mu Q_\nu}{Q^2}\right) Tr[\gamma_i p^i \gamma_\mu \gamma_0 \gamma_\nu] &= 4 \left(\delta_{\mu\nu} - \frac{Q_\mu Q_\nu}{Q^2}\right) p^i [\delta_{i\mu}\delta_{0\nu} + \delta_{i\nu}\delta_{\mu 0}] \\
&= 4 \left[p^i \delta_{\mu\nu} (\delta_{i\mu}\delta_{0\nu} + \delta_{i\nu}\delta_{\mu 0}) - p^i \frac{Q_\mu Q_\nu}{Q^2} (\delta_{i\mu}\delta_{0\nu} + \delta_{i\nu}\delta_{\mu 0}) \right] \\
&= 4 \left[p^i (\delta_{i0} + \delta_{i0}) - p^i \left(\frac{Q_i Q_0}{Q^2} + \frac{Q_0 Q_i}{Q^2} \right) \right] \\
&= 4 \left[(0) - \frac{(\vec{p}\cdot\vec{q}) q_0}{Q^2} + \frac{q_0 (\vec{p}\cdot\vec{q})}{Q^2} \right] \\
&= -4 \left[2\frac{(\vec{p}\cdot\vec{q})\Omega_{nl}}{Q^2} \right],
\end{aligned} \tag{B.1.8}
$$

where $Q_0 = q_0 = \Omega_{nl}$ and $Q_i = q_i = \vec{q}$.

$$Tr[\gamma_0\gamma_\mu\gamma_i\gamma_\nu]k^i = 4[\delta_{0\mu}\delta_{i\nu} - \delta_{0i}\delta_{\mu\nu} + \delta_{0\nu}\delta_{\mu i}]k^i. \tag{B.1.9}$$

$$\begin{aligned}\left(\delta_{\mu\nu} - \frac{Q_\mu Q_\nu}{Q^2}\right) Tr[\gamma_0\gamma_\mu\gamma_i\gamma_\nu]k^i &= 4\left(\delta_{\mu\nu} - \frac{Q_\mu Q_\nu}{Q^2}\right)[\delta_{0\mu}\delta_{i\nu} - \delta_{0i}\delta_{\mu\nu} + \delta_{0\nu}\delta_{\mu i}]k^i \\ &= 4\left[\delta_{\mu\nu}(\delta_{0\mu}\delta_{i\nu} - \delta_{0i}\delta_{\mu\nu} + \delta_{0\nu}\delta_{\mu i})k^i - \frac{Q_\mu Q_\nu}{Q^2}(\delta_{0\mu}\delta_{i\nu} - \delta_{0i}\delta_{\mu\nu} + \delta_{0\nu}\delta_{\mu i})k^i\right] \\ &= 4\left[(0) - \frac{q_0(\vec{q}\cdot\vec{k})}{Q^2} - \frac{q_0(\vec{q}\cdot\vec{k})}{Q^2}\right] = -4\left[2\frac{q_0(\vec{q}\cdot\vec{k})}{Q^2}\right] = -4\left[2\frac{\Omega_{nl}(\vec{q}\cdot\vec{k})}{Q^2}\right].\end{aligned} \tag{B.1.10}$$

$$\begin{aligned}Tr[\gamma_0\gamma_\mu\gamma_i\gamma_\nu]k^i &= 4P^T_{\mu\nu}[\delta_{0\mu}\delta_{i\nu} - \delta_{0i}\delta_{\mu\nu} + \delta_{0\nu}\delta_{\mu i}]k^i \\ &= 4[P^T_{0i} - P^T_{0i} + P^T_{i0}] = 0.\end{aligned} \tag{B.1.11}$$

$$Tr[\gamma_0\gamma_\mu\gamma_0\gamma_\nu]k^i = 4[\delta_{0\mu}\delta_{0\nu} - \delta_{00}\delta_{\mu\nu} + \delta_{0\nu}\delta_{\mu 0}] = 4[2\delta_{0\mu}\delta_{0\nu} - \delta_{\mu\nu}]. \tag{B.1.12}$$

$$\begin{aligned}\left(\delta_{\mu\nu} - \frac{Q_\mu Q_\nu}{Q^2}\right) Tr[\gamma_0\gamma_\mu\gamma_0\gamma_\nu] &= 4\left(\delta_{\mu\nu} - \frac{Q_\mu Q_\nu}{Q^2}\right)[2\delta_{0\mu}\delta_{0\nu} - \delta_{\mu\nu}] \\ &= 4\left[\delta_{\mu\nu}(2\delta_{0\mu}\delta_{0\nu} - \delta_{\mu\nu}) - \frac{Q_\mu Q_\nu}{Q^2}(2\delta_{0\mu}\delta_{0\nu} - \delta_{\mu\nu})\right] \\ &= 4\left[-2 - \frac{q_0^2}{Q^2} + 1\right] = -4\left[1 + \frac{q_0^2}{Q^2}\right] = -4\left[1 + \frac{\Omega_{nl}^2}{Q^2}\right].\end{aligned} \tag{B.1.13}$$

$$Tr[\gamma_\alpha\gamma_\mu\gamma_\beta\gamma_\nu] = 4[\delta_{\alpha\mu}\delta_{\beta\nu} - \delta_{\alpha\beta}\delta_{\mu\nu} + \delta_{\alpha\nu}\delta_{\mu\beta}]. \tag{B.1.14}$$

$$\begin{aligned}\left(\delta_{\mu\nu} - \frac{q_\mu q_\nu}{q^2}\right) Tr[\gamma_\alpha p^\alpha\gamma_\mu\gamma_\beta k^\beta\gamma_\nu] &= 4p^\alpha\left(\delta_{\mu\nu} - \frac{q_\mu q_\nu}{q^2}\right)[\delta_{\alpha\mu}\delta_{\beta\nu} - \delta_{\alpha\beta}\delta_{\mu\nu} + \delta_{\alpha\nu}\delta_{\mu\beta}]k^\beta \\ &= 4\left[p^\alpha(\delta_{\alpha\beta} - 4\delta_\beta + \delta_{\alpha\beta})k^\beta - \frac{p^\alpha}{q^2}(q_\alpha Q_\beta - \delta_{\alpha\beta}q^2 + q_\beta Q_\alpha)k^\beta\right] \\ &= 4\left[-2(\vec{p}\cdot\vec{k}) - \frac{1}{q^2}[(\vec{p}\cdot\vec{q})(\vec{q}\cdot\vec{k}) - (\vec{p}\cdot\vec{k})\vec{q}^2 + (\vec{k}\cdot\vec{q})(\vec{p}\cdot\vec{q})]\right] \\ &= 4\left[-2(\vec{p}\cdot\vec{k}) - 2\frac{(\vec{p}\cdot\vec{q})(\vec{q}\cdot\vec{k})}{\vec{q}^2} + \frac{(\vec{p}\cdot\vec{k})\vec{q}^2}{\vec{q}^2}\right] \\ &= -4\left[(\vec{p}\cdot\vec{k}) + 2\frac{(\vec{p}\cdot\vec{q})(\vec{q}\cdot\vec{k})}{\vec{q}^2}\right].\end{aligned} \tag{B.1.15}$$

Also

$$(\vec{p}\cdot\vec{q})(\vec{q}\cdot\vec{k}) = [\vec{p}\cdot(\vec{p}-\vec{k})][(\vec{p}-\vec{k})\cdot\vec{k}] = (\vec{p}^2+\vec{k}^2)(\vec{p}\cdot\vec{k}) - \vec{p}^2\vec{k}^2 - (\vec{p}\cdot\vec{k})^2, \quad \text{(B.1.16)}$$

$$(\vec{p}\cdot\vec{q}) = \vec{p}^2 - (\vec{p}\cdot\vec{k}), \quad \text{(B.1.17)}$$

$$(\vec{q}\cdot\vec{k}) = (\vec{p}\cdot\vec{k}) - \vec{k}^2. \quad \text{(B.1.18)}$$

Angular Integration:

$$\int d^3\vec{k} = 2\pi\int_0^\infty d\vec{k}\vec{k}^2\int_0^\pi d\theta\sin\theta. \quad \text{(B.1.19)}$$

In all above, $\vec{k}$ and $\vec{p}$ alone represent the magnitude of the spatial vector, respectively.

B.2 Gap equations after performing angular integration

The self consistent equation to determine B, A and C after performing the angular integration are:

$$B(\vec{p}^2,\widetilde{\omega}_n^2) = m_c - \frac{1}{3\pi^2}T\sum_{l=-\infty}^{\infty}\int_0^\infty d\vec{k}\vec{k}^2\sigma_B(\vec{p}^2,\widetilde{\omega}_n^2)\Big[I_0+2I_0'\Big], \quad \text{(B.2.1)}$$

$$\begin{aligned} A(\vec{p}^2,\widetilde{\omega}_n^2) = 1 - \frac{T}{3\vec{p}^2\pi^2}\sum_{l=-\infty}^{\infty}\int_0^\infty d\vec{k}\vec{k}^2\Big[&\sigma_A(\vec{k}^2,\widetilde{\omega}_l^2)[\vec{p}\vec{k}I_1 + \\ &2\vec{p}\vec{k}(\vec{p}^2+\vec{k}^2)(I_2-I_5+I_5') - 2\vec{p}^2\vec{k}^2(I_3+I_4-I_6-I_7+I_6'+I_7')] \\ &+2\Omega_{nl}\widetilde{\omega}_l\sigma_C(\vec{k}^2,\widetilde{\omega}_l^2)[\vec{p}^2I_4-\vec{p}\vec{k}I_2]\Big] \end{aligned} \quad \text{(B.2.2)}$$

and

$$\begin{aligned} C(\vec{p}^2,\widetilde{\omega}_n^2) = 1 - \frac{1}{3\pi^2\widetilde{\omega}_n}T\sum_{l=-\infty}^{\infty}\int_0^\infty d\vec{k}\vec{k}^2\Big[&2\sigma_A(\vec{k}^2,\widetilde{\omega}_l^2)\Omega_{nl}[\vec{k}^2I_4-\vec{k}\vec{p}I_2] + \\ &\widetilde{\omega}_l\sigma_C(\vec{k}^2,\widetilde{\omega}_l^2)[-I_0+2I_0'+2\Omega_{nl}^2I_4]\Big], \end{aligned} \quad \text{(B.2.3)}$$

where

$$I_0 = \int_0^\pi d\theta \sin\theta g^2 D^L(\vec{k}^2, \Omega_{nl}^2), \qquad I_0' = \int_0^\pi d\theta \sin\theta g^2 D^T(\vec{k}^2, \Omega_{nl}^2),$$
$$I_1 = \int_0^\pi d\theta \sin\theta\cos\theta g^2 D^L(\vec{k}^2, \Omega_{nl}^2), \qquad I_2 = \int_0^\pi d\theta \sin\theta\cos\theta \frac{g^2 D^L(\vec{k}^2, \Omega_{nl}^2)}{Q^2},$$
$$I_3 = \int_0^\pi d\theta \sin\theta\cos^2\theta \frac{g^2 D^L(\vec{k}^2, \Omega_{nl}^2)}{Q^2}, \qquad I_4 = \int_0^\pi d\theta \sin\theta \frac{g^2 D^L(\vec{k}^2, \Omega_{nl}^2)}{Q^2},$$
$$I_5 = \int_0^\pi d\theta \sin\theta\cos\theta \frac{g^2 D^L(\vec{k}^2, \Omega_{nl}^2)}{\vec{q}^2}, \qquad I_5' = \int_0^\pi d\theta \sin\theta\cos\theta \frac{g^2 D^T(\vec{k}^2, \Omega_{nl}^2)}{\vec{q}^2},$$
$$I_6 = \int_0^\pi d\theta \sin\theta\cos^2\theta \frac{g^2 D^L(\vec{k}^2, \Omega_{nl}^2)}{\vec{q}^2}, \qquad I_6' = \int_0^\pi d\theta \sin\theta\cos^2\theta \frac{g^2 D^T(\vec{k}^2, \Omega_{nl}^2)}{\vec{q}^2},$$
$$I_7 = \int_0^\pi d\theta \sin\theta \frac{g^2 D^L(\vec{k}^2, \Omega_{nl}^2)}{\vec{q}^2}, \qquad I_7' = \int_0^\pi d\theta \sin\theta \frac{g^2 D^T(\vec{k}^2, \Omega_{nl}^2)}{\vec{q}^2}. \tag{B.2.4}$$

B.2.1 Sum over two Matsubara frequencies

Here we perform explicitly the sum over two Matsubara frequencies $n = 0, -1$.

$$\begin{aligned} B(\vec{p}^2, \widetilde{\omega}_0^2) &= m_c - \frac{1}{3\pi^2} T \int_0^\infty d\vec{k}\vec{k}^2 \Big[\sigma_B(\vec{p}^2, \widetilde{\omega}_0^2)[I_{0(00)} + 2I'_{0(00)}] \\ &\quad + \sigma_B(\vec{p}^2, \widetilde{\omega}_{-1}^2)[I_{0(0-1)} + 2I'_{0(0-1)}] \Big], \end{aligned} \tag{B.2.5}$$

$$\begin{aligned} B(\vec{p}^2, \widetilde{\omega}_{-1}^2) &= m_c - \frac{1}{3\pi^2} T \int_0^\infty d\vec{k}\vec{k}^2 \Big[\sigma_B(\vec{p}^2, \widetilde{\omega}_0^2)[I_{0(-10)} + 2I'_{0(-10)}] \\ &\quad + \sigma_B(\vec{p}^2, \widetilde{\omega}_{-1}^2)[I_{0(-1-1)} + 2I'_{0(-1-1)}] \Big], \end{aligned} \tag{B.2.6}$$

$$
\begin{aligned}
A(\vec{p}^2,\widetilde{\omega}_0^2) &= 1-\frac{T}{3\vec{p}^2\pi^2}\int_0^\infty d\vec{k}\vec{k}^2\Bigg[\Bigg[\sigma_A(\vec{k}^2,\widetilde{\omega}_0^2)[\vec{p}\vec{k}I_{1(00)}+2\vec{p}\vec{k}(\vec{p}^2+\vec{k}^2)(I_{2(00)}-I_{5(00)}+I'_{5(00)}) \\
&\quad -2\vec{p}^2\vec{k}^2(I_{3(00)}+I_{4(00)}-I_{6(00)}-I_{7(00)}+I'_{6(00)}+I'_{7(00)})] \\
&\quad +2\Omega_{00}\widetilde{\omega}_0\sigma_C(\vec{k}^2,\widetilde{\omega}_0^2)[\vec{p}^2I_{4(00)}-\vec{p}\vec{k}I_{2(00)}]\Bigg]+ \\
&\quad \Bigg[\sigma_A(\vec{k}^2,\widetilde{\omega}_{-1}^2)[\vec{p}\vec{k}I_{1(0-1)}+2\vec{p}\vec{k}(\vec{p}^2+\vec{k}^2)(I_{2(0-1)}-I_{5(0-1)}+I'_{5(0-1)}) \\
&\quad -2\vec{p}^2\vec{k}^2(I_{3(0-1)}+I_{4(0-1)}-I_{6(0-1)}-I_{7(0-1)}+I'_{6(0-1)}+I'_{7(0-1)})] \\
&\quad +2\Omega_{0-1}\widetilde{\omega}_{-1}\sigma_C(\vec{k}^2,\widetilde{\omega}_{-1}^2)[\vec{p}^2I_{4(0-1)}-\vec{p}\vec{k}I_{2(0-1)}]\Bigg]\Bigg], \qquad \text{(B.2.7)}
\end{aligned}
$$

$$
\begin{aligned}
A(\vec{p}^2,\widetilde{\omega}_{-1}^2) &= 1-\frac{T}{3\vec{p}^2\pi^2}\int_0^\infty d\vec{k}\vec{k}^2\Bigg[\Bigg[\sigma_A(\vec{k}^2,\widetilde{\omega}_0^2)[\vec{p}\vec{k}I_{1(-10)}+2\vec{p}\vec{k}(\vec{p}^2+\vec{k}^2)(I_{2(-10)}-I_{5(-10)}+I'_{5(-10)}) \\
&\quad -2\vec{p}^2\vec{k}^2(I_{3(-10)}+I_{4(-10)}-I_{6(-10)}-I_{7(-10)}+I'_{6(-10)}+I'_{7(-10)})] \\
&\quad +2\Omega_{-10}\widetilde{\omega}_0\sigma_C(\vec{k}^2,\widetilde{\omega}_0^2)[\vec{p}^2I_{4(00)}-\vec{p}\vec{k}I_{2(00)}]\Bigg]+ \\
&\quad \Bigg[\sigma_A(\vec{k}^2,\widetilde{\omega}_{-1}^2)[\vec{p}\vec{k}I_{1(-1-1)}+2\vec{p}\vec{k}(\vec{p}^2+\vec{k}^2)(I_{2(-1-1)}-I_{5(-1-1)}+I'_{5(-1-1)}) \\
&\quad -2\vec{p}^2\vec{k}^2(I_{3(-1-1)}+I_{4(-1-1)}-I_{6(-1-1)}-I_{7(-1-1)}+I'_{6(-1-1)}+I'_{7(-1-1)})] \\
&\quad +2\Omega_{-1-1}\widetilde{\omega}_{-1}\sigma_C(\vec{k}^2,\widetilde{\omega}_{-1}^2)[\vec{p}^2I_{4(00)}-\vec{p}\vec{k}I_{2(00)}]\Bigg]\Bigg], \qquad \text{(B.2.8)}
\end{aligned}
$$

$$
\begin{aligned}
C(\vec{p}^2,\widetilde{\omega}_0^2) &= 1-\frac{1}{3\pi^2\widetilde{\omega}_0}T\int_0^\infty d\vec{k}\vec{k}^2\Bigg[\Bigg[2\sigma_A(\vec{k}^2,\widetilde{\omega}_0^2)\Omega_{00}[\vec{k}^2 I_{4(00)}-\vec{k}\vec{p}I_{2(00)}]+ \\
&\quad \widetilde{\omega}_0\sigma_C(\vec{k}^2,\widetilde{\omega}_0^2)[-I_{0(00)}+2I'_{0(00)}+2\Omega_{00}^2 I_{4(00)}]\Bigg] \\
&\quad +\Bigg[2\sigma_A(\vec{k}^2,\widetilde{\omega}_{-1}^2)\Omega_{0-1}[\vec{k}^2 I_{4(0-1)}-\vec{k}\vec{p}I_{2(0-1)}]+ \\
&\quad \widetilde{\omega}_{-1}\sigma_C(\vec{k}^2,\widetilde{\omega}_{-1}^2)[-I_{0(0-1)}+2I'_{0(0-1)}+2\Omega_{0-1}^2 I_{4(0-1)}]\Bigg]\Bigg], \qquad \text{(B.2.9)}
\end{aligned}
$$

$$
\begin{aligned}
C(\vec{p}^2,\widetilde{\omega}_{-1}^2) &= 1-\frac{1}{3\pi^2\widetilde{\omega}_{-1}}T\int_0^\infty d\vec{k}\vec{k}^2\Bigg[\Bigg[2\sigma_A(\vec{k}^2,\widetilde{\omega}_{-1}^2)\Omega_{-10}[\vec{k}^2 I_{4(-10)}-\vec{k}\vec{p}I_{2(-10)}]+ \\
&\quad \widetilde{\omega}_{-1}\sigma_C(\vec{k}^2,\widetilde{\omega}_{-1}^2)[-I_{0(-10)}+2I'_{0(-10)}+2\Omega_{-10}^2 I_{4(-10)}]\Bigg] \\
&\quad +\Bigg[2\sigma_A(\vec{k}^2,\widetilde{\omega}_{-1}^2)\Omega_{-1-1}[\vec{k}^2 I_{4(-1-1)}-\vec{k}\vec{p}I_{2(-1-1)}]+ \\
&\quad \widetilde{\omega}_{-1}\sigma_C(\vec{k}^2,\widetilde{\omega}_{-1}^2)[-I_{0(-1-1)}+2I'_{0(-1-1)}+2\Omega_{-1-1}^2 I_{4(-1-1)}]\Bigg]\Bigg], \qquad \text{(B.2.10)}
\end{aligned}
$$

with $\Omega_{nl}=2(n-l)\pi T$, $\omega_n=(2n+1)\pi T$, $\omega_l=(2l+1)\pi T$, $\Omega_{00}=0$, $\Omega_{0-1}=2\pi T$, $\Omega_{-10}=-2\pi T$, $\Omega_{-10}^2=\Omega_{0-1}^2=4\pi^2T^2$, $\Omega_{00}^2=\Omega_{-1-1}^2=0$, $\omega_0=\pi T$, $\omega_{-1}=-\pi T$, and $\omega_0^2=\omega_{-1}^2=\pi^2T^2$. The integrals involved here are the following:

$$
\begin{aligned}
I_{0(00)} &= I_{0(-1-1)} = \int_0^\pi d\theta \sin\theta g^2 D^L(\vec{k}^2, 0) = \int_0^\pi d\theta \sin\theta g^2 D^L(\vec{k}^2), \\
I'_{0(00)} &= I'_{0(-1-1)} = \int_0^\pi d\theta \sin\theta g^2 D^T(\vec{k}^2, 0) = \int_0^\pi d\theta \sin\theta g^2 D^T(\vec{k}^2), \\
I_{1(00)} &= I_{1(-1-1)} = \int_0^\pi d\theta \sin\theta\cos\theta g^2 D^L(\vec{k}^2, 0) = \int_0^\pi d\theta \sin\theta\cos\theta g^2 D^L(\vec{k}^2), \\
I_{2(00)} &= I_{2(-1-1)} = \int_0^\pi d\theta \sin\theta\cos\theta \frac{g^2 D^L(\vec{k}^2, 0)}{Q^2} = \int_0^\pi d\theta \sin\theta\cos\theta \frac{g^2 D^L(\vec{k}^2, 0)}{Q^2}, \\
I_{3(00)} &= I_{3(-1-1)} = \int_0^\pi d\theta \sin\theta\cos^2\theta \frac{g^2 D^L(\vec{k}^2, 0)}{Q^2} = \int_0^\pi d\theta \sin\theta\cos\theta \frac{g^2 D^L(\vec{k}^2)}{Q^2}, \\
I_{4(00)} &= I_{4(-1-1)} = \int_0^\pi d\theta \sin\theta \frac{g^2 D^L(\vec{k}^2, 0)}{Q^2} = \int_0^\pi d\theta \sin\theta \frac{g^2 D^L(k^2)}{Q^2}, \\
I_{5(00)} &= I_{5(-1-1)} = \int_0^\pi d\theta \sin\theta\cos\theta \frac{g^2 D^L(\vec{k}^2, 0)}{\vec{q}^2} = \int_0^\pi d\theta \sin\theta\cos\theta \frac{g^2 D^L(\vec{k}^2)}{\vec{q}^2}, \\
I_{6(00)} &= I_{6(-1-1)} = \int_0^\pi d\theta \sin\theta\cos^2\theta \frac{g^2 D^L(\vec{k}^2, 0)}{\vec{q}^2} = \int_0^\pi d\theta \sin\theta\cos^2\theta \frac{g^2 D^L(\vec{k}^2)}{\vec{q}^2}, \\
I_{7(00)} &= I_{7(-1-1)} = \int_0^\pi d\theta \sin\theta \frac{g^2 D^L(\vec{k}^2, 0)}{\vec{q}^2} = \int_0^\pi d\theta \sin\theta \frac{g^2 D^L(\vec{k}^2)}{\vec{q}^2}, \\
I'_{5(00)} &= I'_{5(-1-1)} = \int_0^\pi d\theta \sin\theta\cos\theta \frac{g^2 D^T(\vec{k}^2, 0)}{\vec{q}^2} = \int_0^\pi d\theta \sin\theta\cos\theta \frac{g^2 D^T(\vec{k}^2)}{\vec{q}^2}, \\
I'_{6(00)} &= I'_{6(-1-1)} = \int_0^\pi d\theta \sin\theta\cos^2\theta \frac{g^2 D^T(\vec{k}^2, 0)}{\vec{q}^2} = \int_0^\pi d\theta \sin\theta\cos^2\theta \frac{g^2 D^T(\vec{k}^2)}{\vec{q}^2}, \\
I'_{7(00)} &= I'_{7(-1-1)} = \int_0^\pi d\theta \sin\theta \frac{g^2 D^T(\vec{k}^2, 0)}{\vec{q}^2} = \int_0^\pi d\theta \sin\theta \frac{g^2 D^T(\vec{k}^2)}{\vec{q}^2}, \\
I_{0(0-1)} &= I_{0(-10)} = \int_0^\pi d\theta \sin\theta\cos\theta g^2 D^L(\vec{k}^2, 4\pi^2 T^2), \\
I_{1(0-1)} &= I_{1(-10)} = \int_0^\pi d\theta \sin\theta\cos\theta g^2 D^L(\vec{k}^2, 4\pi^2 T^2), \\
I_{2(0-1)} &= I_{2(-10)} = \int_0^\pi d\theta \sin\theta\cos\theta \frac{g^2 D^L(\vec{k}^2, 4\pi^2 T^2)}{Q^2}, \\
I_{3(0-1)} &= I_{3(-10)} = \int_0^\pi d\theta \sin\theta\cos^2\theta \frac{g^2 D^L(\vec{k}^2, 4\pi^2 T^2)}{Q^2}, \\
I_{4(0-1)} &= I_{4(-10)} = \int_0^\pi d\theta \sin\theta \frac{g^2 D^L(\vec{k}^2, 4\pi^2 T^2)}{Q^2}, \\
I_{5(0-1)} &= I_{5(-10)} = \int_0^\pi d\theta \sin\theta\cos\theta \frac{g^2 D^L(\vec{k}^2, 4\pi^2 T^2)}{\vec{q}^2}, \\
I_{6(0-1)} &= I_{6(-10)} = \int_0^\pi d\theta \sin\theta\cos^2\theta \frac{g^2 D^L(\vec{k}^2, 4\pi^2 T^2)}{\vec{q}^2},
\end{aligned}
$$

$$
\begin{aligned}
I_{7(0-1)} &= I_{7(-10)} = \int_0^\pi d\theta \sin\theta \frac{g^2 D^L(\vec{k}^2, 4\pi^2 T^2)}{\vec{q}^2}, \\
I'_{5(0-1)} &= I'_{5(-10)} = \int_0^\pi d\theta \sin\theta\cos\theta \frac{g^2 D^T(\vec{k}^2, 4\pi^2 T^2)}{\vec{q}^2}, \\
I'_{6(0-1)} &= I'_{6(-10)} = \int_0^\pi d\theta \sin\theta\cos^2\theta \frac{g^2 D^T(\vec{k}^2, 4\pi^2 T^2)}{\vec{q}^2}, \\
I'_{7(0-1)} &= I'_{7(-10)} = \int_0^\pi d\theta \sin\theta \frac{g^2 D^T(\vec{k}^2, 4\pi^2 T^2)}{\vec{q}^2}.
\end{aligned}
$$

Substituting the values of frequencies, we observe that the self consistent equations with $n = 0$ and $n = -1$ are the same, i.e.,

$$
\begin{aligned}
B(\vec{p}^2, \widetilde{\omega}_0^2) &= m_c - \frac{1}{3\pi^2} T \int_0^\infty d\vec{k}\vec{k}^2 \sigma_B(\vec{p}^2, \pi^2 T^2) \Bigg[[I_{0(00)} + 2I'_{0(00)}] \\
&\quad + [I_{0(0-1)} + 2I'_{0(0-1)}] \Bigg], \qquad \text{(B.2.11)}
\end{aligned}
$$

$$
\begin{aligned}
B(\vec{p}^2, \widetilde{\omega}_{-1}^2) &= m_c - \frac{1}{3\pi^2} T \int_0^\infty d\vec{k}\vec{k}^2 \sigma_B(\vec{p}^2, \pi^2 T^2) \Bigg[[I_{0(0-1)} + 2I'_{0(0-1)}] \\
&\quad + [I_{0(00)} + 2I'_{0(00)}] \Bigg], \qquad \text{(B.2.12)}
\end{aligned}
$$

$$
\begin{aligned}
A(\vec{p}^2, \widetilde{\omega}_0^2) &= 1 - \frac{T}{3\vec{p}^2\pi^2} \int_0^\infty d\vec{k}\vec{k}^2 \Bigg[\sigma_A(\vec{k}^2, \pi^2 T^2) \Bigg[[\vec{p}\vec{k} I_{1(00)} + 2\vec{p}\vec{k}(\vec{p}^2 + \vec{k}^2)(I_{2(00)} - I_{5(00)} + I'_{5(00)}) \\
&\quad - 2\vec{p}^2\vec{k}^2(I_{3(00)} + I_{4(00)} - I_{6(00)} - I_{7(00)} + I'_{6(00)} + I'_{7(00)})] \\
&\quad + [\vec{p}\vec{k} I_{1(0-1)} + 2\vec{p}\vec{k}(\vec{p}^2 + \vec{k}^2)(I_{2(0-1)} - I_{5(0-1)} + I'_{5(0-1)}) \\
&\quad - 2\vec{p}^2\vec{k}^2(I_{3(0-1)} + I_{4(0-1)} - I_{6(0-1)} - I_{7(0-1)} + I'_{6(0-1)} + I'_{7(0-1)})] \Bigg] \\
&\quad - 4\pi^2 T^2 \sigma_C(\vec{k}^2, \pi^2 T^2)[-\vec{p}\vec{k} I_{2(0-1)} + \vec{p}^2 I_{4(0-1)}] \Bigg], \qquad \text{(B.2.13)}
\end{aligned}
$$

$$
\begin{aligned}
A(\vec{p}^2,\widetilde{\omega}_{-1}^2) &= 1-\frac{T}{3\vec{p}^2\pi^2}\int_0^\infty d\vec{k}\vec{k}^2\Bigg[-4\pi^2T^2\sigma_C(\vec{k}^2,\pi^2T^2)[-\vec{p}\vec{k}I_{2(0-1)}+\vec{p}^2I_{4(0-1)}] \\
&\quad +\sigma_A(\vec{k}^2,\pi^2T^2)\Bigg[[\vec{p}\vec{k}I_{1(0-1)}+2\vec{p}\vec{k}(\vec{p}^2+\vec{k}^2)(I_{2(0-1)}-I_{5(0-1)}+I'_{5(0-1)}) \\
&\quad -2\vec{p}^2\vec{k}^2(I_{3(0-1)}+I_{4(0-1)}-I_{6(0-1)}-I_{7(0-1)}+I'_{6(0-1)}+I'_{7(0-1)})] \\
&\quad +[\vec{p}\vec{k}I_{1(00)}+2\vec{p}\vec{k}(\vec{p}^2+\vec{k}^2)(I_{2(00)}-I_{5(00)}+I'_{5(00)}) \\
&\quad -2\vec{p}^2\vec{k}^2(I_{3(00)}+I_{4(00)}-I_{6(00)}-I_{7(00)}+I'_{6(00)}+I'_{7(00)})]\Bigg]\Bigg], \qquad \text{(B.2.14)}
\end{aligned}
$$

$$
\begin{aligned}
C(\vec{p}^2,\widetilde{\omega}_0^2) &= 1-\frac{T}{3\pi^2}\int_0^\infty d\vec{k}\vec{k}^2\Bigg[\sigma_C(\vec{k}^2,\pi^2T^2)\Bigg[[-I_{0(00)}+2I'_{0(00)}] \\
&\quad -[-I_{0(0-1)}+2I'_{0(0-1)}+8\pi^2T^2I_{4(0-1)}]\Bigg] \\
&\quad +4\sigma_A(\vec{k}^2,\pi^2T^2)[\vec{k}^2I_{4(0-1)}-\vec{k}\vec{p}I_{2(0-1)}]\Bigg], \qquad \text{(B.2.15)}
\end{aligned}
$$

$$
\begin{aligned}
C(\vec{p}^2,\widetilde{\omega}_{-1}^2) &= 1-\frac{T}{3\pi^2}\int_0^\infty d\vec{k}\vec{k}^2\Bigg[4\sigma_A(\vec{k}^2,\pi^2T^2)[\vec{k}^2I_{4(0-1)}-\vec{k}\vec{p}I_{2(0-1)}]+ \\
&\quad \sigma_C(\vec{k}^2,\pi^2T^2)\Bigg[[-I_{0(0-1)}+2I'_{0(0-1)}+8\pi^2T^2I_{4(0-1)}] \\
&\quad +[-I_{0(00)}+2I'_{0(00)}]\Bigg]\Bigg]. \qquad \text{(B.2.16)}
\end{aligned}
$$

Appendix C

Gap equation in magnetic field

In this Appendix we present some calculations of Chapter 4.

C.1 Zero temperature and magnetic field

The Schwinger propagator in a uniform magnetic field is given by

$$\begin{aligned} S(k) &= \int_0^\infty d\tau \frac{\mathrm{e}^{-\tau(k_\parallel^2+k_\perp^2\frac{\tan(|q_fB\tau|)}{|q_fB\tau|}+M^2)}}{\cosh(|q_fB\tau|)}\Bigg[\Bigg(\cosh(|q_fB\tau|)(M-\not{k}_\parallel)- \\ &\quad (M-\not{k}_\parallel)i\gamma^1\gamma^2\sinh(|q_fB\tau|)\Bigg)-\frac{\not{k}_\perp}{\cosh(|q_fB\tau|)}\Bigg], \end{aligned} \tag{C.1.1}$$

where $k_\parallel^2 = k_0^2 + k_3^2$ and $k_\perp^2 = k_0^2 + k_3^2$. The trace of Eq. (**??**) is given by

$$\begin{aligned} Tr[S(k)] &= \int_0^\infty d\tau \frac{\mathrm{e}^{-\tau(k_\parallel^2+k_\perp^2\frac{\tan(|q_fB\tau|)}{|q_fB\tau|}+M^2)}}{\cosh(|q_fB\tau|)}Tr\Bigg[\Bigg(\cosh(|q_fB\tau|)(M-\not{k}_\parallel)- \\ &\quad (M-\not{k}_\parallel)i\gamma^1\gamma^2\sinh(|q_fB\tau|)\Bigg)-\frac{\not{k}_\perp}{\cosh(|q_fB\tau|)}\Bigg]. \end{aligned} \tag{C.1.2}$$

As $Tr[\not{k}] = 0$, $Tr[\gamma^1\gamma^2] = 4\delta^{12} = 0$, and $Tr[M\mathbb{I}] = 4M$, Eq. (**??**) becomes

$$\begin{aligned} Tr[S(k)] &= 4M\int_0^\infty d\tau \frac{\mathrm{e}^{-\tau(k_\parallel^2+k_\perp^2\frac{\tan(|q_fB\tau|)}{|q_fB\tau|}+M^2)}}{\cosh(|q_fB\tau|)}\cosh(|q_fB\tau|), \\ &= 4M\int_0^\infty d\tau \mathrm{e}^{-\tau(k_\parallel^2+k_\perp^2\frac{\tan(|q_fB\tau|)}{|q_fB\tau|}+M^2)}. \end{aligned} \tag{C.1.3}$$

Introducing the infra-red and ultraviolet cut-offs, we have

$$Tr[S(k)] \;=\; 4M\int_{\tau_{uv}^2}^{\tau_{ir}^2} d\tau \mathrm{e}^{-\tau(k_\parallel^2+k_\perp^2\frac{\tan(|q_fB\tau|)}{|q_fB\tau|}+M^2)}. \tag{C.1.4}$$

Since

$$M = m_c + \frac{4\alpha_{\text{eff}}(0)}{3}\int \frac{d^4k}{(2\pi)^4} Tr[S(k)], \tag{C.1.5}$$

using Eq. (**??**) in Eq. (**??**), we have

$$M = m_c + \frac{16M\alpha_{\text{eff}}(0)}{3}\int \frac{d^4k}{(2\pi)^4}\int_{\tau_{uv}^2}^{\tau_{ir}^2} d\tau \mathrm{e}^{-\tau(k_\parallel^2+k_\perp^2\frac{\tan(|q_fB\tau|)}{|q_fB\tau|}+M^2)}, \tag{C.1.6}$$

or

$$M = m_c + \frac{16M\alpha_{\text{eff}}(0)}{3}\int \frac{d^2k_\perp}{(2\pi)^2}\frac{d^2k_\parallel}{(2\pi)^2}\int_{\tau_{uv}^2}^{\tau_{ir}^2} d\tau \mathrm{e}^{-\tau(k_\parallel^2+k_\perp^2\frac{\tanh(|q_fB\tau|)}{|q_fB\tau|}+M^2)}. \tag{C.1.7}$$

As

$$\int_{-\infty}^{\infty}\frac{d^2k_\parallel}{(2\pi)^2}e^{-\tau k_\parallel^2} = \frac{1}{4\pi\tau}, \qquad \int_{-\infty}^{\infty}\frac{d^2k_\perp}{(2\pi)^2}e^{-\tau k_\perp^2\frac{\tanh(|q_fB\tau|)}{|q_fB\tau|}} = \frac{|q_fB|}{4\pi\tanh(|q_fB\tau|)}, \tag{C.1.8}$$

our final gap equation expression is of the form

$$M = m_c + \frac{M\alpha_{\text{eff}}(0)}{3\pi^2}\frac{1}{2}\sum_{f=u,d}|q_fB|\int_{\tau_{uv}^2}^{\tau_{ir}^2} d\tau\frac{\mathrm{e}^{-\tau M^2}}{\tau\tanh(|q_fB\tau|)}. \tag{C.1.9}$$

The factor (1/2) is due to the fact that our gap equation at zero temperature and magnetic field considers $N_f = 2$, and in the case of magnetic field each flavor gets separated by electric charge.

C.2 Finite temperature and magnetic field

At finite temperature, we replace k_0 by ω_n such that the gap equation is expressed as

$$M = m_c + \frac{4\alpha_{\text{eff}}(0)}{3}T\sum_n\int \frac{d^3k}{(2\pi)^3} Tr[S(k)], \tag{C.2.1}$$

or

$$M = m_c + \frac{16M\alpha_{\rm eff}(0)T}{3}\sum_n \int \frac{d^3k}{(2\pi)^3}\int_{\tau_{uv}^2}^{\tau_{ir}^2} d\tau {\rm e}^{-\tau(\omega_n^2+k_3^2+k_\perp^2\frac{\tan(|q_fB\tau|)}{|q_fB\tau|}+M^2)}. \tag{C.2.2}$$

Since

$$\int \frac{d^3k}{(2\pi)^3} = \int_{-\infty}^{\infty}\frac{dk_3}{(2\pi)}\frac{d^2k_\perp}{(2\pi)^2}, \qquad \sum_{n=-\infty}^{\infty} e^{-\tau\omega_n^2} = \Theta_2(0, e^{-4\pi^2\tau T^2}),$$
$$\int_{-\infty}^{\infty}\frac{dk_3}{(2\pi)}\frac{d^2k_\perp}{(2\pi)^2}{\rm e}^{-\tau(k_3^2+k_\perp^2\frac{\tanh(|q_fB\tau|)}{|q_fB\tau|})} = \frac{|q_fB|}{8\pi^{3/2}\sqrt{\tau}\tanh(|q_fB\tau|)}, \tag{C.2.3}$$

where $\Theta_2(x,y)$ is the Jacobi theta function. Using Eq. (**??**) in Eq. (**??**), we have

$$M = m_c + \frac{2M\alpha_{\rm eff}(0)T}{3\pi^{3/2}}\frac{1}{2}\sum_{f=u,d}|q_fB|\int_{\tau_{uv}^2}^{\tau_{ir}^2} d\tau\frac{\Theta_2(0,e^{-4\pi^2\tau T^2}){\rm e}^{-\tau M^2}}{\sqrt{\tau}\tanh(|q_fB\tau|)}. \tag{C.2.4}$$

Bibliography

[1] I. G. Aznauryan *et. al.*, *Int. J. Mod. Phys. E* **22**, 1330015 (2013).

[2] R. Alkofer, C. S. Fischer and L. V. Smekal, *Phys. Rev. D* **52**, 191 (2002);
P. Maris, A. Raya, C. D. Roberts and S. M. Schmidt, *Eur. Phys. J. A***18**, 231 (2003).

[3] D. Dudal, O. Oliveira, N. Vandersickel, *Phys. Rev. D* **81**, 074505 (2010).

[4] A. Ahmad and A. Raya, *J. Phys. Conf. Ser.* **418**, 012009 (2013).

[5] A. Bashir, A. Raya and J. Rodríguez-Quintero, *Phys. Rev. D* **88**, 054003 (2013).

[6] K. G. Klimenko, *Z. Phys. C* **54**, 323 (1992);
K. Farakos, N. E. Mavromatos, *Int. J. Mod Phys. B* **12**, 809 (1998) ;
V. P. Gusynin, V. A. Miransky, I. A. Shovkovy, *Phys. Rev. D* **52**, 4747 (1995).

[7] A. Bazavov, T. Bhattacharya, M. Cheng, C. DeTar, T. H. Ding, S. Gottlieb, R. Gupta, P. Hegde, U. M. Heller and F. Karsch, *Phys. Rev. D* **85**, 054503 (2012).

[8] A. Ahmad, A. Ayala, A. Bashir, E. Gutiérrez and A. Raya, *J. Phys.: Conf. Ser.* **651**, 012018 (2015).
A. Ahmad, *et. al.*, *QCD phase diagram from constant mass approximation*, in progress.

[9] P. Maris and P. C. Tandy, *Phys. Rev. C* **60**, 055214 (1999).

[10] T. Matsubara, *Prog. Theor. Phys.* **14**, 351 (1955).

[11] E. Braaten and A. Nieto, *Phys. Rev. Lett.* **73**, 2402 (1994).

[12] E. Gutiérrez, A. Ahmad, A. Ayala, A. Bashir and A. Raya, *J. Phys. G* **41**, 075002 (2014).

[13] S-X. Qin, L. Chang, H. Chen, Y-X. Liu and C. D. Roberts, *Phys. Rev. Lett.* **106**, 172301 (2011);
S-X. Qin , L. Chang, Liu Y-X and C. D. Roberts, *Phys. Rev. D* **84**, 014017 (2011).

[14] C. D. Roberts, *Phys. Part.Nucl* **30**, 223 (1999).

[15] J. A. Müller, *Ph. D Thesis*, Darmstadt (2011).

[16] C. S. Fischer and J. Luecker, *Prog. Part. Nucl. Phys.* **67**, 200 (2012);
C. S. Fischer and J. Luecker, *Phys. Lett. B* **718**, 1036 (2013).

[17] H. L. L. Roberts, A. Bashir, L. X. Gutiérrez-Guerrero, C. D. Roberts and D. J. Wilson, *Phys. Rev. C***83**, 065206 (2011).

[18] M. A. Bedolla, J. J. Cobos-Martínez, and A. Bashir, *Phys. Rev. D* **92**, 054031 (2015).

[19] D. Ebert, T. Feldmann and H. Reinhardt, *Phys. Lett. B* **388**, 154 (1996).

[20] E. Bilgici, F. Bruckmann, C. Gattringer and C. Hagen, *Phys. Rev. D* **77**, 094007 (2008).

[21] K.-I. Wang, Y.-X. Liu, L. Chang, C. D. Roberts and S. M. Schmidt, *Phys. Rev. D* **87**, 074038 (2013);
Z.-F. Cui, Y.-L. Du and H.-S. Zong, *Int. J. Mod. Phys. Com. Ser.* **29**, 1460232 (2014).

[22] T. Klähn, and T. Fischer, *Astrophys. J.* **810** 2, 134 (2015).

[23] K. Raya, A. Bashir, S. Hernández-Ortiz, A. Raya, and C. D. Roberts, *Phys. Rev. D* **88**, 096003 (2013).

[24] K.-I. Wang, et. al., *Phys. Rev. D* **86**, 114001 (2012).

[25] F. Márquez, A. Ahmad, M. Buballa and A. Raya, *Phys. Lett. B* **747**, 529 (2015).

[26] A. Ahmad, *et. al.*, *QCD phase diagram from vector vector contact interaction*, *in progress.*

[27] I. Bogolubsky, E. M. Ilgenfritz, M. Muller-Preussker and A. Sternbeck, *Proc. Sci., LAT2007*, 290 (2007);
A. Cucchieri and T. Mendes, *Proc. Sci., LAT2007*, 297 (2007);
A. C. Aguilar, D. Binosi and J. Papavassiliou, *Phys. Rev. D* **78**, 025010 (2008);
D. Dudal, J. A. Gracey, S. P. Sorella, N. Vandersickel and H. Verschelde, *Phys. Rev. D* **78**, 065047 (2008);
P. Boucaud, J. Leroy, A. L. Yaouanc, J. Micheli, O. Pène and J. Rodríguez-Quintero, *JHEP* **06.099** (2008);
O. Oliveira and P. Silva, *Proc. Sci., LAT2009*, 226 (2009);
I. Bogolubsky, E. M. Ilgenfritz, M. Muller-Preussker and A. Sternbeck, *Phys. Lett. B* **676**, 69 (2009);
C. S. Fischer, A. Maas and J. M. Pawlowski, *Ann. Phys.* **324**, 2408 (2009);

A. C. Aguilar, D. Binosi and J. Papavassiliou, *Phys. Rev. D* **78**, 025010 (2009);
A. Ayala, A. Bashir, D. Binosi, M. Cristoforetti and J. Rodríguez-Quintero, *Phys. Rev. D* **86**, 074512 (2012).

[28] C. Bernard *et al.* (MILC Collaboration) *Phys. Rev. D* **71**, 034504 (2005);
M. Cheng *et al. Phys. Rev. D* **74**, 054507 (2006);
S. Borsányi *et al. JHEP* **1009.073** (2010);
Y. Aoki *et al.*, *Phys. Lett. B* **643**, 46 (2006);
A. Bazavov *PoS Lattice* 182 (2011);
Z. Fodor and S. D. Katz, *JHEP* **03. 014** (2002);
R. V. Gavai and S. Gupta *Phys. Rev. D* **71**, 114014 (2005);
A. Li, A. Alexandru, X. Meng and K. F. Liu, *Nucl. Phys. A* **830**, 633 (2009);
P. C de Forcrand and S. Kratochvila, *Nucl. Phys. B* **153**, 62 (2006);
S. Sharma, *Adv. HEP* **2013**, 452878 (2013);
P. Cea, L. Cosmai and A. Papa, *Phys. Rev. D* **89**, 074512 (2014).

[29] K. Osterwalder and R. Schrader, *Commun. Math. Phys.* **31**, 83 (1973).

[30] A. M. Polyakov, *Phys. Lett. B* **72**, 477 (1978).

[31] J. Braun, L. M. Haas, F. Marhauser, and J. M. Pawlowski, *Phys. Rev. Lett.* **106**, 022002 (2011).

[32] C. S. Fischer, *Phys. Rev. Lett.* **103**, 052003 (2009).

[33] C. S. Fischer and J. A. Muller, *Phys. Rev. D* **80**, 074029 (2009).

[34] C. S. Fischer, A. Mass and J. A. Muller, *Eur. Phys. J. C* **68**, 165 (2010).

[35] Y. Nambu and Jona-Lasinio, *Phys. Rev.* **122**, 345 (1961).

[36] K. Kashiwa, H. Kouno and M. Yahiro, *Phys. Rev. D* **80**, 117901 (2009).

[37] T. K. Mukherjee, H. Chen and M. Huang, *Phys. Rev. D* **82**, 034015 (2010).

[38] S. Benic, *Phys. Rev. D* **88**, 077501 (2013).

[39] H. Feng, P Yin, W. Sun and H. Zong, *Sci. China Phys. Mech. Astron.* **56**, 1116 (2013).

[40] C. S. Fischer, J. Luecker and C. A. Welzbacher, *Phys. Rev. D* **90**, 034022 (2014);

[41] A. Cucchieri and T. Mendes, *PoS. Latt.* **206**, (2011).

[42] Y. Aoki *et al.*, *JHEP.* **06 088** (2009);
S. Gupta, X. Luo, B. Mohanty, H. G. Ritter and N. Xu, *Science* **332**, 1525 (2011);
A. Bazavov *et al. Phys. Rev. D* **85**, 054503 (2012);

[43] A. Ahmad and A. Raya, *Invese magnetic catalysis in a confining contact interaction model for quarks*, submitted.

[44] C. R. Duncan and C. Thompson, *Astrophys. J.* **392**, L9 (1992).

[45] T. Vachaspati, *Phys. Lett. B* **265**, 258 (1991).

[46] K. Enqvist and P. Olesen, *Phys. Lett. B* **319**, 178 (1993).

[47] V. Skokov, A. Y. Illarionov and V. Toneev, *Int. J. Mod. Phys. A* **24**, 5925 (2009);
V. Voronyuk *et al.*, *Phys. Rev. C* **83**, 054911 (2011);
A. Bazdak and V. Skokov, *Phys. Lett. B* **710**, 171 (2012);
W. T. Deng and X. G. Huang, *Phys. Rev. C* **85**, 044907 (2012).

[48] D. E. Kharzeev, L. D. McLerran and H. J. Warringa, *Nucl. Phys. A* **803**, 227 (2008);
K. Fukushima, D.E. Kharzeev and H.J. Warringa, *Phys. Rev. D* **85**, 045104 (2008).

[49] A. Shovkovy, *Lect. Notes Phys.* **871**, 13 (2012);

[50] P. Buividovich *et. al.*, *Phys. Lett. B* **682**, 484 (2010);
V. Braguta *et. al.*, *LATTICE2010*, 190 (2010);
V. P. Gusynin and V. A. Miransky, I. A. Shovkovy, *Nucl. Phys. B* **462**, 249 (1996);
R. Gatto and M. Ruggieri, *Phys. Rev. D* **82** 054027 (2010);
K. Kashiwa, *Phys. Rev. D* **83**, 117901 (2011);
A. J. Mizher *et al.*, *Phys. Rev. D* **82**, 105016 (2010);
M. Loewe, F. Márquez, C. Villavicencio and R. Zamora, *Int. J. Mod. Phys. A* **30**, 1550123 (2015).

[51] G. S. Bali, *et al.*, *Phys. Rev. D* **86**, 071502 (2012);
G. S. Bali, *et al.*, *JHEP* **1202.044** (2012).

[52] M. Ferreira, P. Costa, O. Lourenço, T. Frederico and C. Providência, *Phys. Rev. D* **89**, 116011 (2014).

[53] M. Ferreira, P. Costa, D. P. Menezes, C. Providencia, and N. Scoccola, *Phys. Rev. D* **89**, 016002 (2014);
E. S. Fraga, B. W. Mintz, and J. Schaffner-Bielich, *Phys. Lett. B* **731**, 154 (2014).

[54] R. L. S. Farias, K. P. Krein and M. B. Pinto, *Phys. Rev. C* **90**, 025203 (2014).

[55] A. Ayala, M. Loewe and R. Zamora, *Phys. Rev. D* **91**, 016002 (2014).

[56] A. Ayala, M. Loewe, A. J. Mizher and R. Zamora, *Phys. Rev. D* **90**, 036001 (2014).

[57] A. Ayala, C. A. Dominguez, L. A. Hernndez, M. Loewe and R. Zamora, *Phys. Rev. D* **92**, 096011 (2015).

[58] F. Bruckmann, G. Endrodi and T. G. Kovacs, *JHEP* **04.112** (2013).

[59] V. A. Miransky and I. A. Shovkovy, *Phys. Rev. D* **66**, 045006 (2002).

[60] A. Ayala, C. A. Dominguez, L. A. Hernndez, M. Loewe and R. Zamora, *arXiv:1510.09134 [hep-ph]* (2015).

[61] J. Schwinger, *Phys. Rev.* **82**, 664 (1951).

[62] A. Andronic, P. Braun-Munzinger and J. Stachel,*Nucl. Phys. A* **834**, 237C (2010);
J. Cleymans, H Oeschler, K. Redlich and S. Wheaton, *Phys. Rev. C* **73**, 034905 (2006);
L. Kumar (for the STAR Collaboration), *Nucl. Phys. A* **904**, 256c (2013);
S. Das (for the STARCollaboration) *Nucl. Phys. A* **904**, 891c (2013);
L. Kumar, *Pramana* **84**, 5 (2015).

[63] D. Griffiths, *Introduction to Elementary Particles. Wiley*, (1987).

[64] M. R. Pennington, Lectures given with title *"Swimming with Quarks"*, XI Mexican School of Particles and Fields, Xalapa, Aug. 2004.

[65] R. Alkofer, W. Detmold, C. S. Fischer, and P. Maris, *Phys. Rev. D* **70**, 014014 (2004).

[66] A. Bashir, A. Raya, I. C. Clöet and C. D. Roberts, *Phys. Rev. C* **78**, 055201 (2008):
C.P. Hofmann, A. Raya and S. Sánchez-Madrigal, *Phys. Rev. D* **82**, 096011 (2010).

[67] J. C. Collins and M. J. Perry, *Phys. Rev. Lett.* **34**, 1353 (1975).

[68] N. Cabibbo and G. Parisi, *Phys. Lett. B* **59**, 67 (1975).

[69] M. Le Bellac, *Thermal Field Theory*, *Cambridge University Press*, (1996).